12-2009

Experimental and Theoretical Investigation of Adsorption of Water Vapor on Carbon Nanotubes

Pyoungchung Kim
University of Tennessee - Knoxville

To the Graduate Council:

I am submitting herewith a dissertation written by Pyoungchung Kim entitled "Experimental and Theoretical Investigation of Adsorption of Water Vapor on Carbon Nanotubes." I have examined the final electronic copy of this dissertation for form and content and recommend that it be accepted in partial fulfillment of the requirements for the degree of Doctor of Philosophy, with a major in Civil Engineering.

Sandeep Agnihotri, Major Professor

We have read this dissertation and recommend its acceptance:

Chris Cox, Terry L. Miller, David J. Keffer

Accepted for the Council:

Carolyn R. Hodges

Vice Provost and Dean of the Graduate School

(Original signatures are on file with official student records.)

To the Graduate Council:

I am submitting herewith a dissertation written by Pyoungchung Kim entitled "Experimental and Theoretical Investigation of Adsorption of Water Vapor on Carbon Nanotubes." I have examined the final electronic copy of this dissertation for form and content and recommend that it be accepted in partial fulfillment of the requirements for the degree of Doctor of Philosophy, with a major in Civil Engineering.

Sandeep Agnihotri, Major Professor

We have read this dissertation
and recommend its acceptance:

Chris Cox

Terry L. Miller

David J. Keffer

Accepted for the Council:

Carolyn R. Hodges
Vice Provost and Dean of the Graduate School

Experimental and Theoretical Investigation of Adsorption of Water Vapor on Carbon Nanotubes

A Dissertation
Presented for the
Doctor of Philosophy
Degree
The University of Tennessee, Knoxville

Pyoungchung Kim

December 2009

Acknowledgments

Isaiah 43:1 *"But now, this is what the LORD says--he who created you, O Jacob, he who formed you, O Israel: "Fear not, for I have redeemed you; I have summoned you by name; you are mine."*

I would like to express my sincere gratitude to my advisor Prof. Sandeep Agnihotri for the continuous support of my Ph.D study and research, for his patience, motivation, enthusiasm, and immense knowledge. His guidance helped me in all the time of research and writing of this dissertation. I could not have imagined having a better advisor and mentor for my Ph.D study.

Besides my advisor, I would like to thank my dissertation committee: Dr. Chris Cox, Dr. Terry Miller, and Dr. David Keffer for their encouragement, insightful comments, and hard questions. I want to thank my former colleagues, Yijing Zheng and Liangcheng Yang, for their help and support.

I could not imagine my life without my family. my father and mother are those who sincerely raised me with scarifying their whole life. My elder brother, PyoungHo and sister Jiyon, thanks for being supportive and caring siblings.

Words fail me to express my appreciation to my lovely wife, Hyoung Yon Kim whose dedication, love and persistent confidence in me, has taken the load off my shoulder. I would also thank my sweet daughter, Katie Arin and son, Ryan JuHyoung, for giving me happiness and encouragement with bright smile. I would also thank my wife's family for letting me take her hand in marriage and accepting me as a member of the family warmly.

Abstract

The adsorption of water in nanoporous materials becomes an important issue in the environmental fate and applications when one considers the practical use of these materials as adsorbents for hazardous organic compounds in the diverse environments.

In this study, the complexity of water-SWNTs interaction was investigated by morphological and chemical characterization techniques, by gravimetric adsorption measurement and by interpretation of experimental adsorption isotherms by fitting to several existing semi-empirical water adsorption models. Commercially available SWNTs samples were measured for chemical and physical characterization such as O% by x-ray photoelectron spectroscopy, I_D/I_G by Raman spectroscopy and surface and porosity by nitrogen adsorption at 77 K. Water adsorption isotherms and kinetics on SWNTs were performed by custom-built gravimetric measurement (detection limit = 0.1 μg).

Water adsorption isotherms data obtained gravimetrically from T= 5, 20, 35 ^{o}C were consequently fitted to several semi-empirical models that were developed to interpret adsorption isotherms of water in common carbonaceous adsorbents. The applicability of these models was evaluated by high correlation coefficients and the significance of temperature sensitive water-specific sample properties such as the degree of primary sites, sizes of water clusters aggregating on primary sites and filling micropore and equilibrium constants. Those fitting parameters were evaluated by comparison to the results obtained from characterization type experiments. Conclusively, the Do & Do equation, as modified by Marban et al., is the most suitable semi-empirical equation for

predicting from experimental isotherms alone the size of molecular clusters that facilitate adsorption in SWNTs. This model can deconvoluted the experimental isotherms into two pseudo-isotherms: adsorption onto hydrophilic groups and filling of micropores, and quantifying the concentration of hydrophilic functional groups, as well as determining the micropore volume explored by water. Isosteric heat of water adsorption calculated from experimental isotherms and that for pseudo-isotherms; functional groups and micropore isotherms, on SWNTs was similar to those available in the current literature reportedly estimated by calorimetric or molecular simulation technique. This research approach may be useful in interpreting experimental water adsorption to aide purely theoretical methods of studying the behavior of water as well as to better understand the environmental fate of carbon materials.

TABLE OF CONTENTS

Lists of Figures

Lists of Tables

1. Introduction

1.1. Background

1.1.1. Carbon nanotubes

Since carbon nanotubes (CNTs) were discovered by Sumio Iijima in 1991,[1] they have been found to possess their remarkable physical and chemical properties, which are connected with cylindrical nanostructure.[2] The inner hollow porosity of CNTs can hold atoms or molecules through capillarity and adsorption, which makes them useful in potential applications in electronic devices,[3] energy storage,[4] and drug delivery.[5] Carbon nanotubes are mainly categorized as single-walled carbon nanotubes (SWNTs) and multi-walled carbon nanotubes (MWNTs).

Single-walled carbon nanotubes (SWNTs) consist of rolled up sheets of carbon hexagons which exhibit the planar sp^2 bonding of graphite. SWNTs are one atom thick uniform cylindrical structures of carbon that often agglomerate into bundles by van der Waal force (Figure 1.1). SWNTs contain 0.7–1.5 nanometers in diameter and 100 nm to 10 μm in length. Multi-walled carbon nanotubes (MWNTs) consist of multiple rolled layers of graphite. MWNTs contain from 5 to 40 nanometers in diameter and 2 to 10 micrometers in length. The spacing between adjacent layers is about 0.34 nanometers, close to the spacing observed between sheets of graphite.[6] MWNTs exist not as bundles but as aggregation of isolated CNTs (Figure 1.2).[7]

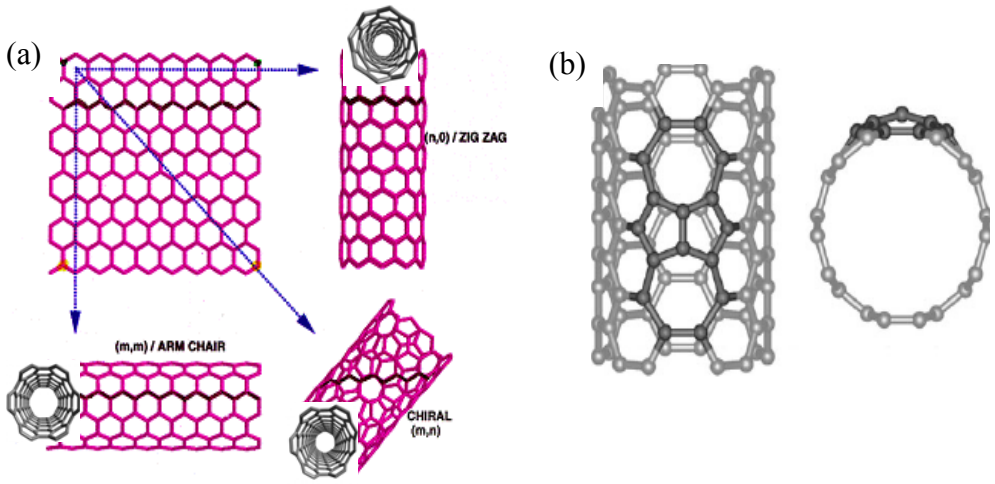

Figure 1.1 (a) Roll-up of a graphene sheet leading to the three types of CNTs (b) Stone-Wales defect on the sidewall of a nanotube

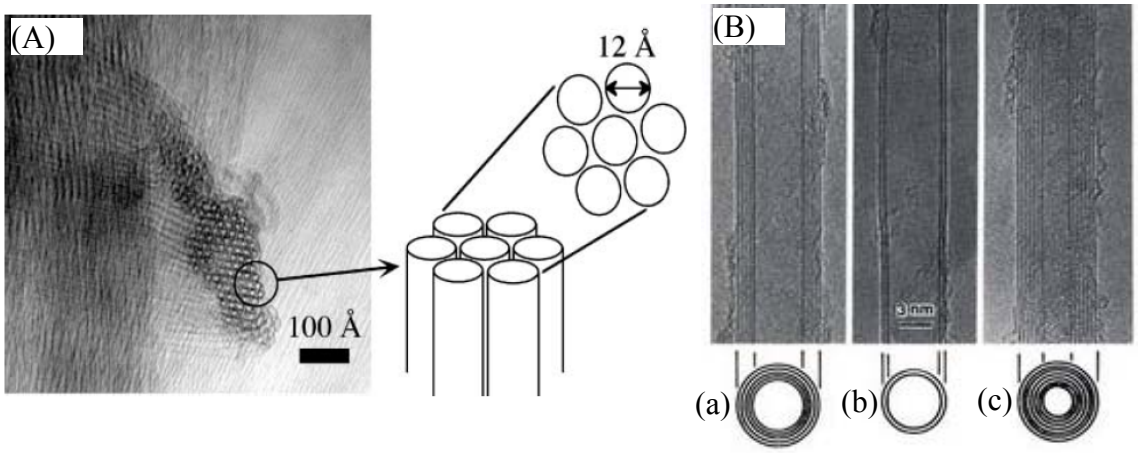

Figure 1.2 (A) Structure of single-walled carbon nanotubes (B) Multi-walled carbon nanotubes; A cross-section of each tube is illustrated. (a). Tube consisting of five graphitic sheets, diameter 6.7nm. (b). two-sheet tube, 5.5 nm in diameter. (c). Seven-sheet tube, 6.5 nm in diameter including 2.2 nm in inner diameter. [8]

1.1.2. Synthesis and purifications

1.1.2.1. Synthesis

Carbon nanotubes can be produced by three synthesis methods[9]; electric arc-discharge, laser ablation, and chemical vapor deposition (CVD). Electric arc-discharge technique[10] uses two graphite electrodes between which carbon atoms are generated through an electric arc discharge at T > 3,000 ^{o}C (Figure 1.3). Nanotubes are formed in the presence of suitable catalyst metal particles (Fe, Co or Ni). Synthesis of MWNTs does not need any metal catalyst for arc discharge, while that of SWNTs required mixed metal catalysts to be inserted into anode electrode. Average diameters of the tube produced by this method are 1.3 - 1.4 nanometers and maximum production rate are 120 g/day. It has been reported that content of SWNTs produced by this method is 80 % by volume. Laser ablation technique[11] uses intense laser beam to irradiate a mixture of graphite and metal catalysts in a flow of inert gas to generate atomic carbon followed by formation of nanoutbes at T > 3,000 ^{o}C. This method can control the diameter of SWNTs with 1.4 nm depending on reaction temperature. Maximum production rate is 50 g/day. Chemical vapor deposition technique[12] applies metal catalysts to decompose gaseous hydrocarbons (benzene, ethanol, acetylene, propylene, methane, ethylene, CO, etc) as the carbon source and consequently grow carbon nanotubes over them in a temperature 300 – 1,200 ^{o}C. CVD method can control over diameter depending on the size of catalyst particles, shell number and growth rate of CNTs. Average diameter of the tubes is 1 nm and maximum production rate is 50 kg/day. However, compared to arc-discharge and laser ablation techniques, CVD method produces higher density of defect and less tensile strength of CNTs because of lower reaction temperature. Content of SWNTs produced by CVD method is 30 – 50 wt%, while that of MWNT is 30 – 99 wt%.

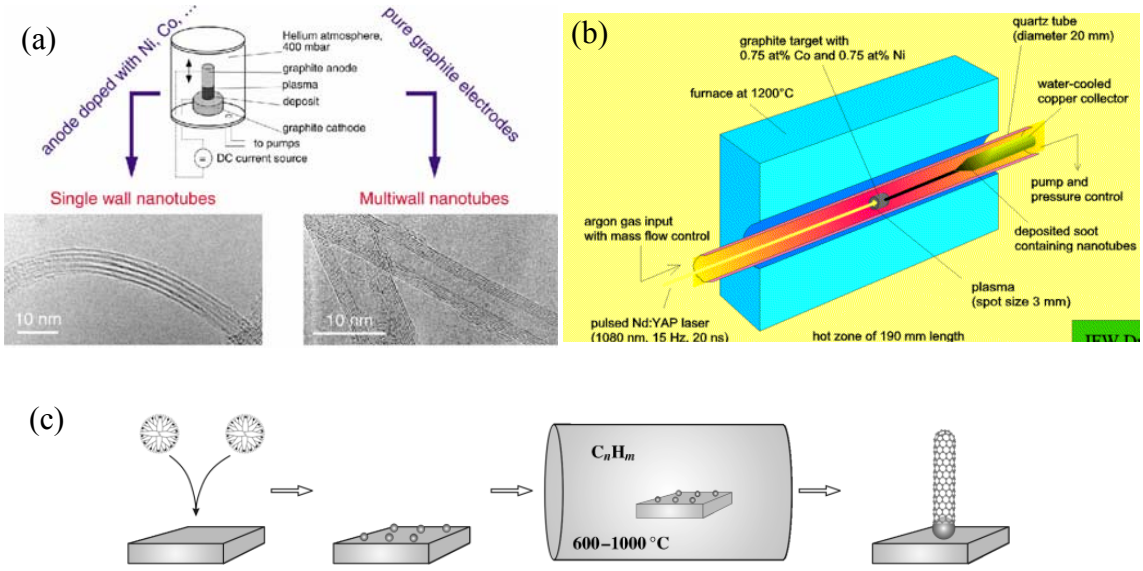

Figure 1.3 Experimental set up for synthesis of carbon nanotubes (a) Arc discharge (b) Laser ablation (c) Chemical vapor deposition.

1.1.2.2. Impurity

Synthetic processes of carbon nanotubes generate both carbonaceous and metal catalytic impurities owing to the graphite and metal catalysts sources.[13] Arc-discharge and laser ablation techniques generate by-products such as fullerenes, amorphous carbon, graphite particles coming from unvaporized graphite rods and graphitic polyhedrons with enclosed metal particles in the synthetic process of SWNTs. CVD synthesis method also by-produces impurities such as aromatic carbon, amorphous carbon, polyhedral carbon with enclosed metal particles at high temperature (> 1,000 ^{o}C).

1.1.2.3. Purification

As-synthesized CNTs containing impurity should be purified to obtain high quality tubes and to chemically functionalize nanotube sidewalls for further applications.[13] Fullerene with solubility can be separated from carbon nanotubes by certain organic solvents such as toluene. Amorphous carbons containing high density of defects are easily removed by general purification methods. However, impurities such as graphite particles and polyhedral carbon with enclosed metal catalytic particles are very difficult to remove because such impurities contain a similar oxidation rate to carbon nanotubes. Metal impurity encapsulated by carbon layers is unable to dissolve or expose in chemical solutions. Therefore, highly efficient purification methods of as-synthesized CNTs are required to obtain high purity tubes.

Carbon nanotubes are purified by basically three methods, namely, chemical, physical and a combination of both. Chemical oxidation method basically removes amorphous carbonaceous materials and metal particles by high selectivity of chemical oxidation with destroying surface structure and cutting CNTs and introducing oxygenated functional groups (-OH, -COOH and -C=O). Chemical oxidation includes gas phase oxidation (using a mixture of Cl_2, H_2O, and HCl, a mixture of Ar, O_2 and H2O or a mixture of O_2, SF_6 and $C_2H_2F_4$), liquid phase oxidation (using a mixture of H_2O_2 and HCl, a mixture of H_2SO_4, HNO_3, $KMnO_4$ and NaOH and refluxing, etc) and electrochemical oxidation. For example, Chiang et al.[14] reported using gas phase oxidation (a mixture of Ar and O_2 followed by HCl acidification) that encapsulated metal catalysts are oxidized to oxidation products, which break carbon shells and are exposed to concentrated hydrochloric acid to be dissolved into iron particles. This method produced 99.9% pure

SWNTs with a yield of ~ 30 wt% of raw materials. For liquid phase oxidation, Dujardin et al.[15] reported used sonication in concentric nitric acid followed by refluxing under stirring at 120 - 130 ^{o}C for 4 hours to purify as-synthesized SWNTs that 30 – 50 % of SWNTs from the raw sample were yielded and metal impurity was reduced to ~1 wt%. For electrochemical oxidation, Fang et al. used electrochemical cyclic voltammetric (CV) oxidation in KOH solution and removed amorphous carbon. Unlike chemical purification which destroys the structure of CNTs or changes their natural surface properties, physical based purification is applied to elucidate the inherent physical and chemical properties of CNTs and to remove graphite particles. Based on the different physical properties between CNTs and impurities such as aspect ratio, physical size, solubility, gravity and magnetism, filtration, chromatography, centrifugation, electrophoresis, and high temperature annealing (1,400-2,800 ^{o}C) have been extensively investigated. Combination of chemical and physical methods facilitates the purification of CNTs. Bandow et al.[16] used the combination of microfiltration with air oxidation in which large carbon nanosoots (CNS) in raw samples are separated by filtration followed by removing CNTs attached to the CNTs walls by air filtration at 450 ^{o}C for 20 min. Then, metal particles were removed by concentric HCl (36 %) for 1 – 2 days at room temperature. From this method, greater than 90% pure CNTs were obtained.

1.1.3. Property

Carbon nanotubes are unique nanostructures with remarkable electrical and thermal properties, which are characterized by helicity and defects of carbon surface.[17] As with helicity of rolled graphene sheet, chiral indices (n, m) in graphene sheet are

rolled to tubes by (n = m) value, the armchair typed nanotubes possess metallic property (Figure 1.3). If graphene sheet is rolled by different values between n and m values, zigzag (n, 0) or chiral (n, m) typed nanotubes present semi-conductive property. Diameters of carbon nanotubes depend on the helicity of carbon layer. For example, diameter of (10:10) SWNTs is 1.4 nm while that of (20:20) SWNTs is 2.7 nm. This is based on the distance between carbon atom centers on opposite sides of CNTs.[6] Surface defects, which are produced in the process of synthesis and purification, also affect property of carbon nanotubes. It is observed that any materials contain surface defects. Carbon nanotubes also contain mainly two types of defects[18]; one type is a point defect in the form of atomic vacancies. Another form of defects is the Stone Wales defect, which are rearranged by a pentagon and heptagon pair. Defects on CNTs weaken the tensile strength of tubes, change electric property of armchair typed CNTs from conductivity into semi-conductivity, and reduce the thermal conductivity of tubes. Likewise, defects on carbon surface are covalently bonded with oxygen functional groups during purification, which also changes the chemical property of CNTs from hydrophobic to hydrophilic.

1.1.4. Adsorption property

SWNT bundles aggregated by van der Waals interaction give rise to adsorption sites such as internal porosity (1), interstitial channels (2) between adjacent SWNTs, peripheral grooves (3) and external surface of the bundles (4)[19] (Figure 1.4). These different sites play an important role in adsorption capacity. Adsorption capacity of internal porosity (1) depends on pore diameter. Width of interstitial channels produced

from SWNT bundles (2) depends on the diameter size of SWNTs. For example, the width of interstitial channel increases with the pore diameter of bundles of SWNTs. It is known that width of interstitial channels ranges of 0.3-0.5 nm, which accommodates one or more rows of adsorbate molecules. As a result, adsorption capacity of the interstitial channels is traceable. Peripheral grooves (3) on a nanotubes bundle contain 0.4-0.5 nm of a partial slit pore where adsorption capacity is traceable. External surfaces (4) of SWNT bundles are adsorbed by electrically neutral gas molecules. Adsorption capacity depends on purity and opening of carbon nanotubes. As-produced carbon nanotubes are usually found that both ends are closed and most of the inner cavities are hard to be available for adsorption sites. As-produced SWNTs are required to remove impurities and open the ends of SWNTs. Pristine CNTs contain uncharacterized impurities such as amorphous carbon, fullerene, and catalytic metal particles (e.g. Co, Fe or Ni). These impurities can misrepresent adsorption properties of CNTs. Impurities, therefore, should be removed by purification process.

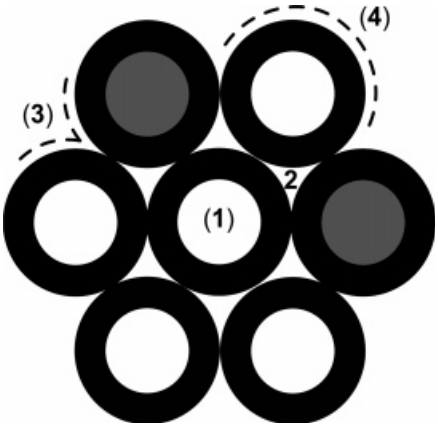

Figure 1.4 A cross-section of SWNTs illustrated adsorption sites of SWNTs bundles : (1) Internal porosity, (2) Interstitial channels, (3) Grooves, (4) External surface[20]

1.1.5. Comparison of carbon nanotubes to activated carbons

Carbon nanotubes containing remarkable physical and morphological properties are attractive carbon materials as a replacement of activated carbons. However, owing to simpler processes and cheaper cost for activated carbons, it is still hard to replace activated carbons with carbon nanotubes in some areas. However, carbon nanotubes are very attractive materials rather in applications not in economic. Comparison of carbon nanotubes to activated carbons presented in Table 1 is, therefore, essential to realizing the full potential applicability of CNTs.

Activated carbons are extremely cheap and produced from various carbonaceous sources such as coal, nutshells and wood by physical or chemical activation processes. For example, physical reactivation applies carbonation using pyrolysis in the range 600 – 900 ^{o}C and in absence of air followed by activation or oxidation using oxidizing atmospheres (CO_2, oxygen, or steam) in the range of 600 – 1,200 ^{o}C. Chemical activation process applies simultaneous process in carbonation and activation using soaking raw materials into chemicals (acid, strong base or salt like phosphoric cid, potassium hydroxide, zinc chloride). Activated carbons are high surface area and high porosity carbons made of small hexagonal rings organized into graphene sheets. Typical Brunauer, Emmett, and Teller (BET) surface areas for activated carbons are 1,000 – 3,000 m^2/g. Although the BET surface area of CNTs (~ 2,000 m^2/g) is not sometimes as high as in activated carbons, surface area of CNTs is more accessible because CNTs have percolated pore structure which is useful for ion or molecule migration.

Table 1.1 Summary of commonly recognized properties of Activated Carbons and Carbon Nanotubes. (Y-yes, N-no)

Property	Activated Carbons	SWNTs
Composition	**Reference**	**Reference**
Carbon (primary element)	Y Bansal, 1998[21]	Y Ijima, 1991[1]
Ash	Y Smisek, 1970	Y Li & Zhang, 2005
Pre-adsorbed moisture	Y Bansal, 1986[22]	Y Mawhinney et al., 2000[23]
Chemical Properties		
Surface-oxygen is common	Y Chingombe et al., 2005[24]	Y Curulli et al., 2005[27]
Reactive to strong acids and bases	Y Biniak et al., 1997[25]	Y Kuznetsova et al., 2001[28]
Annealing, ozonation etc. alter chemistry	Y Villacanas et al., 2006[26]	Y Lafi et al., 2005[29]
Physical Properties		
BET surface area of 100s to 1,000s m^2/g	Y Bansal, 1998[21]	Y Cinke et al., 2002[32]
Pore width less than 2 nm in micropores	Y Ruthven, 1984[30]	Y Dresselhaus, 2000[33]
Micropore volume is at least 10% of total	Y Alcaniz et al., 2001[31]	Y Agnihotri et al., 2004[34]
Adsorption Capacities		
Moisture uptake ≈ micropore volume	Y Do & Do, 2000[35]	Y Kim & Agnihotri, 2008[37]
Organic uptake ≈ total pore volume	Y Bansode et al., 2003[36]	Y Agnihotri et al., 2005[38]
Polar, nonpolar, aromatic, linear	Y Qi & Levan, 2005[39]	Y Crespo & Yang, 2006[42]
Nitroaromatics > pore, non-polar…	Y Radovic, 2001[40]	Y Chen et al., 2007[43]
H_2 storage = 2 to 4% at 100 atm, 25 ^oC	Y Jung et al., 2009[41]	Y Jorda et al., 2007[44]
SO_2 uptake = 10's mg/g at flue gas conc.	Y Lua & Guo, 2001[45]	Y Long & Yang, 2001*[47]
NO_x uptake= 10's mg/g at flue gas conc.	Y Pietrzak & Bandosz, 2007[46]	Y Long & Yang, 2001*[47]
Adsorbent Structure		
Heterogeneous	Y Liu & Monson, 2006[48]	Y Shi & Johnson, 2003[49]
Structural order		
Limited number of possible structural arrangements for most generality	N 	Y 
Pores are unconnected for ease in modeling actual samples	N	Y
Porosity can also be characterized from non adsorption techniques	N	Y
Cost	$0.05~$1.00 per gram	$50~1,000 per gram

* estimated from MWNTs

Carbon nanotubes contain narrower pore size distribution than activated carbons, which provides high selectivity of target molecules in membrane application. Carbon nanotubes are also more conductive than activated carbons. CNTs consist of a mix of metallic, semiconducting, and insulating materials. A substantial fraction of electrical property depends on chirality of CNTs structure.

1.1.6. Applications

Electrical and thermal properties as well as morphological properties of carbon nanotubes provide potential applications to scientific fields. Remarkable electrical and thermal conductivity of carbon nanotubes is applied for a paper battery in which carbon nanotubes act as electrodes[50], gas sensors based on carbon nanotubes transistors,[51] and flat panel displays with electron emission of carbon nanotubes[52]. Morphological property such as uniformed cylindrical tubes is used for nanotube membranes which exclude ions and other particles due to a combination of small pore size and pore charge effects. Adsorption sites and capacity of carbon nanotubes also extend their potential applications to energy storage[4], catalyst supports[53, 54] and removal of pollutants in the environments.[55, 56]

1.1.7. Consideration for applications-Water adsorption

Water is ubiquitous in the environment and is essential to understand its behavior in the carbon nanotubes. Adsorption of water in carbon nanotubes may become an important issue in realizing potential applications. For example, application of CNTs to water desalination, nanosyringes, drug delivery and high performance membranes is

required to understand the equilibrium and thermodynamic and transport properties of water confined carbon nanotubes. Application of oxidized CNTs to chemical sensors for NO_2 and NH_3 is needed to consider water vapor because target vapors and water are hydrophilic and both are competitive to adsorption sites.[57] For removal of volatile organic vapors in the carrier gas streams, the presence of water vapor can reduce total organic adsorption capacity owing to the competition of water with volatile organic vapors, as is the case with activated carbons.[58]

1.1.7.1. Water adsorption mechanism into micropore filling

As it is mentioned above (Table 1.1), nanocarbons have apparently different geometric configuration from typical activated carbon but include the micropores and mesopores as much as those in microporous activated carbon. Water adsorption isotherms in SWNTs, therefore, are almost the same with that in microporous activated carbons. Water adsorption in carbon pores is mainly affected by the presence of surface functional groups and by pore size. The surface functional groups facilitate adsorption of water at low relative pressures by forming hydrogen bonds after which the aggregation of water molecules into ring-like clusters occurs. These clusters then fill micropores corresponding to vapor pressures.[35] Absence of surface functional groups leads to higher relative pressure at which micropore filling can be observed.[6] Using experimental and molecular simulation methods, Ohba et al.[59] suggested that water clusters formed on the functional groups located at the pore entry of hydrophobic carbon pores exhibited a shift from hydrophilic to hydrophobic after entering the pore. Ohba and Kaneko[60] also showed that the number of molecules that form a cluster, i.e., the cluster size, increase with larger pore size or a decreased concentration of surface functional groups(Figure 1.5).

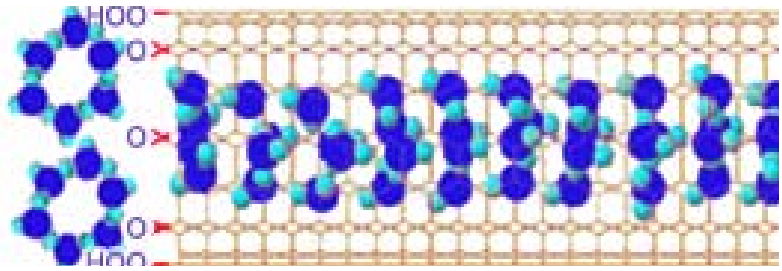

Figure 1.5 Schematic of water adsorption by functional groups on SWNTs.[61]

Estimating the thermodynamic properties of water adsorbed in SWNTs is as important as measuring adsorption capacities and kinetics. Recently, experimental methods and molecular simulation were employed to study the temperature dependency of water adsorption isotherm in carbon nanopores. Striolo et al.[62] suggested that for carbon slit pores and carbon nanotubes an increase of temperature causes the isotherm to shift rightwards, i.e., towards an increasing relative pressure, while a decreasing temperature exhibits narrower hysteresis. Kimura et al.[63] used microcalorimetric and x-ray diffraction techniques to estimate heats of adsorption in carbon nanopores and concluded that at higher vapor pressures several small clusters combine to form a large highly ordered cluster that fills the micropore. Some related studies have developed new equations for calculating the heat of water adsorption in carbon pores.[64, 65] Furmaniak et al.[66] derived an equation by incorporating temperature dependency in the fitting parameters of the Do & Do equation.[35] These methods may describe the thermodynamic behavior of water in the porous carbon with sufficient accuracy; however, they may be limited in application to the samples tested in the particular study.

1.1.7.2. Existing water adsorption isotherm models

In spite of such a tremendous effort to better understand the adsorption of water in SWNTs, it remains ambiguous and not fully understood. SWNT nanocarbons have both micropores and mesopores[19] much like in a typical activated carbon, although the differences in the pore geometry of these two carbon types are obvious. The adsorption of water in the pores of activated carbons is known to be mediated by surface chemistry. Several semi-empirical water adsorption models incorporating the role of surface chemistry can be found in the literature. Therefore, it seems reasonable to apply these models to water-nanotube experimental data to first determine their applicability to novel carbons, and second, attempt to extract reliable molecular scale information about interactions of water with SWNTs. To the best of our knowledge, the Dubinin-Serpinsky (D.S) equation[67] remains to be the only common water-activated carbon isotherm model which has been applied to SWNTs.[68] Several recent studies have reported water isotherms in SWNTs [61, 69] without further analysis of the isotherm data by semi-empirical models that are readily available. The DS equation is one of the most common equations but is also one of the simplest water adsorption models. However, several detailed semi-empirical isotherm models have recently been developed. These models can provide more fundamental information about the behavior of water in porous carbons. Typically these models [35, 70-75] can predict the concentration of surface functional groups, the molecular size of water clusters, the water adsorption capacity in the micropores as well as on the surface functional groups, and also estimate the adsorption equilibrium rate constants. Such models are, for example, the Dubinin-Astakov (DA) equation,[70] the Talu-Meunier equation,[71] the Cooperative multi-molecular sorption (CMMS) theory,[72] the Do

and Do equation[35] and its several modifications.[73-75] However, each of these models was applied to a specific carbon adsorbent. For example, the CMMS [72] theory and the Do and Do[35] equation revised by Lagorsse et al.[73] were fitted to the water adsorption isotherms measured on carbon molecular sieves. Similarly, the DA [70] equation, the Do and Do[35] equation and its interpretation by Zimny et al.,[74] and Marban et al.,[75] were used to describe the data collected for water adsorption on activated carbon and activated carbon fibers.

1.2. Research Objective

The main objective of this study is to explore the adsorption properties of water vapor in SWNTs. The adsorption properties such as adsorption isotherm types, adsorption kinetics as well as water adsorption mechanism such as interaction of water vapor with surface functional groups and with nanopores are investigated by gravimetrically measuring water adsorption isotherms and applying existing several adsorption equations. The selected appropriate isotherm equation, Do & Do model modified by Marban et al. is also applied to obtain adsorption parameters in various SWNTs. The adsorption parameters could be used to understand the adsorption mechanism such as the average size of water clusters growing on the surface functional groups and those migrating inside the pores of nanotubes and the limiting water adsorption capacities in different temperatures on SWNTs. Specific goals of this study are following.

1.2.1. Adsorption equilibrium and kinetics of water vapor in carbon nanotubes and its comparison with activated carbon

The development and application of an experimental setup is reported to allow measurement of water uptake during adsorption-desorption equilibrium and kinetics with a resolution of 0.1 μg of gravimetric microbalance system. This setup is applied to study water adsorption in several commercially available single-walled carbon nanotubes (SWNTs) for comparison with activated carbons. Experimental water adsorption isotherms on SWNTs and activated carbons were curve-fitted to DS equation and Do & Do equation. The kinetics of water adsorption was also curve-fitted to the linear-driving force (LDF) model.

1.2.2. Application of water adsorption models in activated carbon to that in single walled carbon nanotubes

The objective of this study is to understand the interactions of water in novel SWNT nanocarbons by implementing the semi-empirical tools developed for common carbonaceous materials such as activated carbons. This is accomplished by applying several water-carbon isotherm models whose relevance to SWNTs remains unreported in the literature. We gravimetrically measured water adsorption isotherms on several commercially available SWNTs. Each isotherm was fitted to the DS equation [67], DA equation [70], CMMS theory [72] and the Do & Do equation [35]. We are able to identify the Do & Do equation modified by Marban et al. [75], to be the most suitable equation that we tested for interpreting the water adsorption isotherms of SWNT with sufficient details. We suggest that this equation could be an appropriate model to determine from empirical

data alone the concentration of surface functional groups, the average size of water clusters growing on the surface functional groups and those migrating inside the pores of nanotubes, and the limiting water adsorption capacities. Such data should be useful in supporting molecular simulation studies of water adsorption in SWNTs which remains to be the most popular approach for understanding the microscopic behavior of water in nanocarbons [60, 76].

1.2.3. Effect of Surface Oxygen and Temperature on External and Micropore Adsorption of Water in Single-Walled Carbon Nanotubes by Gravimetric Experiments

The objective of this study was to collect water isotherms on multiple SWNT samples and apply a previously modified version[75] of the Do & Do water-isotherm model[35] in order to extract from experimental data the heat of water adsorption in SWNTs, the size of water clusters, the concentration of primary sites and the limiting pore volume. In our previous study,[37] we tested the applicability of several common water-isotherm equations to experimental isotherms collected for SWNTs and activated carbons at T = 20 ^{o}C. We concluded that a model suggested by Marban et al.[75] (Cluster Formation Induced Micropore Filling, CIMF model) is the most suitable equation for interpreting the experimental water-SWNT isotherms. Using this model we were able to deconvolute experimental isotherms into micropore and functional group fractions, and estimate cluster sizes, the concentration of functional groups and the micropore volume. In this publication, we are applying this equation to data collected at multiple temperatures, and have estimated the total and separated heats of water adsorption on

functional groups and in micropores of several SWNT samples. The heats of adsorption (46 to 48 kJ/mol) are found to be similar to those reported in literature by theoretical calculations[77, 78] as well as calorimetric measurements.[79] In micropores, the heat of adsorption is found to be inversely related to the size of water clusters. As posited, the value of parameters representing the concentration of surface functional groups and micropore volumes decreased with an increasing temperature and was discovered to relate to total % O and pore widths determined by independent sample characterizations.

1.3. Research Design

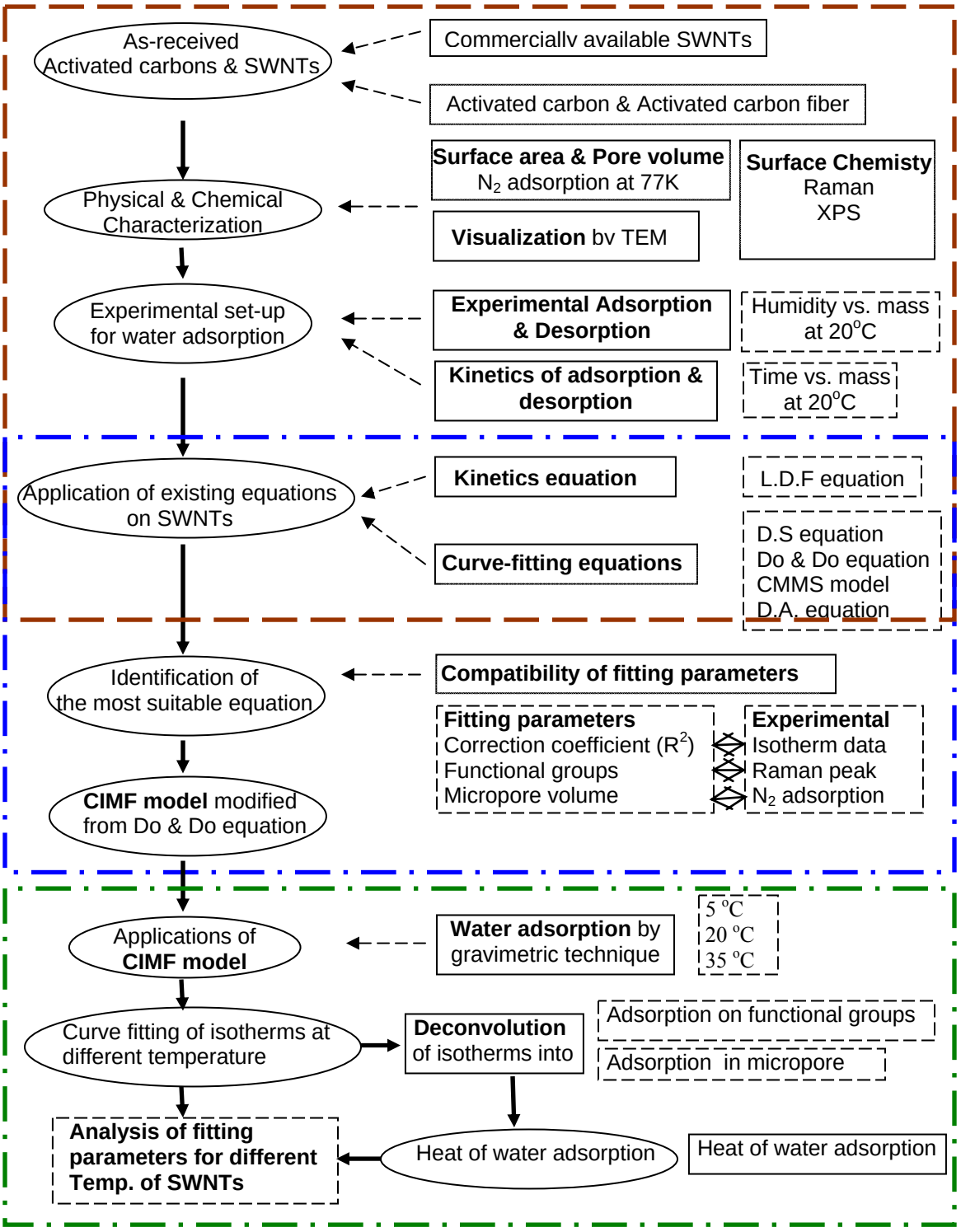

2. Methodology

2.1. Sample information

SWNT samples selected for this study are commercially produced and were purified by the manufacturers. The sample description, morphologies and characterization details were presented in Table1. Samples were purchased from MER Corporation, Tucson, AZ in 2001, from Carbon nanotechnologies Inc., Houston, TX in 2006. and from Carbon Solutions, Riverside, CA in 2006.

The MER sample was produced by the electric arc method. This sample contained 95-98wt% pure SWNTs. The residual contamination consisted of <0.5 wt.% Ni/Co catalyst and <5 wt.% of amorphous and graphitic carbons (manufacture information). It is referred to as SWNT1 (EA95). According to the manufacturer, the as-produced nanotubes were initially refluxed in a 2-3 M nitric acid solution for 45 hours followed by centrifuged to purify nanotubes. The purified sample was then washed 3-4 times by deionized water through re-centrifugation to remove the acid trapped in SWNTs. The purified SWNTs were extracted by hollow-fiber cross-flow filtration after the solution pH was raised up to 11.

The carbon nanotechnologies sample was produced by the HiPco chemical vapor deposition (CVD) processes. The sample contained 90 wt.% pure SWNTs, 12 wt.% Fe catalyst and some amprphous and graphitic carbon. It is referred to as SWNT2 (CVD90). This sample was also purified by using the same method as described above according to the manufacturer information.

The Carbon Solutions samples are 70-90% and 80-90% SWNTs. Here, the samples are referred to as SWNT3 (CS70) and SWNT4 (CS80), respectively. Sample

CS70 was reportedly concentrated from an as-produced material by air oxidation method. It contained a lower concentration of surface functionality, mainly –COOH. The residual mass is supposedly 7 to 10 wt% Ni/Y catalyst and other carbonaceous impurities. Sample SWNT4, on the other hand, is purified with nitric acid. It contains a higher concentration of surface oxides, primarily –COOH. According to the manufacturer, this sample contains 4-6 atomic% carboxylic acid with residual mass being 5 to10 wt% Ni/Y catalyst and other carbons. All SWNT samples contained some fraction of open-ended nanotubes, which was determined by an experimental and molecular simulation method developed in our previous work.[25-28] This parameter is an indication of the available porosity. It was found that only 50%, 55% and 0% SWNTs were open or unblocked, respectively, in samples SWNT1, SWNT3 and SWNT4.[28] The fraction of open-ended nanotubes will have obvious implications on any adsorption measurements, such as those reported in this manuscript.

Activated carbon sample was obtained from Calgon Carbon Corp., Pittsburgh, PA (type F-300). Here it is referred to as AC. Activated carbon fiber sample was provided by American Kynol Inc., New York (type ACF10). This is a non-woven fiber sample. It was produced from novolac resin by polymerization of phenol and formaldehyde. This sample is referred to as ACF10. However, some quantities of SWNT samples SWNT3 and SWNT4 were heated to 600 ^{o}C for several hours in 10 millitorr or less vacuum to modify the concentration of surface functional groups [29]. Prior to the water adsorption tests by the gravimetric method, the heat-treated samples were stored under vacuum to minimize the effects of atmosphere on the sample properties, if any.

2.2. Sample characterization

2.2.1 SWNTs morphology

The nanostructure and impurity of SWNTs were measured with a high resolution transmission electron microscope (HRTEM, JEM-2010, JEOL Ltd., Japan) that is available at the HTML at Oak Ridge National Laboratory (ORNL). This electron microscope uses a 200kV electron source and has a resolution of 2.8 Å . The SWNT samples analyzed by TEM were prepared by the dissolution of the samples in 1% Poly(vinylpyrrolidone) (PVP) solution followed by 10 min sonication. A drop of PVP-SWNT solution was placed on a carbon holey grid and was dried in air. The carbon holey grid was mounted on a TEM sample holder and was then analyzed for the presence of carbon nanotubes. Figure 2.1 showed that Sample SWNT1 (Fig.2.1.a) is extremely purified without any residuous impurity. SWNT2 (Fig.2.1.b) and SWNT3 (Fig.2.1.c) contained dark particles which are identified as metal catalysts or amorphous carbons. In particular, Sample SWNT2 contained significant dark particles

2.2.2 Nitrogen adsorption at 77 K

Samples were analyzed by standard N_2 adsorption at 77 K (Autosorb 1-c by Quantachrome Instruments). 20 ~ 30 mg of sample was outgassed at 140 ^{o}C (or 600 ^{o}C for samples referred to here as heat-treated). N_2 adsorption isotherms were obtained in the relative pressure, P/P_o, range of 10^{-6} to 0.99, where P is actual pressure and P_o is the saturation pressure of N_2 at 77 K. For each sample, the physical properties such as surface area, pore volumes, pore size distributions were extracted from the experimental N_2 isotherm data by application of appropriate equations in the Autosorb 1 Software.

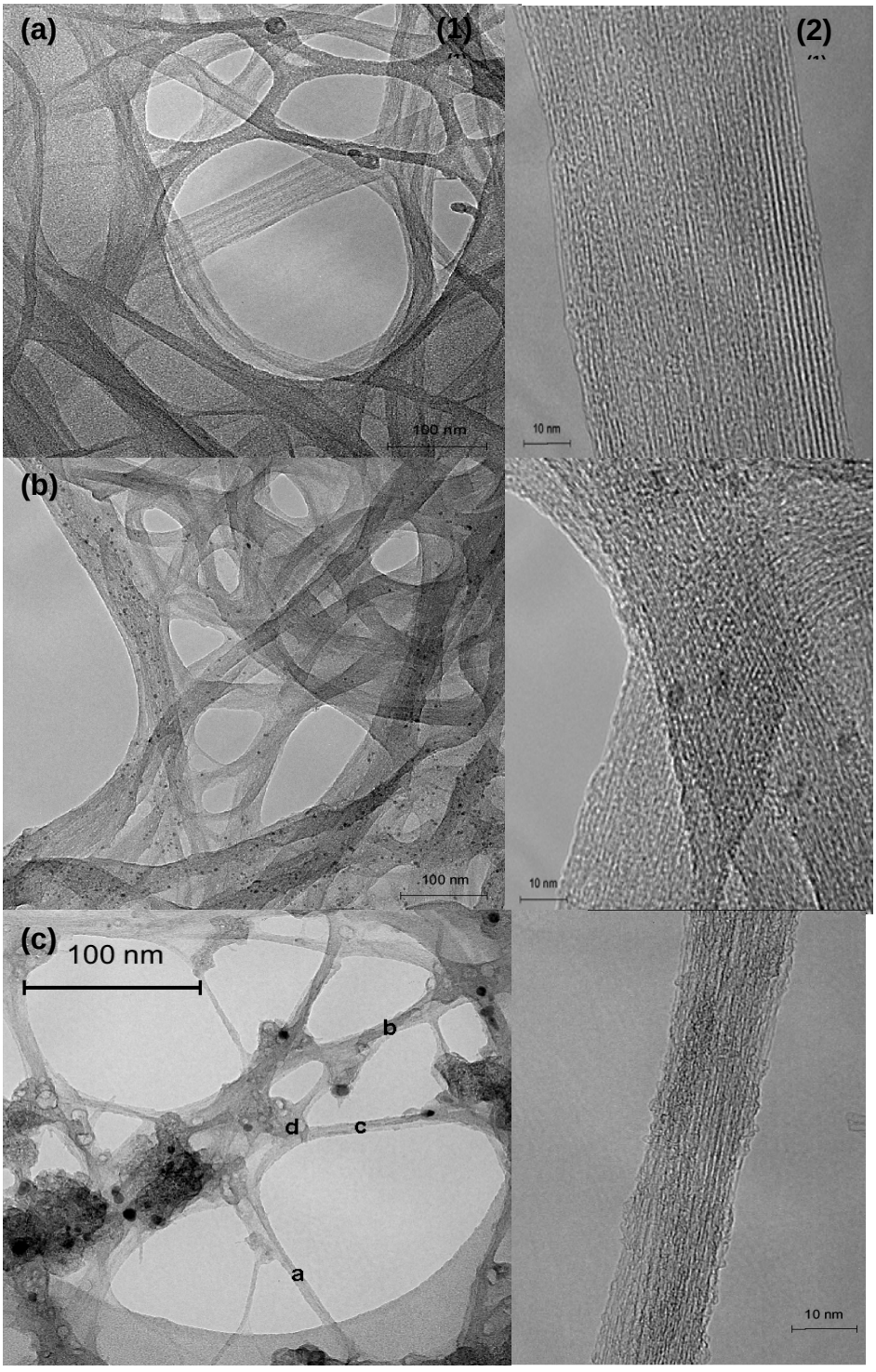

Figure 2.1 TEM image of SWNTs. (a) SWNT1 (EA95) (b) SWNT2 (CVD90), (c) SWNT3 (CS70) and (1) magnification =30,000, (2) magnification=230,000

Table 2.1 provides the summary of the sample characterization data. For SWNTs, the typical micropore volume was found to be only a fraction of the total pore volume (0 to 25%, depending upon the sample). Activated carbons had a slightly higher fraction of microporosity (25% to 40%). Nevertheless, the differences in porosities of SWNTs and activated carbons appeared inclusive to determine if nanocarbons offer special advantages in pore volumes when compared with traditional microporous activated carbons. The effect of heat-treatment on the porosity of SWNT samples and activated carbon samples seemed insignificant; however, the sample SWNT4 exhibited a significant increase in the surface area and micropore volume upon heat-treatment. This sample was known to contain an unusually high concentration of surface functional groups. It is very likely that heat treating this sample unblocked some pores, thus, increasing the amount of adsorption as evident by an enhanced surface area and pore volume for the treated sample.

Table 2.1 Physical characteristics of SWNT samples studied

			Surface area (m^2/g)		Pore volume (cm^3/g)		Pore size [c] (nm)
			Total[a]	Micropore	Total	$C_{\mu N_2}$ [b]	
SWNT	SWNT1 (EA95)	-	507	352	0.57	0.16	1.52
	SWNT2 (CVD90)	-	637	98	1.38	0.05	0.9
	SWNT3 (CS70)	-	631	229	1.06	0.10	1.1
		treated [e]	717	172	1.13	0.09	-
	SWNT4 (CS80)	-	80	1	0.20	0	1.1
		treated [e]	268	182	0.40	0.05	-
AC	AC	-	810	331	0.71	0.18	3.5[d]
	ACF10	-	786	476	0.61	0.24	3.1[d]

[a] Total BET surface area
[b] Micropore volume determined from standard N2 adsorption at 77K
[c] This value is extracted from the Raman Spectra of samples. It is the SWNT size which had the largest radial breathing mode (RBM) peak.[80]
[d] Average pore size determined from standard N_2 adsorption at 77 K
[e] Samples were outgassed at 600 ^oC for 12 h. Other samples were outgassed at 140 ^oC.

2.2.3. Spectral analysis for surface chemistry of SWNTs

2.2.3.1. Raman spectroscopy

The Raman scattering technique is basically a vibrational molecular spectroscopy. When light is interacted with materials, light is scattered with keeping its energy constant (Rayleigh scattering) or with changing its energy (Raman scattering). Light source is monochromatic light from a laser in the visible, near infrared or near ultraviolet range. The amount of energy lost or gained is presented as a change in energy (wavelength) of the irradiating photon. The change in energy is introduced by molecule's polarizability which represents the ability of an applied electric field to induce dipole moment in an atom or molecule. Raman scattering by molecule's polarization is characteristic for a particular bond in the molecule.

Raman spectroscopy is mainly used to characterize electronic structure, the presence of defect and diameter of carbon nanotubes. All carbon structures contribute to the Raman spectra with a four-band feature such as radial breathing mode (RBM) peaks (100~300 cm^{-1}), D –band (~1350 cm^{-1}), G-band (~1582cm^{-1}), and D'-band (~1516cm^{-1}). RBM peaks are used to measure the diameter of carbon nanotubes through the calculation with the following equation. Spectra are presented in Figure 2.2 with the dominant diameter calculated using the equation (2.1)

$$\omega_{RBM} = 12.5 + \frac{223.5}{R(nm)} \tag{2.1}$$

where ω_{RBM} is the RBM frequency, $R(nm)$ is nanotube diameter with the unit of nanometer. Table 2.1 provides a summary of the characterization data.

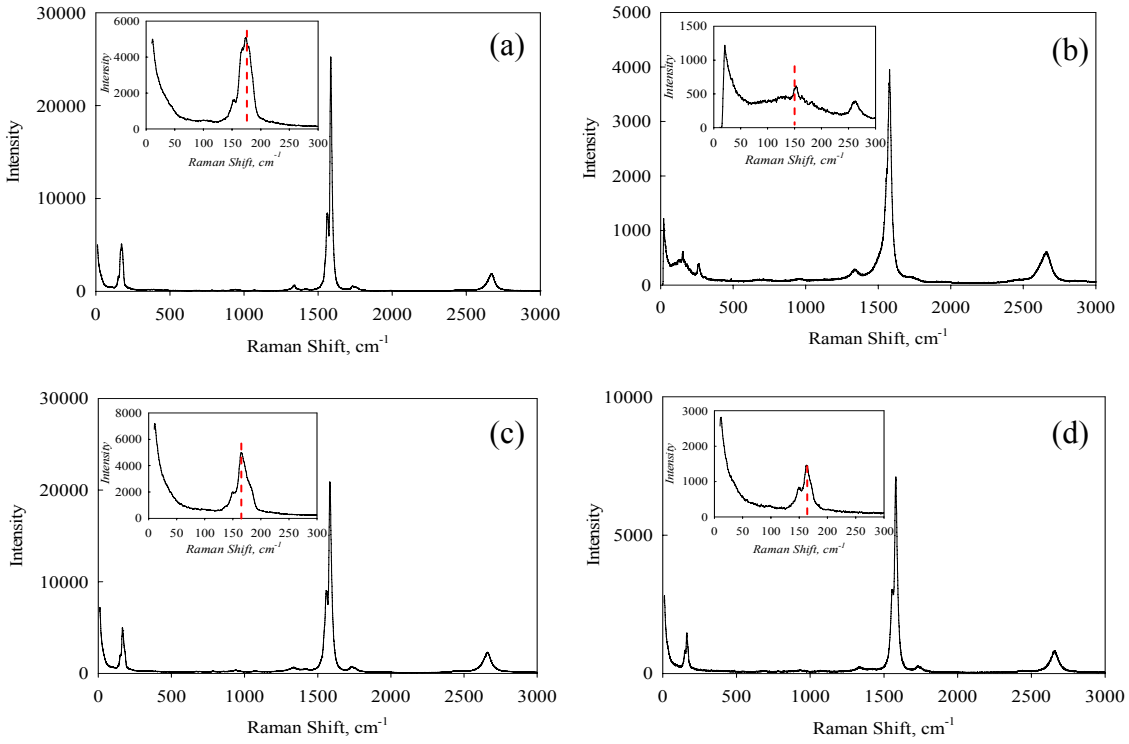

Figure 2.2 Raman spectra of samples (a) SWNT1, (b) SWNT2, (c) SWNT3 and (d) SWNT4 measured at $\lambda_{excitation} = 532$ nm. The inset is the radial breathing mode (RBM) frequency region in the spectra. Experiments were performed on solid samples using T6400 Raman research system by JY Horiba. *R* was calculated by the relation $\omega_{RBM} = 10.0 + 234.0/R(nm)$ which accounts for the slight shift in RBM frequencies due to nanotubes present in bundles as opposed to individually dispersed. *R* presented in Table 2.1 is the one calculated from cm^{-1} highlighted by (- - - -) in the inset.

The D-band is used as a probe of disruption in the hexagonal framework due to the double resonance process which is activated in the first order scattering process of sp^2 carbons. The D-band provides direct evidence of structural disorder such as finite particle size, curvature effects of the grapheme, defects caused by pentagons or hepagons and graphitic or nanoscale carbon particle materials on the tubes. The G-band results from intramolecular vibration between carbon atom and the in-plane stretching of the C-C bonds in grapheme. The G-band is independent of the defect and originated from a single

resonance process. The D'-band is also a double-resonance Raman feature induced by disorder and defects. The intensity of D-band normalized with respect to that of G-band (I_D/I_G) is usually used to estimate the defect concentration in SWNTs.

The trends in surface chemistry as estimated by fitting the water adsorption isotherms were also observed directly from surface analysis by Raman spectroscopy (Figure 2.3.). The spectra were obtained by Nicolet 6700 FT-IR-Raman by Thermo Fisher. The excitation λ is in the near infrared region (λ= 946nm). The instrument is fitted with a liquid N_2 cooled high sensitivity Ge detector. It was operated at a power rating of 0.06 W (less than 5% of maximum power) to minimize sample heating which could be one of the major drawbacks of a non-dispersive Raman technique.

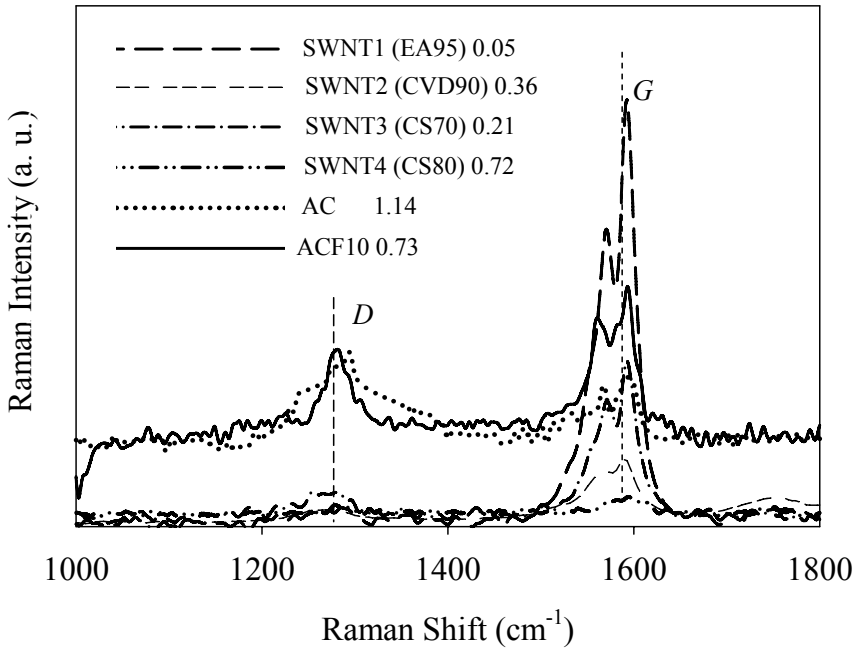

Figure 2.3 Raman spectra of carbon nanotubes and activated carbon samples (λ= 946nm). I_D/I_G ratio is presented in the legend. Shoulder peak at 1550 cm^{-1} is due to resonance from metallic nanotubes. It is not included in the calculated I_D/I_G ratio.

Samples were prepared by grinding approximately 0.05% (w/w) adsorbent in KBr powder. Spectra were collected at 10 different points on the pellet. The spectra were corrected by subtracting spectras of blank pellets. Average of 10 spectra is presented in Figure 5. It is known that for carbon samples the peak originating at approximately 1,350 cm^{-1} Raman shift (D peak) is related to the sp^2-sp^3 covalently bonded C and that at 1,580 cm^{-1} Raman shift (G peak) represents the pristine sp^2-sp^2 graphitic structure. The I_D/I_G intensity ratio is commonly used to estimate the degree of functionalization.

2.2.3.2. X-ray photoelectron spectroscopy (XPS)

The XPS for surface chemical analysis technique, can provide useful information about surface functional groups present in carbon materials. X-ray sources in XPS are generated by bombarding a metallic anode with high-energy electrons (10 to 15 KeV). The anode material determines the characteristic X-ray energy and the width of the X-ray line. The most commonly used materials are Mg and Al with principal photon energies of 1253.6 and 1486.6 eV respectively. The bombardment of the sample with X-ray results in 3 step emission process as following. 1) the electron is promoted from its ground state to the final state above the Fermi level, 2) the electron is transported to the surface and 3) the electron escapes into the vacuum. The kinetic energies of the emitted electrons forming the spectral peaks in Figure 2.4 are measured using an electrostatic charged-particle energy analyzer from which the binding energies of the escaping electrons can be calculated from (Eq. 2.2),

$$E_b = h\upsilon - E_{kin} - W_f \qquad \text{(Eq. 2.2)}$$

where E_b is the binding energy (eV) in the solid, $h\upsilon$ is the energy of the incident photon, E_{kin} is the electron kinetic energy, and W_f is the different in work functions between the sample and detector material assuming there is no electrical charging at the sample surface. The surface specificity of XPS is a result of the fact that the average net distance traveled in a solid by an electron before being scattered, the attenuation length (AL), is very short. The AL is dependent on the electron kinetic energy and the type of materials such as elements, inorganic or organic compounds. The average depth of the photoelectrons released from the surface is about 4nm. Thus XPS is highly surface specific.

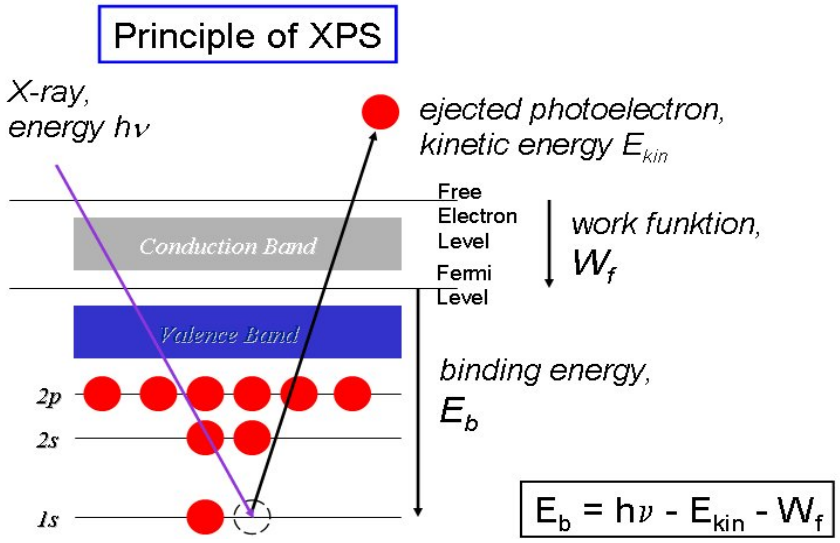

Figure 2.4 Schematic of XPS

The surface chemistry of samples was measured as total atomic surface oxygen (% O) by x-ray photoelectron spectroscopy (Thermo Scientific K-Alpha XPS). The % O peak is typically used to estimate the total concentration of oxygenated functionality.[81] The spectra were recorded using monochromatic Al K-alpha radiation at a pass energy of 25 eV and power of 300W. The base pressure of the analysis chamber was 2 x 10^{-9} mbar and the operating pressure was maintained at approximately 2 x 10^{-7} mBar while the charge compensation (a combination of low energy Ar ions and low energy electrons) system was active. The atomic % O peak was calculated from the areas of oxygen 1s (525-545 eV) peaks using Thermo Scientific's Avantage software (v3.85) (Figure 2.5).

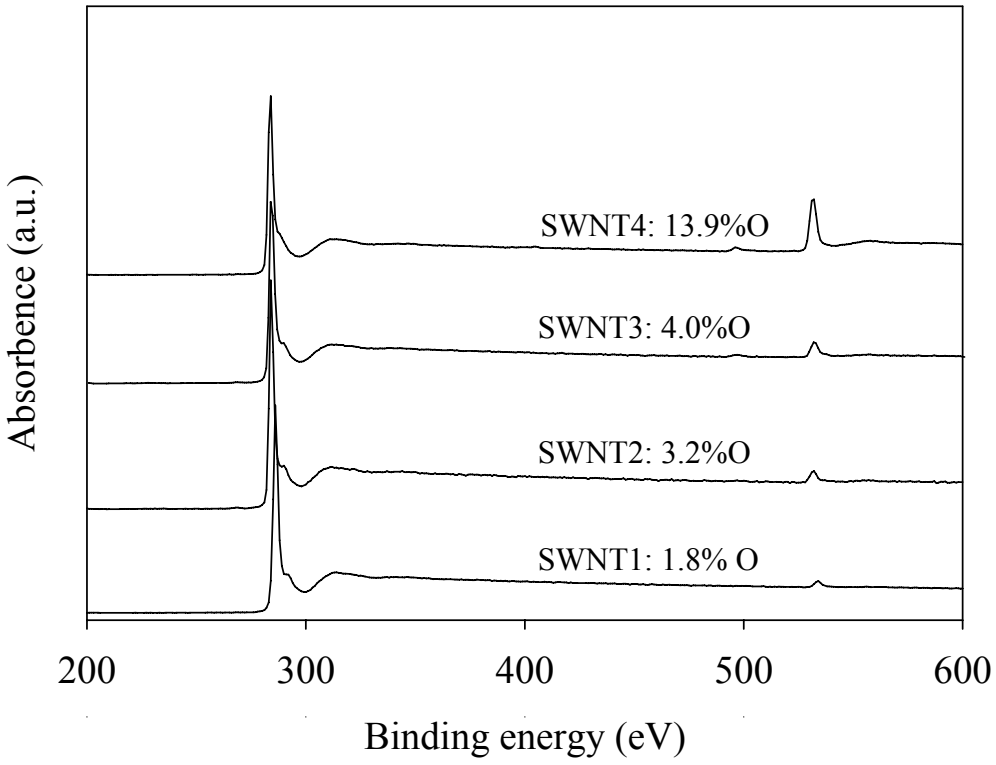

Figure 2.5 XPS survey scans of SWNT samples analyzed in this work. Survey scans for activated carbon samples have not been provided for clarity.

2.3. Experimental gravimetric technique

2.3.1. Gravimetric microbalance system description and operation.

Water vapor adsorption experiments were performed by gravimetric techniques. The experimental setup consists of a high-sensitivity microbalance (Cahn Digital Recording Balance, DRB - 200), customized sampling and gas handling system, and a data acquisition system (Figure 2.6). The microbalance has a detection limit of 0.1 μg. A custom-made 30" long and 3" inner diameter quartz hangdown is fitted to the balance on the sampling side. The sample pan is fashioned from a nickel-chromium wire mesh as opposed to conventional non-permeable sample pans to reduce mass transfer resistance between solid-fluid phases. The sample pan is suspended inside the hangdown tube by a Ni-Cr hangdown wire. The hangdown tube has one inlet gas port at the bottom and several exit ports along the length of the tube with 1" spacing. During experimentation, the carrier gas is allowed to continuously flow out of the exit port into the laboratory fume hood maintained under normal atmospheric pressures. An upper limit of 400 sccm flow rate was determined by trial and error in order to maintain the stability of 3 – 5 mg sample in the sample pan. The experiments are conducted at only 200 sccm total flow rate for additional precaution. For single-component adsorption, such as adsorption of water vapor, only one exit port is utilized and other ports are sealed to minimize losses. The temperature of sample chamber is controlled with an electrical heating tape a variac. The gas generation system consists of ultrahigh purity N_2 (99.999% UHP N_2) as carrier gas. The carrier gas is initially passed through a gas drier/purifier, containing anhydrous $CaSO_4$, to remove any trace gas contaminants. Mass flow controllers are used to control

the gas flow rates. A portion of carrier gas is allowed to purge through double-distilled water in a fritted glass bubbler. This creates a vapor saturated or "wet" stream of carrier gas. The wet gas is mixed with remaining dry carrier gas to generate controlled water vapor concentrations in the carrier gas streams. The concentration of water vapor is monitored by a relative humidity probe (Cole-Parmer Instrument, Digi-Sense) upstream of the sample pan which dictates the flow rates of wet and dry streams. The gas generation system is a manually operated. The electronics of gravimetric balance is similar to that of a thermogravimetric analyzer. The gravimetric balance is coupled with a data acquisition system that gathers mass, time and temperature data every 2 seconds during operation. The schematic of our experimental setup is provided in Figure 2.6.

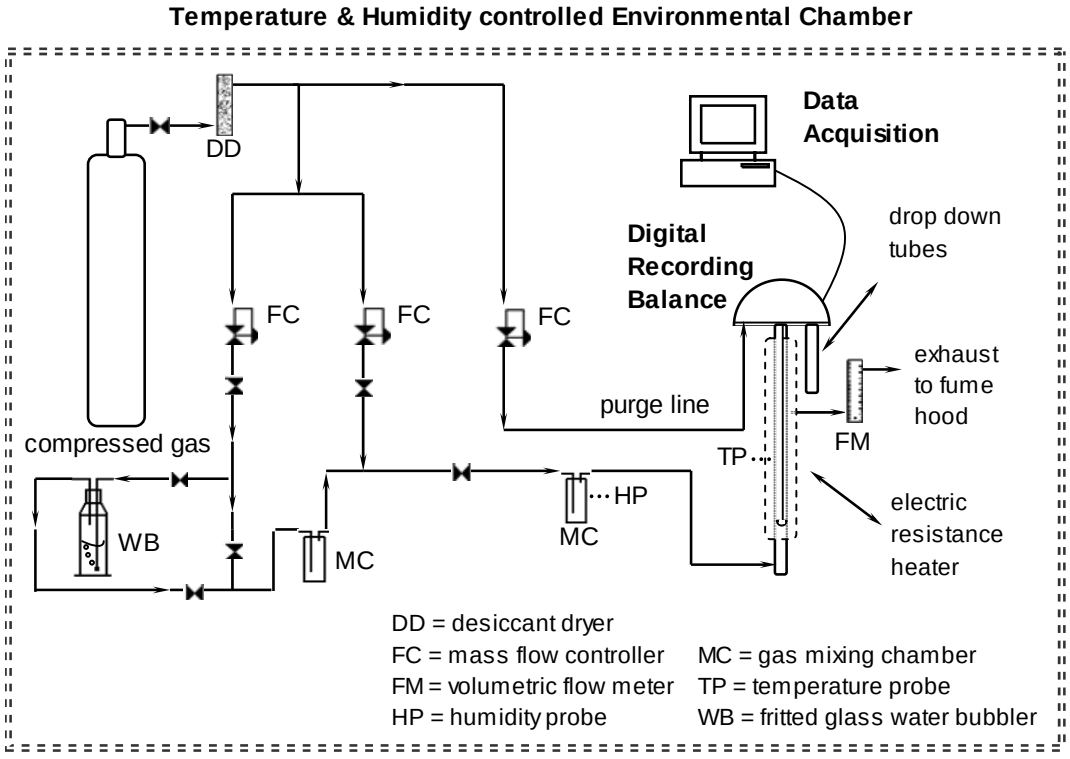

Figure 2.6 Schematic of experimental setup for adsorption of water vapor in carbon nanotubes.

2.3.2. Water adsorption kinetics of gravimetric technique

The entire experimental setup is operated in an 8' x 8' x 8' environmental chamber. The chamber is maintained at 20 ± 0.5 ^{o}C, which is also the balance operating temperature during data collection. It is emphasized that sufficient relative humidity (RH) in the chamber was found to be essential for high sensitivity measurements. The humidity in the chamber was maintained at least 50 ± 1%. We found that low humidity levels caused slight vibrations in the sample hangdown wire, due most likely to buildup of static charge on the micro-balance. This lead to μg level fluctuations in the data collected. Figure 2.7. shows the adsorption kinetics measured at two different humidity conditions in the chamber. The experiments were conducted at isothermal condition of 20 ^{o}C. The characteristic adsorption curve is apparent for the experiment conducted in the presence of higher humidity surrounding the microbalance. Most importantly, data collection with a resolution of 0.1 μg could be observed in the kinetics curve obtained under precisely monitored humidity in the chamber.

Prior to each test, 200 cm^3/min flowrate of UHP-N_2 is established through the experimental setup. The gravimetric balance is then zeroed and calibrated while the carrier gas is allowed to flow through the hangdown tube without the sample. This step is essential to compensate for the buoyancy related corrections that are typically needed after collecting adsorption data. The adsorbate sample (3 – 5 mg) is placed on the sample pan and its initial weight is measured upon reaching equilibrium with the carrier gas. The sample is then heated to 140 ^{o}C in carrier gas for approximately 3 h to desorb any volatile gases and vapors physically adsorbed during storage. The sample is allowed to cool down

to the operating temperature (20 ± 1 ºC). For accuracy, the entire environmental chamber is maintained at the operating temperature for adsorption experiments. The sample weight is measured upon equilibrium, and is reported as the dry weight on the basis of which all adsorption capacities are reported. Desired concentrations of water vapor, measured as relative to the saturation pressure P/P_o where P is actual pressure of water vapor and P_o is the saturation pressure, are created in the carrier gas by adjusting the flow rate through the nanopure water in the fritted glass bubbler and the dry gas stream. The flowrate of water vapor, estimated from the rate of evaporation of water in the bubbler (0.02 to 10 ml/h), is much less than the total gas flow rate to not offset the zero correction of the balance. The vapor laden carrier gas is allowed to flow through the sample. The sample adsorbs some vapor and gains mass until equilibrium is achieved. The sample weight is continuously monitored as a function of time. Adsorption equilibrium is assumed when no increase in sample mass (< 1 μg = 10x detection limit) is observed for a continuous 15 min period. The net gain in sample mass is normalized to its dry weight, and is reported as the adsorption capacity in equilibrium with the concentration of water vapor present in the carrier gas. Upon equilibrium, the vapor concentration is manually increased to obtain another data point in a similar manner. The entire adsorption isotherm is thus obtained point-by-point by progressively increasing the concentration of water vapor and measuring the equilibrium adsorption capacity at each vapor concentration. Desorption isotherm is also obtained in a similar manner by measuring adsorption capacities with a decreasing trend in concentration of water vapor.

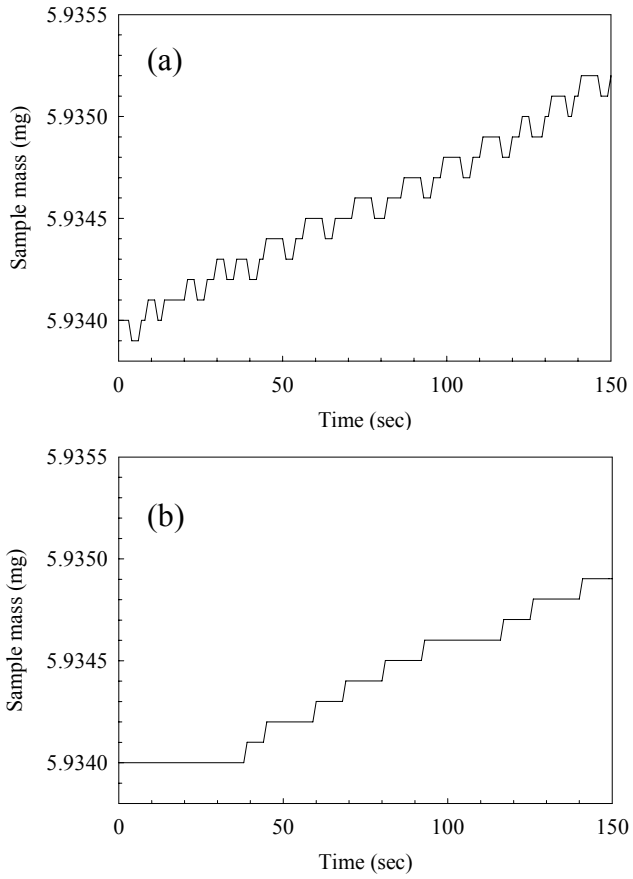

Figure 2.7 Effect of humidity in the air surrounding the microbalance. (a) RH = 40% and (b) RH = 50%. Concentration of water vapor in carrier gas = 0.05 P/P_o. Adsorbent = SWNT sample SWNT1. Temperature = 20 ^oC. P_o = 0.0234 bar.

Figure 2.8 represents a typical experiment in which both, sample mass and water vapor, are monitored as a function of time. It was observed that higher vapor concentrations ($P/P_o > 0.15$) reach the desired constant value much faster than the lower concentrations. Since a constant gas phase concentration is implicit to adsorption, this transient behavior of the water vapor concentration in a step change is taken into account in the analysis of adsorption kinetics presented later in this publication. The kinetic analysis only included that mass vs. time data which was collected when the concentration reached at least 75% of the desired steady state concentration.

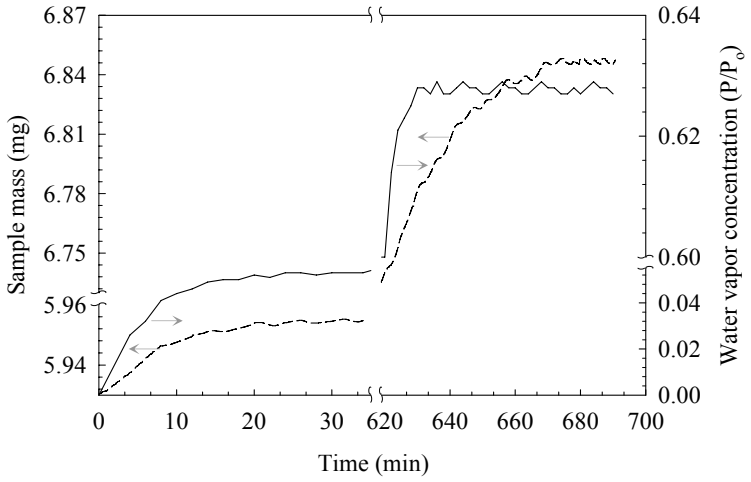

Figure 2.8 Gas-phase concentration of water vapor (——) and sample mass (- - - - -) measured as a function of time in a typical adsorption experiment.

2.4. Existing water isotherm models

The DS equation (Eq.2.3) is one of the simplest models. It assumes adsorption of one water molecule per active site, and is often fitted to the lower part of the isotherm [68]. It is the most commonly used equation to estimate as a fitting parameter the concentration of primary adsorption sites (i.e., hydrophilic functional groups) on the carbon surface.

$$\frac{P}{P_o} = \frac{C_\mu}{c\left(1 - kC_\mu\right)\left(S_o + C_\mu\right)} \tag{2.3}$$

where, C_μ is micropore volume by water, S_o (mmol/g) is the number of primary adsorption sites which increases with the degree of oxidation of a carbon surface (typical $0.05 < S_o < 5$ mmol/g), c (unitless) is a ratio of the desorption rate to the adsorption rate, and k (g/mmol) is a parameter representing the loss of secondary sites upon water adsorption. The parameter k affects the maximum amount of water that can adsorb on a

sample; it does not, however, affect the initial adsorption behavior. The DS equation was selected for data fitting because of a lesser number of parameters to be fitted in the data modeling and the ability of the model to *quantify* the hydrophilic surface chemistry.

The DA equation (Eq. 2.4) is based on the change of Gibbs free energy, $A = RT\,ln(P_o / P)$. It is a common model to describe the adsorption isotherm of gases and vapors. Water adsorption isotherm is usually described by two similar forms of the fundamental DA equation [82]: type I for adsorption on surface functional groups and type V for adsorption in the micropores. Such modified DA equation [70] can be applied to interpret the total water adsorption isotherm.

$$C_\mu = S_o\, exp\left[-\left(\frac{A}{E_{H_2O(I)}}\right)^{n(I)}\right] + C_{\mu S}\, exp\left[-\left(\frac{A}{E_{(H_2O(V)}}\right)^{n(V)}\right] \tag{2.4}$$

where $E_{H_2O(I)}$ and $E_{H_2O(V)}$ (kJ/mol) , respectively, are characteristic energy related to water adsorption on functional groups and in the carbon pores; $C_{\mu s}$ is the maximum adsorption capacity of water (mmol/g); $n_{(I)}$ and $n_{(V)}$ describe the surface heterogeneity (unitless); the definition of other parameters is similar to those in Eq. 2.3. Parameters $E_{H_2O(I)}$, $E_{H_2O(V)}$, $C_{\mu s}$, $n_{(I)}$, $n_{(V)}$ and S_o are fitting parameters.

The CMMS model [72] (Eq. 2.5-1 or 2.5-2) was developed by Malakhov and Volkov [83]. It has been modified by Rutherford [72] to describe the water adsorption isotherm in highly nanoporous carbon adsorbents such as carbon molecular sieves. The CMMS model considers adsorption of one water molecule per functional group followed by adsorption of two water molecules by hydrogen bonding. This configuration forms a

triad of water molecules which then allows secondary interactions to form dimers, trimers, etc. The CMMS model can describe the types IV and V water adsorption characteristics. The CMMS model (Eq. 2.5-1) is used to describe the water adsorption isotherm for samples with high concentration of surface functional groups. It employs the BET type equation to describe the adsorption contributions of the functional groups. The CMMS model (Eq. 2.5-2) uses the Langmuir type equation to describe the adsorption on surface functional groups, and is therefore, applied to samples with less surface oxidation which often exhibit type V adsorption characteristics.

$$C_{\mu} = \frac{S_o b_{BET}\left(\frac{P}{P_o}\right)}{\left(1 - K_{as}\left(\frac{P}{P_o}\right)\right)\left(1 + b_L\left(\frac{P}{P_o}\right)\right)} + \frac{C_{\mu S} K_o \left(\frac{P}{P_o}\right)}{\left(K_o\left(\frac{P}{P_o}\right) + w_{1\,sin\,g}^2\right)} \tag{2.5-1}$$

$$C_{\mu} = \frac{S_o b_L\left(\frac{P}{P_o}\right)}{\left(1 + b_L\left(\frac{P}{P_o}\right)\right)} + \frac{C_{\mu S} K_o \left(\frac{P}{P_o}\right)}{\left(K_o\left(\frac{P}{P_o}\right) + w_{1\,sin\,g}^2\right)} \tag{2.5-2}$$

Where, $$w_{1\,sin\,g} = \frac{1}{2}\left(1 - K_1\left(\frac{P}{P_o}\right) + \sqrt{\left(1 - K_1\left(\frac{P}{P_o}\right)\right)^2 + 4K_o\left(\frac{P}{P_o}\right)}\right) \tag{2.5-3}$$

where K_o and K_1, respectively, are the equilibrium constants representing the interaction of water molecules with the functional group and with the side unit on the functional group respectively; K_{as} is the constant of adsorption of the side associate; b_{BET} and b_L are BET constant (Eq. 2.5-1) and Langmuir affinity constant (Eq. 2.5-2) respectively. Parameters K_o, K_1, K_{as}, b_{BET}, and S_o are fitting parameters for BET type

water adsorption isotherm. Parameters K_o, $K_{1,}$ b_L, and S_o are fitting parameters for Langmuir type water adsorption isotherm.

The Do and Do equation[35] (Eq. 2.6) assumes that water molecules chemically bond with the functional groups located in the mesopores and at the entrance to the micropores. The cluster of water molecules grows to the size of a pentamer (5 molecules, approximate 0.6 nm width) on the functional groups. The pentamers attain sufficient dispersive energy to migrate into the micropores and, thus, fill the micropores. The BET equation is used to describe the adsorption of water on functional groups. The overall water adsorption isotherm is deconvoluted into the two distinct isotherms: adsorption on functional groups and filling of micropores.

$$C_\mu = \underbrace{S_o \frac{K_f \Sigma_{i=1}^{n} i * \left(\frac{P}{p_o}\right)^i}{1 + K_f \Sigma_{i=1}^{n} \left(\frac{P}{p_o}\right)^i}}_{\text{Adsorption on functional groups}} + \underbrace{C_{\mu s} \frac{K_\mu \left(\frac{P}{P_o}\right)^6}{K_\mu \left(\frac{P}{P_o}\right)^6 + \left(\frac{P}{P_o}\right)}}_{\text{Micropore filling}} \qquad (2.6)$$

where the definition of S_o and $C_{\mu s}$ remains unchanged; K_f and K_μ, respectively, are the equilibrium rate constants for the chemisorption of water on functional groups and water filling of micropore (unitless); and n is the average number of molecules in the fully developed water cluster on the surface functional groups.

Several versions derived from the fundamental Do and Do equation have been proposed in the recent years by Lagorsse et al., [73], Zimny et al., [74], and Marban et al., [75]. The Lagorsse et al., version of the Do and Do equation (Eq. 2.7) is similar to the original

Do and Do equation with a minor alteration that the clusters of water molecules adsorbed in the micropores composed of 7 molecules as opposed to 5 molecules [73] . The model was applied to an extremely microporous activated carbon such as carbon molecular sieves.

$$C_{\mu} = S_o \frac{\sum_{n=1}^{7} n\left(K_f \times \frac{P}{P_o}\right)^n}{1+\sum_{n=1}^{7}\left(K_f \times \frac{P}{P_o}\right)^n} + \frac{K_{\mu}\left(K_f \times \frac{P}{P_o}\right)^7}{1+K_{\mu}\left(K_f \times \frac{P}{P_o}\right)^7}\left(C_{\mu s} - S_o \frac{\sum_{n=1}^{7} n\left(K_f \times \frac{P}{P_o}\right)^n}{1+\sum_{n=1}^{7}\left(K_f \times \frac{P}{P_o}\right)^n}\right) \tag{2.7}$$

where the definition of S_o, $C_{\mu s}$, K_f , K_{μ} and *n* remains unchanged.

The Zimny's et al., version (Eq. 2.8) replaced the BET type equation with a Langmuir type equation to describe the water adsorption from functional groups; although no rational explanation was provided for this alteration [74]. Also, they introduced a new fitting parameter, *m*, speculating the variability in the cluster size entering the micropores, and omitted the fitting parameter *n* that described the variability in cluster size forming on the functional groups. The total number of fitting parameters remained unchanged. This model is also expected to have limited application to extremely hydrophobic microporous carbon adsorbents.

$$C_{\mu} = S_o \frac{b_L\left(\frac{P}{P_o}\right)}{1+b_L\left(\frac{P}{P_o}\right)} + C_{\mu s}\frac{K_{\mu}\left(\frac{P}{P_o}\right)^m}{K_{\mu}\left(\frac{P}{P_o}\right)^m + \left(\frac{P}{P_o}\right)} \tag{2.8}$$

where the definition of S_o, $C_{\mu s}$, K_{μ} remains unchanged with the parameters of Do and Do equation, b_L is Langmuir affinity constant, and *m* is the number of water molecules forming the clusters migrating into the micropores.

The Marban et al., version of the Do and Do equation (Eq. 2.9) is also called a cluster formation induced micropore filling (CIMF) isotherm model [75]. The CIMF model is similar to the original equation; however, this model assumed a variable size for the water cluster adsorbed in the micropores. This introduces a new fitting parameter, *m*, in the equation in addition to the parameter, *n*. This parameter was introduced upon the assumption that the cluster size will not always be fixed to a pentamer [35] or a heptamer [73] but it would depend upon the concentration of the functional groups and the pore width.

$$C_{\mu} = S_O \frac{K_f \sum_{i=1}^{n} i * \left(\frac{P}{P_O}\right)^i}{1 + K_f \sum_{i=1}^{n} \left(\frac{P}{P_O}\right)^i} + C_{\mu s} \frac{K_{\mu} \left(\frac{P}{P_O}\right)^{m+1}}{K_{\mu} \left(\frac{P}{P_O}\right)^{m+1} + \left(\frac{P}{P_O}\right)} \qquad (2.9)$$

where the definition of S_o, $C_{\mu s}$, K_f, K_{μ} and *n* remains unchanged and *m* is the cluster size adsorbing into the micropores (unitless, n > m).

2.5. Kinetics of Water Adsorption.

Adsorption kinetics is most useful in designing and assessing adsorbent beds. The chemical potential driving force (CPDF) model is the most rigorous formulation to describe adsorbate mass transport inside an adsorbent particle. It simplifies to the Fickian diffusion (FD) model.[30, 84] The FD model is fundamentally adequate to describe pure gas adsorption kinetics. It considers integration of two parameters within and above Henry's law region: a constant diffusivity of pure gas in the Henry's law region and a function of the adsorbate loading.[85] However, the FD model requires large computational times for the process simulation under realistic conditions.[86] While the CPDF or FD models of gas

transport in adsorbent particles provide a more realistic mechanism, the linear driving force (LDF) model (Eq. 2.10)[87] is frequently used to describe the adsorption kinetics of water vapor, nitrogen, oxygen and carbon dioxide on heterogeneous adsorbents such as activated carbons and molecular sieves.[74, 88-90] The LDF approach is more practical than the FD model as the characteristics of adsorption kinetics of a single pore are essentially lost when evaluating the overall uptake on a heterogeneous porous solid. Since SWNTs are heterogeneous adsorbents, it is obvious to apply this model to the kinetics data obtained from high-sensitivity adsorption measurements.

$$\frac{M_t}{M_e} = 1 - e^{-kt} \tag{2.10}$$

where M_t is the mass uptake in time t, M_e is the equilibrium uptake for the given pressure increment, and k is the rate constant.

3 Results and discussion

3.1. Adsorption equilibrium and kinetics of water vapor in carbon nanotubes and its comparison with activated carbon

3.1.1. Water Adsorption Isotherms

Isotherms of water vapor adsorption and desorption on carbon nanotube and activated carbon samples were measured at P/P_o between 0 and 0.94 (Figure 3.1.). Sample SWNT1 showed a slow and an almost insignificant rise in the adsorption capacity until 0.4 P/P_o, a sharp increase between 0.4 and 0.6 P/P_o, followed by a slow rise in adsorption capacity from 0.6 to 0.94 P/P_o. Therefore, majority of water vapor uptake by this sample would take place in the 40% to 60% relative humidity range (relative humidity = 100 x P/P_o). The activated carbon sample ACF10 exhibited a similar isotherm characteristic with a slow increase until 0.3 P/P_o, a shape increase between 0.3 and 0.6 P/P_o followed by only a marginal increase in adsorption. This adsorption isotherm is a type V characteristic, which is typical for water adsorption on microporous carbon adsorbents. Samples SWNT2, SWNT3 and AC also exhibited type V characteristics. However, sample SWNT4 showed an abrupt increase at the initial low relative pressure ($P/P_o < 0.05$) and a monotonous increase in adsorption capacity up to 0.94 P/P_o with no apparent sharp uptake of water. This is either a type IV or type V characteristics. The morphology of nanotubes in this sample is similar to that of sample SWNT3. It has been reported that functional groups affect the relative pressure value at which the adsorption on secondary sites becomes appreciable.[67, 91, 92] Therefore, the ambiguity of the adsorption type for sample SWNT4 is most likely due to a much higher

concentration of functional groups that would shift the isotherm rise to a lower P/P_o and change the isotherm characteristics to that of an increasingly steeper type IV isotherm.[70]

Desorption equilibrium of water exhibited slightly higher capacities for all test samples which resulted in a perceptible hysteresis (Figure 3.1.). Extensive studies of water and carbon adsorption-desorption interactions has suggested at least two factors: surface oxides and pore dimensions. The accepted explanation[93] for activated carbons is that smaller pores constrict the opening to wider pores such that desorption is not observed until the vapor pressure is reduced to that corresponding to the smaller pore size. However, this only explains the hysteresis in sample AC. The lack of hysteresis in ACF10 is most likely due to a uniform pore size which was observed from pore size distribution estimated by standard N_2 adsorption at 77 K. Similar explanation, however, can not be extended to carbon nanotubes as small size nanotubes constricting opening to large nanotubes is an unlikely sample geometry. However, the trends are consistent with the hysteresis loops observed for simulated water adsorption isotherms in carbon nanopores.[6] It has been proposed that water molecules clustering around hydrophilic functional groups induce a continuous adsorbed phase at lower relative pressures.[94] When the pore size decreases, the water molecule-pore interaction potential increases at lower relative pressure in a way such that the conditions of hysteresis arise at lower water vapor concentrations.[91]

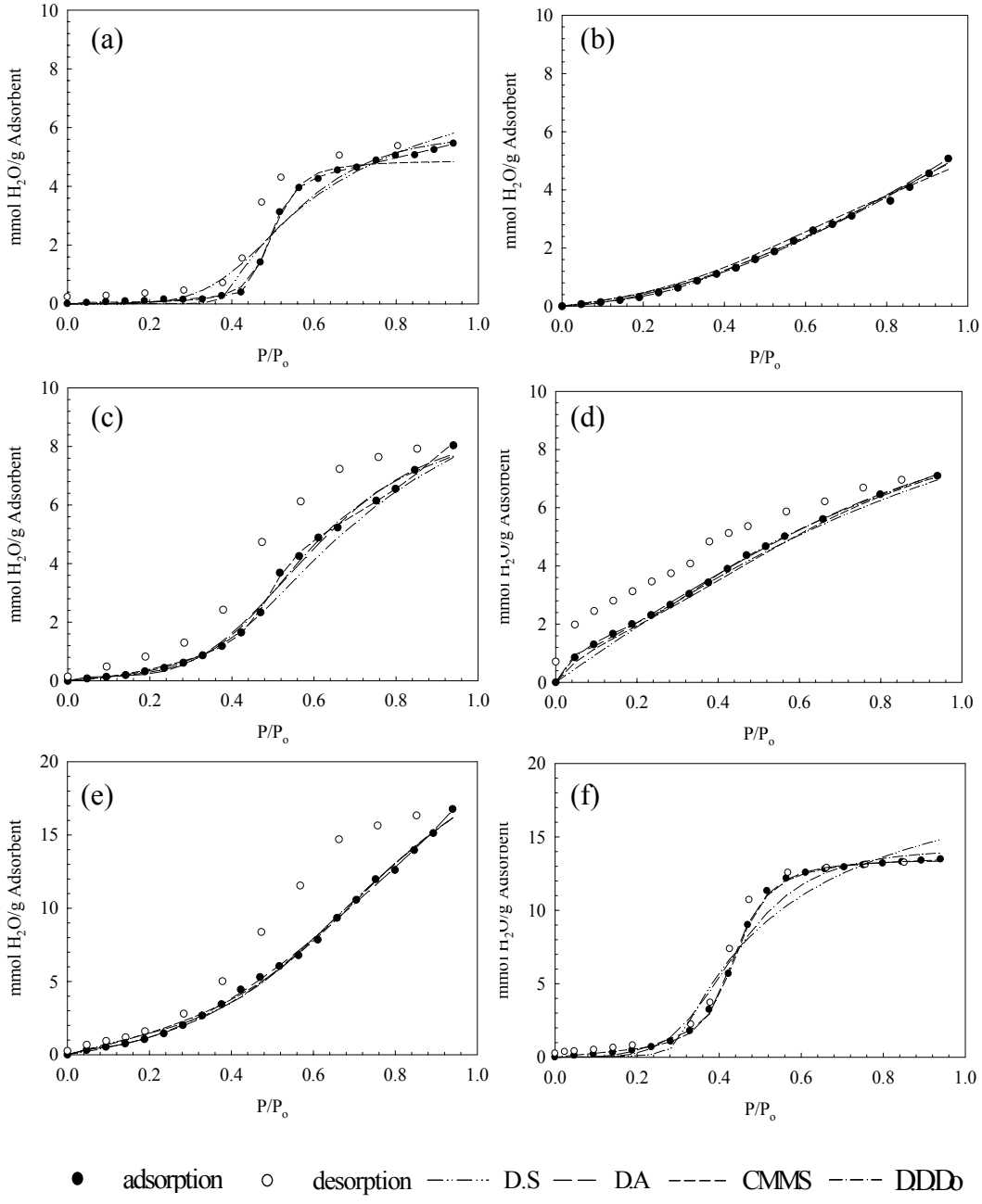

Figure 3.1 Water vapor adsorption isotherms and fits to common isotherm models for carbon nanotube samples (a) SWNT1, (b) SWNT2, (c) SWNT3, (d) SWNT4, and activated carbon (e) AC and (f) ACF10.

3.1.2 Kinetics of Water Adsorption

The LDF model was applied to the kinetics of water uptake at all equilibrium data points. As a representation of the data fitting, Figure 3.2 compares the experimentally measured mass versus time data with that calculated by the LDF model for both adsorption and desorption. A near perfect fit to the experimental data is observed in all cases. It should also be noted that the experimental data presented here is complementary to that presented in Figure 2.5 where the relevance of high-sensitivity kinetic measurements with 0.1 μg precision is apparent. The adsorption kinetics in Figure 3.2.a shows that the LDF model is applicable to the data with approximately 95% accuracy and the prediction of sample mass within ± 0.0032 mg of experimental data. It is to be noticed that in this adsorption step, sample CS70 adsorbed only 0.003 mg of total water, which could also be modeled to the LDF equation with accuracy greater than 95% and prediction of sample mass within 0.0004 mg. Desorption kinetics in Figure 3.2.b also showed applicability to the LDF model with 95% accuracy and prediction of water uptake within ± 0.0035 mg.

The rate constants, k, were calculated as a function of P/P_o by the LDF model for adsorption and desorption (Figure 3.3.). It should be noted that all values of k presented here were determined from fitting the LDF model to the mass vs. time data collected after the gas phase concentration had reached 75% of the desired value in an adsorption step. This correction was needed because the mass change in the initial time period of a step change reflects a gas-phase concentration in transition as opposed to a constant value. The effect of such a correction on k values was negligible. For example, the k value for

sample SWNT3 calculated using the mass vs. time data for the entire adsorption step of P/P_o = 0.05 to 0.1 was found to be 2.60 x 10^{-3} s^{-1}. The same value for the truncated date set was 2.67 x 10^{-3} s^{-1} which shows that the effect of a transient vapor concentration on k values is minimal; however, it should be noted that larger step changes will result in more deviant values which is also why the increments in P/P_o were kept as small as 0.05 in the isotherm measurements.

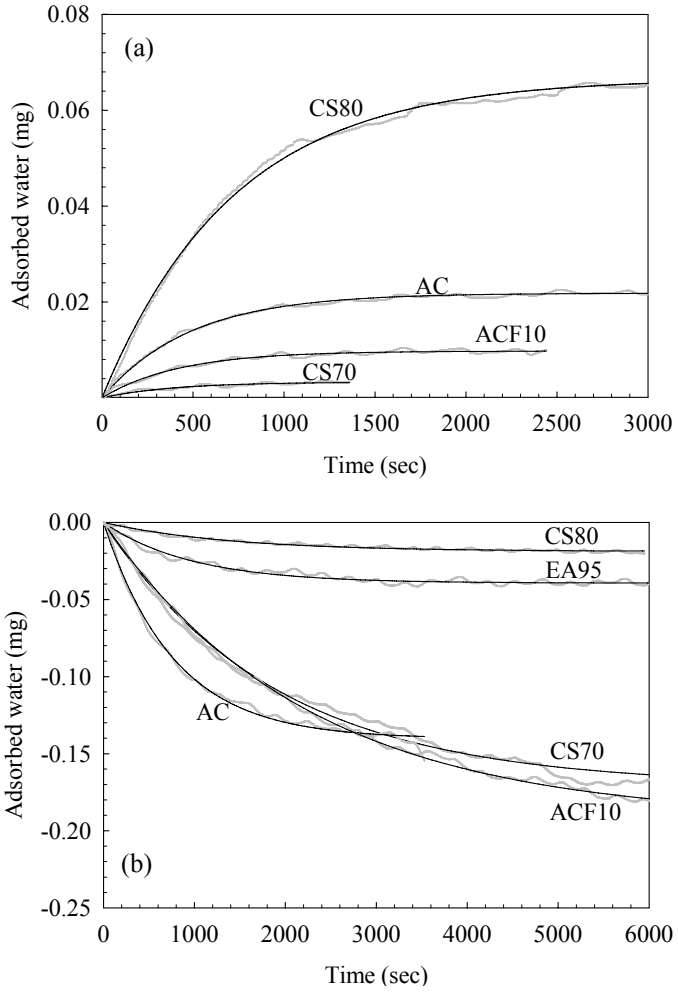

Figure 3.2 Kinetics of water adsorption at P/P_o = 0.05 (a) and desorption from P/P_o = 0.6 to 0.5 (b). The experimental data is presented as grey lines. The smooth line represents the fit to the LDF equation.

Sample SWNT1 showed no kinetic rate constant values up to 0.4 P/P_o due to little to no uptake of water, followed by sharply increasing rate constants up to 0.6 P/P_o most likely due to capillary condensation and then decreased up to 0.94 P/P_o due to pore filling. Sample SWNT3 showed a high rate constant at the initial P/P_o followed by a steady decrease up to 0.5 P/P_o. This trend is similar to that of samples AC and ACF10. It has been suggested that the rate constants decrease with increasing surface coverage by water molecules,[95, 96] which shows a similarity between water kinetics in nanotubes and that in activated carbons. The rate constant of SWNT3 steeply increased until 0.6 P/P_o followed by a steady decrease, much like in sample SWNT1 and ACF10. On the contrary, the kinetic rate constant of sample AC at P/P_o = 0.6 decreases which may imply that the higher concentration of functional groups is associated with the blocking or resistance of entering water clusters into micropore.[29, 92] Sample SWNT4 showed a higher kinetic rate constant at the initial P/P_o and fluctuating values without discernible peaks. It is very likely due to an extremely hydrophilic surface such that the distinction between near saturation of primary sites and initiation of capillary condensation are essentially lost by high concentration of functional groups. The general trends in adsorption rate constants were much smoother in sample ACF10 with clear distinction of two peaks representing, respectively, the adsorption on primary sites and capillary condensation. It could be noticed that these peaks occurred at P/P_o values same as those at which the points of inflexion occurred in the adsorption isotherms. This indicates that of all samples tested here, ACF10 is relatively a more homogenous adsorbent than carbon nanotubes. The more random dependence of k on P/P_o for carbon nanotubes might be attributed to the impurities in nanotube samples. We expect the contributions of impurities to be lumped into the data provided here. Our experimental technique is not capable of differentiating

water adsorption on nanotubes from that on impurities in nanotube samples; however, we guesstimate that the adsorptive contributions of impurities might be separated by modeling impurities as non-porous carbon, the water adsorption characteristics of which will obviously be much different from those of porous carbons.

The desorption rate constants profiles for samples SWNT1, SWNT3 and AC showed trends mirrored to the adsorption kinetic profile, such that increasing desorption rate constants were observed in the same P/P_o range in which decreasing trends were observed for adsorption rates constants. This is most likely due to the hysteresis between water adsorption and desorption curves.[44] Sample ACF10 showed similar trends between adsorption and desorption kinetic profiles. It is the only sample where the hysteresis was insignificant. This characteristics is similar to that observed in the carbon molecular sieves consisting of uniformed pore size distribution,[48] and further indicates the high degree of homogeneity of the adsorbent surface. In general, the desorption rate constant for all test samples at the lowest $P/P_o = 0$ were considerably lower than the adsorption rate constants. This is due to the fact that the strong interaction between water and the pore walls in the smallest micropores limits diffusion. Additionally, it may be more difficult to break hydrogen bonding between water molecules and functional groups.[89, 95, 97] In other words, water molecules adsorb more easily than they desorb. The general adsorption and desorption rate constants of carbon nanotubes under pure carrier gas ($P/P_o = 0$) were not much different from those for activated carbons, which indicates a similarity in water desorption characteristics regardless of differences in pore geometries. It is to be noted that these k values and its trends with respect to P/P_o are similar to those reported in the activated carbon literature.[98]

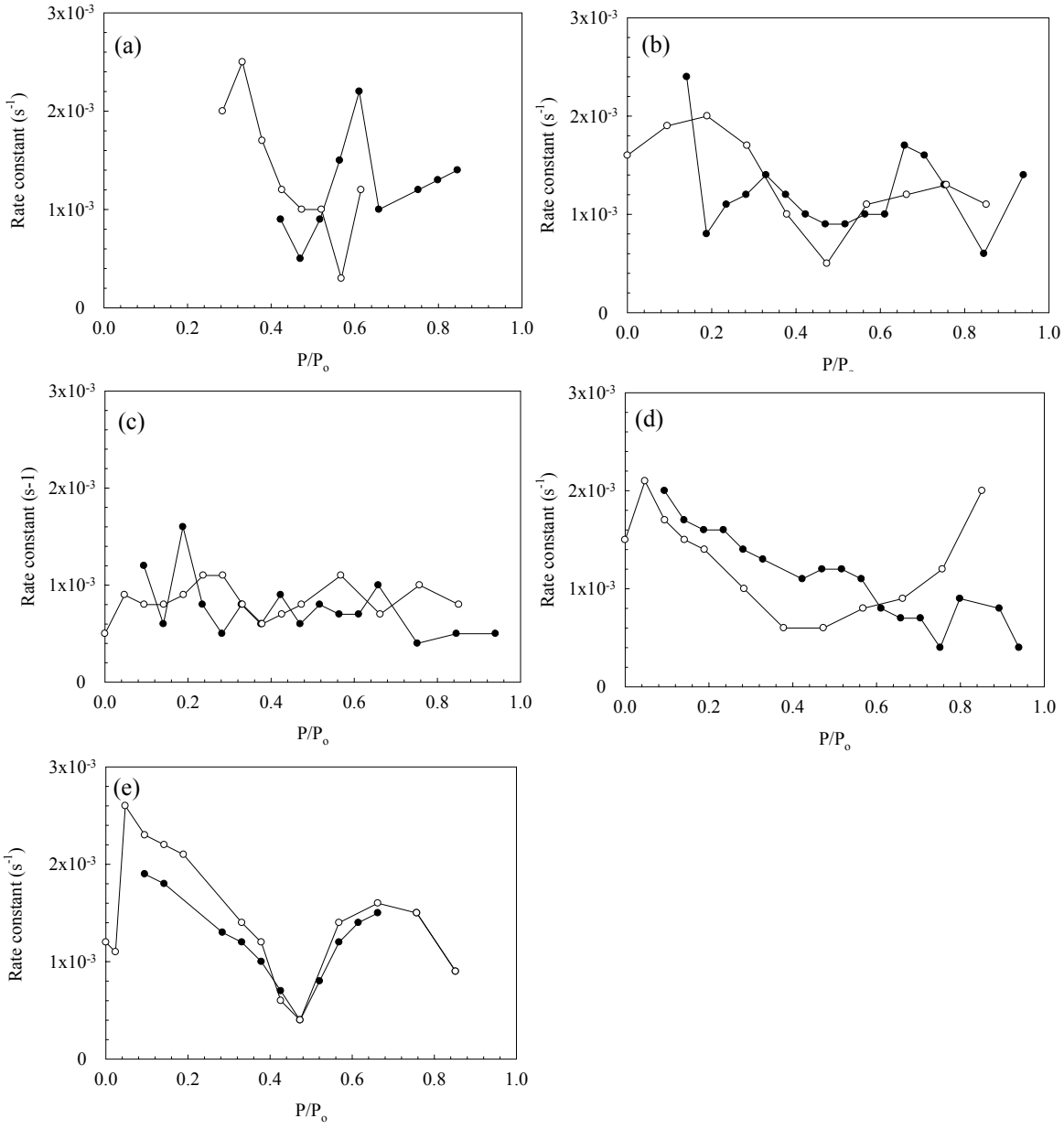

Figure 3.3 Rate constants, k, of water adsorption (●) and desorption (○) calculated from the LDF model fitted to the adsorption kinetics at 20 intermediate points from 0 to 0.94 P/P_o. Sample (a) SWNT1 (EA95) (b) SWNT3 (CS70), (c) SWNT4 (CS80), (d) AC and (e) ACF.

3.1.3. Summary

An experimental set up is developed that allows real-time measurement of water vapor adsorption kinetics with a resolution of 0.1 μg. Adsorption equilibrium and kinetics of water vapor were measured gravimetrically on several commercially available carbon nanotubes and activated carbon samples. Water adsorption in SWNTs followed typical type V adsorption isotherms. The kinetics data was fitted to the linear-driving force model. It is emphasized that the application of the LDF. We found that water adsorption characteristics of nanotubes are similar to that of activated carbons. Precise measurement of water adsorption on small sample sizes, as reported here, is attractive due to the availability of novel adsorbent materials in limited quantities. Additionally, due to the employment of high-sensitivity analytical techniques this study can provide insightful examination on the realism of the methodology and inter-molecular potentials commonly used in molecular modeling water and nanotubes, which is the most common tool for studying adsorption of water in nanocarbons.

3.2 Application of water adsorption models in activated carbon to that in single walled carbon nanotubes

3.2.1 Water adsorption isotherms and Modeling

Data fitting as a tool is used to extract meaningful fundamental information about the behavior of water adsorbed in carbon nanopores from experimental data alone. Data fitting to understand water-nanotube interactions is performed, in particular, to predict the

water adsorption on functional groups and in the micropores from several water adsorption isotherm models present in the literature, such as the D.S. equation, the D.A. equation, the CMMS model and the Do and Do equation. We used the curve fitting toolbox provided in Matlab (version 7.0), of which non-linear least square optimizer was used to determine the values of model parameters. The Trust Region algorithm was employed as an iterative procedure for nonlinear curve fitting under the boundary condition of non-negative values of zero or higher for all fitting parameters. All adsorption isotherms were fitted to all water adsorption isotherm models.

The fit to the experimental data is also presented in Figure 3.1. as continuous lines. The fitting parameters for each sample are provided in the Supplementary Information. The criteria to identify the most applicable model were high correlation coefficient ($R^2 >$ 0.995) between experimental and fitted isotherm, and the relevance of the fitting parameters S_o and $C_{\mu s}$ as determined by other empirical methods. These parameters are common to all models, and of all parameters these are the only fitting parameters that can be related to the physical properties of a sample relatively easily. Here, the trends in the values of S_o and $C_{\mu s}$, respectively, are compared with the sample characterization results from Raman scattering and standard N_2 adsorption at 77 K. It is known that the Raman spectra of a carbon sample exhibits peaks at approximately 1,350 cm^{-1} Raman shift (D peak) and 1,580 cm^{-1} Raman shift (G peak). The intensity ratio I_D/I_G is commonly used for a qualitative estimate of the total degree of functionalization and, in principle, should be extendable to the hydrophilic component of total surface chemistry. Therefore, if one were to follow the trends in the I_D/I_G ratio then those trends should also exist in the values

of S_o. Briefly the experiments were performed with a Fourier Transform (FT) Raman equipment ($\lambda_{excitation}$ = 946 nm), and the S_o calculated from the D.S. equation was found related to the I_D/I_G intensity ratio in spectra regardless of the sample. Here we are extending this comparison to all models tested. The other fitting parameter, $C_{\mu s}$, is the micropore volume from fitting various models to the water adsorption data. In principle, this value should be relatable to the micropore volume by standard N_2 adsorption (77 K) technique ($C_{\mu N_2}$); furthermore, the former should be less than the latter because water does not fill the micropores as completely as N_2 [91].

All models fitted very well with most SWNT and activated carbon samples with $R^2 \geq 0.995$. This compatibility is apparent in Figure 3.1 where a near perfect overlap between the experimental isotherms and the fitted isotherms can be observed for these samples. However, only the D.S equation and the Do and Do equation were found to be not as compatible as other equations to sample SWNT1 and the activated carbon sample ACF10 (Figure 3.1.). The adsorption data and the curve fitting for samples SWNT1 and ACF10 showed $R^2 \approx 0.97$ for the Do and Do equation and $R^2 \approx 0.9$ for the D.S equation. In general, the D.S equation is used to describe only the initial region of an isotherm ($0 < P/P_o < 0.3$) [35]. Therefore, it is suggested that the D.S equation may not be the most suitable model for a detailed evaluation of water adsorption in microporous carbon adsorbents.

The S_o values calculated from all models were compared to the I_D/I_G ratio obtained from the Raman spectra of the samples (Figure 3.4.a, λ = 946 nm). It was observed that the sample-to-sample trends in the S_o values did follow those in the I_D/I_G

ratio; thus, corroborating the credibility of the fitting methodology and supporting our hypothesis that the trends in S_o values should be tractable from those in the surface chemistry as measured by the I_D/I_G ratio in a sample's Raman spectra. However, the S_o calculated from the CMMS theory did not follow trends closely; especially for samples SWNT4, AC and ACF10. Furthermore, the absolute values of S_o calculated from the DA equation were abnormally high compared to those calculated from all other models for any given sample. Therefore, based upon the criteria of *quantification* of hydrophilic surface chemistry (i.e, S_o values) D.S and Do and Do equations appeared most appropriate to both SWNTs and activated carbons.

The comparison of water micropore volume, $C_{\mu s}$, with the N_2 adsorption (77 K) micropore volume suggested that the CMMS theory and the D.A equation did not follow the applicability criteria of $C_{\mu s} < C_{\mu N_2}$) (Figure 3.4.b) This criterion was only fulfilled by the $C_{\mu s}$ calculated from the Do and Do equation which also followed the sample-to-sample trends when compared with the corresponding $C_{\mu N_2}$ values. It was also noticed that for sample SWNT4 $C_{\mu s} > C_{\mu N_2}$ irrespective of the isotherm model. This is because this sample has a very high concentration of surface functional groups which would block the pores for an electrically neutral N_2 molecule but allow polar H_2O molecules to grow into clusters and migrate into the internal volume of the pores.

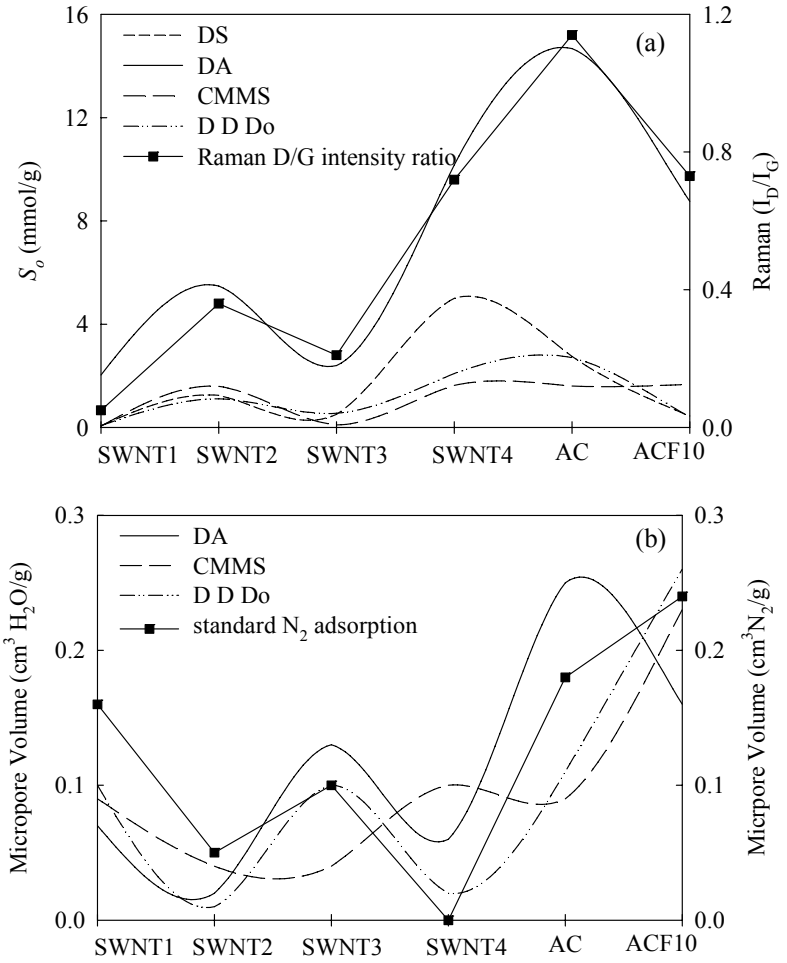

Figure 3.4 (a) Trends in surface chemistry estimated from water adsorption as fitting parameter, S_o, and experimentally determined from Raman scattering of samples. (b) Trends in micropore volume calculated from water adsorption as fitting parameter, $C_{\mu s}$, and experimentally determined from standard N_2 adsorption at 77 K, $C_{\mu N_2}$. This parameter is not calculated from DS equation. Notice the $C_{\mu s}$ for sample SWNT4 were larger than N_2 micropore volume due most likely to an excessive concentration of hydrophilic functional groups.

Based upon the above discussion, the Do and Do equation was found to be successfully fulfilling all criteria for a water-activated carbon isotherm model to be applicable to the water-SWNT isotherms. Furthermore, this equation is also able to deconvolute an extremely hydrophilic type IV or an extremely hydrophobic type V water isotherm into two fractions: adsorption on the functional groups and that in the micropores. Additionally, this is the only equation which can predict as fitting parameters the average number of water molecules forming clusters around the functional groups (parameter *n*) and the critical size of a cluster penetrating into the micropores. In the present form, the size of a three-dimensional water cluster entering the pores is restricted to five molecules which relates to a 0.6 nm wide cluster. Recently, using molecular simulations to study water adsorption inside hydrophobic nanopores, Kaneko and co-workers reported the growth of water clusters to a critical size of 0.6 nm [99] which is remarkably similar to the cluster size used in this equation.

3.2.2. Comparison of several versions of the Do and Do equation

The Do and Do equation satisfactorily fitted the experimental data of all SWNT samples and AC samples with $R^2 > 0.997$ (Figure 3.1.). However, for extremely hydrophobic samples, i.e., samples SWNT1 and ACF10, the R^2 values were approximately 0.97 (Fig. 3.1.). Although, these correlation coefficients are sufficiently high, it still indicates that this equation may not be most suitable for extremely hydrophobic microporous carbons, which has also been suggested by other researchers [100].

The three versions of the Do and Do equation were fitted to the water adsorption isotherm data of all samples (Figure 3.5). The applicability of these models was evaluated by the same criteria of goodness of fit ($R^2 > 0.99$), relevance of the fitted S_o values to the measured I_D/I_G ratio in the Raman spectra of any given sample, and the comparison of micropore volume by water adsorption to that by N_2 adsorption, i.e., $C_{\mu s} < C_{\mu N_2}$.

The Lagorsse's version of the Do and Do equation was found to be less compatible with the extremely hydrophobic sample SWNT1 and the extremely hydrophilic sample SWNT4 with $R^2 < 0.95$; otherwise this equation fitted well with other samples with $R^2 \geq 0.99$. The Zimny's version was also found to fit all samples with $R^2 \geq 0.99$ except for the activated carbon sample AC. However, only the CIMF model exhibited $R^2 \geq 0.995$ between the experimental and fitted isotherm for all samples regardless of nanotubes or activated carbons. This observation indicated that the critical size of water clusters entering into the micropore (i.e., parameter m) is an important variable which had been kept fixed in equations other than the CIMF model.

The comparison of S_o values with the I_D/I_G ratio of the respective samples clearly indicated that the Lagorsse's version and the CIMF model were more compatible than the Zimny's version (Figure 3.6a). Furthermore, since it was known that the sample SWNT4 was extremely hydrophilic, it is obvious that the S_o values of this sample should be greater that those of other SWNT samples irrespective of the isotherm model used in its calculation. This secondary criterion was fulfilled by all isotherm models reported in Figure 3.1.

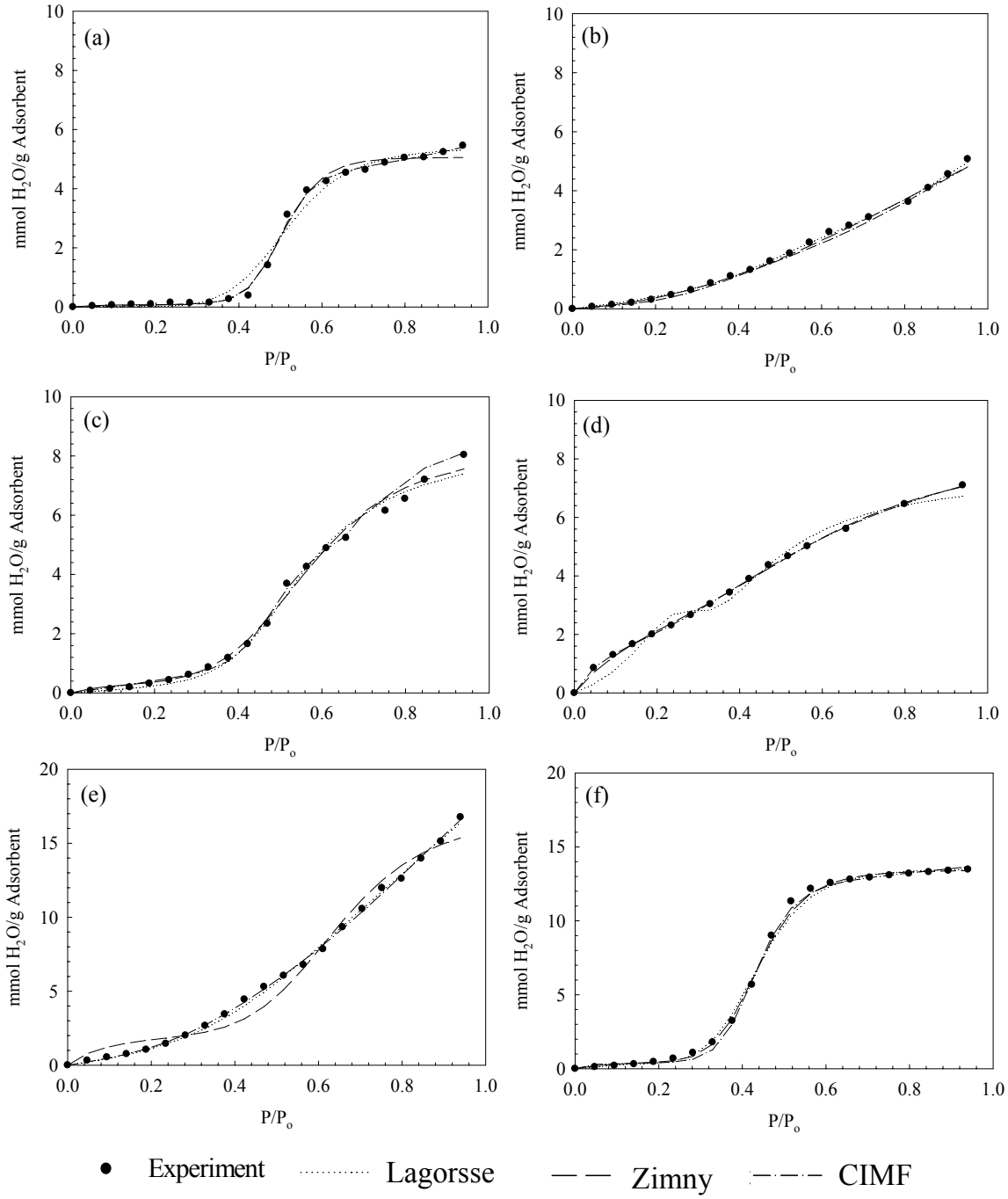

Figure 3.5 Water vapor adsorption isotherms and fits to Lagorsse et.al. equation, Zimny et. al. equation, and CIMF model for carbon nanotube samples (a) SWNT1, (b) SWNT2, (c) SWNT3, (d) SWNT4, and activated carbon (e) AC and (f) ACF10.

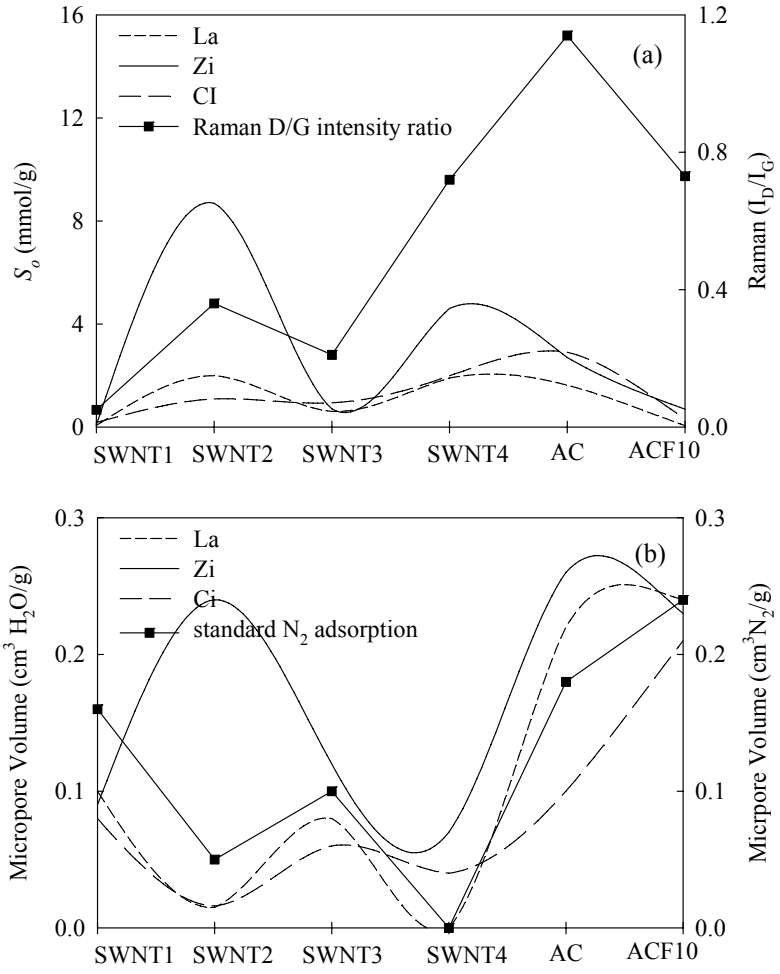

Figure 3.6 (a) Trends in surface chemistry estimated from water adsorption as fitting parameter, S_o, and experimentally determined from Raman scattering of samples. The I_D/I_G ratio is reproduced from Fig. 2 for clarity. (b) Trends in micropore volume calculated from water adsorption as fitting parameter, $C_{\mu s}$, and experimentally determined from standard N_2 adsorption at 77 K, $C_{\mu N2}$. In the legend, La = fit to the Lagorsse et.al. version [73] Eq. 5; Zi = fit to the Zimny et. al. version [74] Eq. 6; and CI = fit to the CIMF model by Marban et al., [75] Eq. 7. Notice that the $C_{\mu s}$ for sample SWNT4 should be non zero and larger than N_2 micropore volume.

However, here only the CIMF model seemed to follow this additional criterion. Upon comparing the sample micropore volumes by water and N_2, and applying the condition $C_{\mu s} < C_{\mu N_2}$, the Lagorsse's version and the CIMF model were again found to be more compatible than the Zimny's version (Figure 3.6b). However, when the water micropore volume of the sample SWNT4 was calculated from Zimny's version, it was found to be negligible which is an unrealistic result as this sample contained same pore sizes as in sample SWNT3 but a much higher concentration of hydrophilic functional groups which might block N_2 molecules but should facilitate some water molecules to enter into the micropores. Therefore, overall the CIMF model by the Marban et al., [75] was found to be the most applicable and most informative model to interpret the water isotherm data collected for SWNTs.

3.2.3. Analysis of water-SWNT isotherms by the CIMF model

The fit to the CIMF model and the water adsorption isotherms of SWNTs and activated carbon samples is presented in Figure 3.7. The fitting parameters are presented in Table 3.1. Also presented in Figure 3.8 are the calculated isotherms for water adsorption on the surface functional groups and in the micropores. The total fitted isotherm is the sum of these two individual isotherms and is found to be almost perfectly overlapping the experimental data regardless of the sample type. It is observed that the highly hydrophilic samples such as SWNT4 had a much higher fraction of water uptake by the functional groups. Similarly, extremely hydrophobic samples such as SWNT1 and ACF10 exhibited a much lower contribution of adsorption on functional groups. To

further explore the accuracy of the deconvoluted isotherms, we conducted additional water adsorption experiments on samples SWNT3 and SWNT4 after reducing the concentration of their surface functional groups by heat treating these samples in vacuum at 600 ^{o}C. These additional isotherms are also presented in Figure 3.7. As expected, the water uptake decreased upon heat treatment for both samples due to loss of surface functionality. Furthermore, the appearance of a type V characteristic became more obvious upon heat treatment, and most importantly, the experimental isotherms of heat treated samples now very closely followed the micropore filling contribution of the total isotherms of untreated samples predicted from the CIMF model. This suggests that heat treatment must have removed a large fraction of surface functional groups. Therefore, CIMF model is most suitable for deconvoluting an experimental water-SWNT adsorption isotherm with great accuracy.

In general, the water adsorption curve by functional groups appeared to monotonically increase until approximately P/P_o = 0.6 and then rise up sharply. This behavior corresponds with the characteristic type III isotherm, and is associated with growth and accumulation of water clusters around the functional groups on a nonporous carbon [92]. The adsorption capacity attributable to the functional groups appeared to be directly related to the hydrophilicity of the samples. The effect of hydrophilicity was observed in the micropore filling isotherm also such that the samples with a higher degree of functionalization (i.e., larger S_o values in Table 3.1.) exhibited a left-hand shift in the micropore filling isotherm. In other words, higher degree of hydrophilicity not only caused more water uptake by the functional groups but also facilitated micropore filling at a lower vapor concentrations.

Table 3.1 Fitting parameters from the CIMF model.

Adsorbent	S_o (mmol/g)	$C_{\mu s}$ (cm^3/g)	K_f	K_μ	n	m
SWNT1	0.17	0.08	2	6999	14	12.8
SWNT2	1.09	0.02	1	70	8	4.6
SWNT3	0.94	0.06	2	1744	11	10.4
SWNT4	1.99	0.04	13	8	4	3.1
AC	2.90	0.10	2	7	9	3.2
ACF10	0.32	0.21	122	3099	10	9.6

The comparison of equilibrium rate constants for majority of SWNT samples indicated a significantly larger value of rate constants for adsorption in micropores than adsorption on functional groups ($K_\mu >> K_f$), which supports the observation that at any given concentration of water vapor, adsorption in micropores is significantly higher than that on the functional groups.

We also found that the fitting parameters could be related to the physical and chemical properties of the samples. The number of water molecules in a cluster grown onto the functional groups and those filling the micropores (i.e., parameters, *n* and *m*) were found to follow trends opposite to the I_D/I_G ratio in the Raman spectra of the sample (Fig. 3.8a). For example, the sample SWNT1 exhibited the highest *n* and *m* values of 14 and 12.8, respectively, which should correspond to a 0.8 to 0.9 nm wide cluster. This sample is known to be extremely hydrophobic as evidenced by a very low I_D/I_G ratio in its Raman spectra and further supported by the lowest value of the S_o parameter among all samples. On the other hand, for sample SWNT4 the *n* and *m* parameters were 4 and 3.1, respectively, which corresponded to a cluster size smaller than 0.6 nm that has been reported in the literature [99]. This sample is extremely hydrophilic as indicated from a high

I_D/I_G ratio in its Raman spectra as well as a large value of S_o parameter. Therefore, we can conclude that a higher concentration of oxidation groups will result in the formation of smaller clusters of water molecules on both functional groups as well as in micropores. This conclusion is not unrealistic if one were to assume that the majority of oxidation groups will exist on the pore entry as opposed to on the SWNT surface, and therefore, will constrict the pore opening resulting in the pore to appear smaller in width. Our observation is consistent with that from molecular simulations where the cluster size was found dependent on the hydrophobicity of the nanopores . It was also noticed that the sample-to-sample trends of I_D/I_G ratio and the same for S_o parameter were directly related. This indicated that trends in the global surface chemistry by Raman scattering experiments can indeed be extended to the hydrophilic component of the total surface chemistry estimated from data fitting. Furthermore, the values of *m* parameter were found to be somewhat directly related to the dominant or the average pore size in the adsorbent (Figure 3.8b), which is an obvious result as wider pores should facilitate adsorption of larger clusters of water molecules so long as the concentration of the functional groups blocking the pores is not excessive. We noticed that for any given sample the *m* values were also directly related to the difference in the micropore volumes by N_2 and water adsorption (i.e., $C_{\mu N_2}$ - C_s) (Figure 3.8b). Larger differences in micropore volumes were observed for samples with higher *m* values. This is a realistic observation as larger clusters will fill the pores more incompletely than smaller clusters, thus exhibiting more deviant values of a sample's micropore volume from water adsorption.

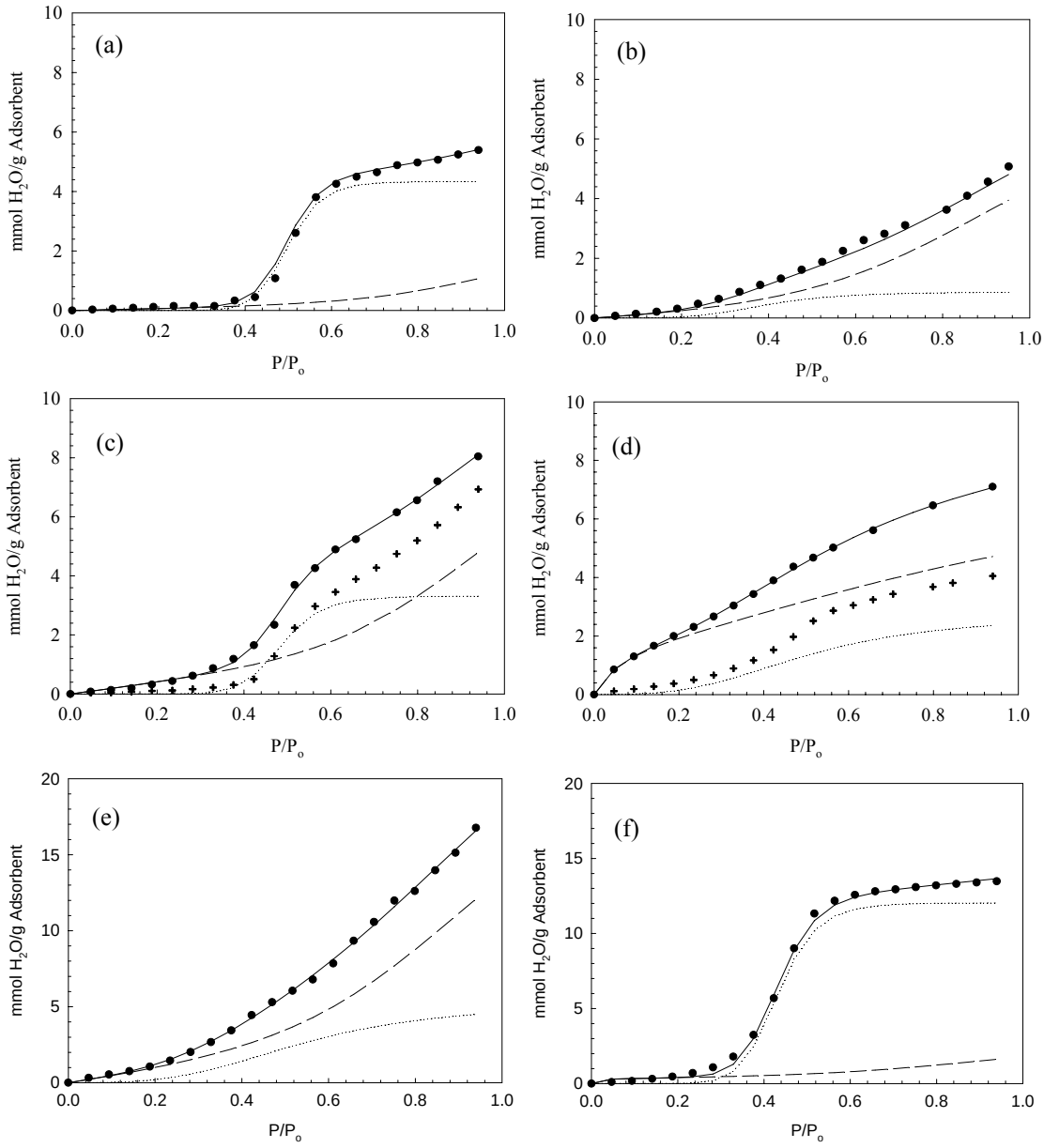

Figure 3.7 Water vapor adsorption isotherms and fits to the CIMF models for carbon nanotube samples (a) SWNT1, (b) SWNT2, (c) SWNT3, (d) SWNT4, and activated carbon (e) AC and (f) ACF10. Notice that the isotherms for samples heat treated at 600 ^{o}C under vacuum (+) are lower than original isotherms, follow type V characteristics, and more closely resemble the micropore filling component of the total isotherm fitted to CIMF model

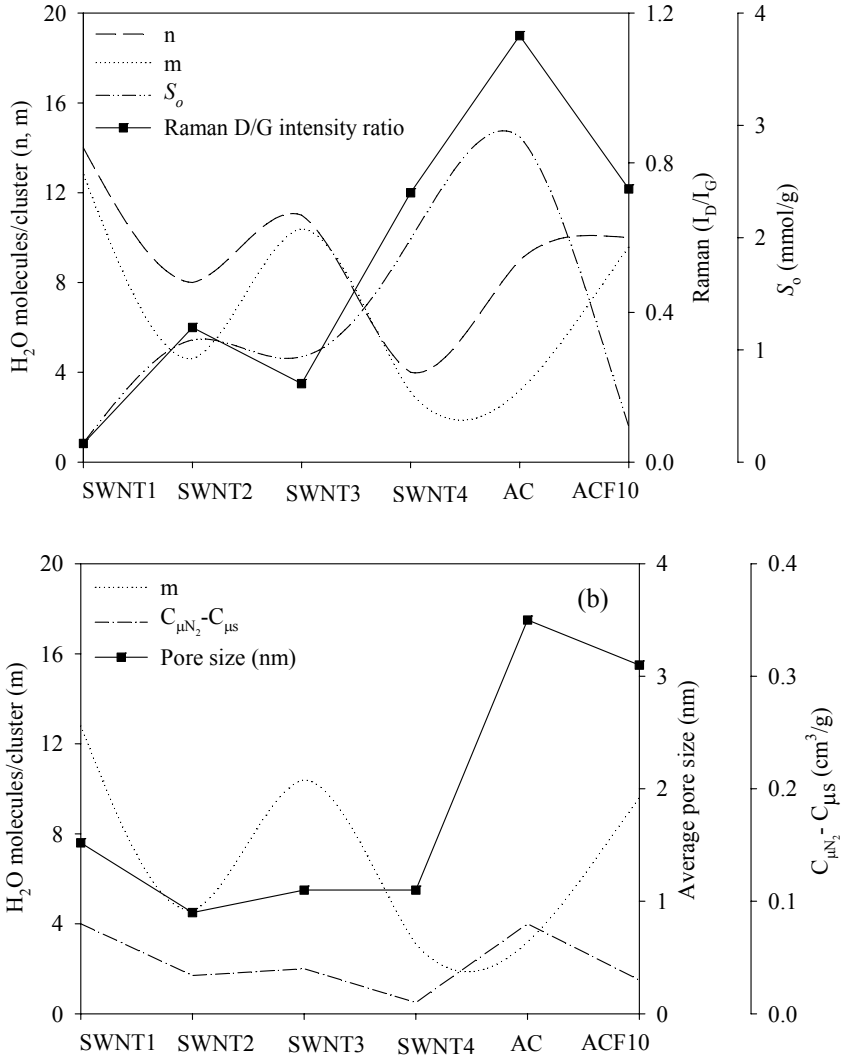

Figure 3.8 (a) Trends in the number of water molecules in clusters on functional groups (*n*) and clusters migrating into the micropores (*m*) as predicted from the CIMF model, and inverse trends observed in the samples' chemistry analyzed from Raman scattering and S_o parameter that quantifies the hydrophilicity of the sample. The I_D/I_G ratio is reproduced from Figure 4 for clarity. (b) Trends in values of *m* parameter, physical pore size from Table 1 and micropore volume remaining unfilled by water molecules.

3.2.4. Summary

We have applied several semi-empirical equations developed to interpret the adsorption isotherms of water in common carbonaceous materials to the water adsorption isotherms collected on SWNT samples. The applicability of each model was evaluated by high correlation coefficient of $R^2 > 0.99$, and physical significance of fitting parameters such as the concentration of functional groups must relate to the D/G intensity ratio in the Raman spectra of the sample, the water adsorption micropore volume should be lower than that by standard N_2 adsorption at 77 K and the size of water clusters should be relatable to the average pore size. We conclude that the Do and Do equation modified by Marban et al. is one of the most suitable equation for predicting from SWNTs' experimental isotherms alone the size of water clusters facilitating adsorption, deconvoluting experimental isotherms into individual contributions from hydrophilic groups and filling of micropores, quantifying the concentration of hydrophilic functional groups, and determining the micropore volume.

3.3 Effect of Surface Oxygen and Temperature on External and Micropore Adsorption of Water in Single-Walled Carbon Nanotubes by Gravimetric Experiments

3.3.1. Experimental Isotherms and Data Fitting

Adsorption isotherms of water vapor in SWNTs and activated carbon measured at 5, 20 and 35 ^{o}C are presented in Figure 3.9. All samples exhibited a decreasing adsorption capacity and a rightward shift in the isotherm heel due to an increase in temperature.

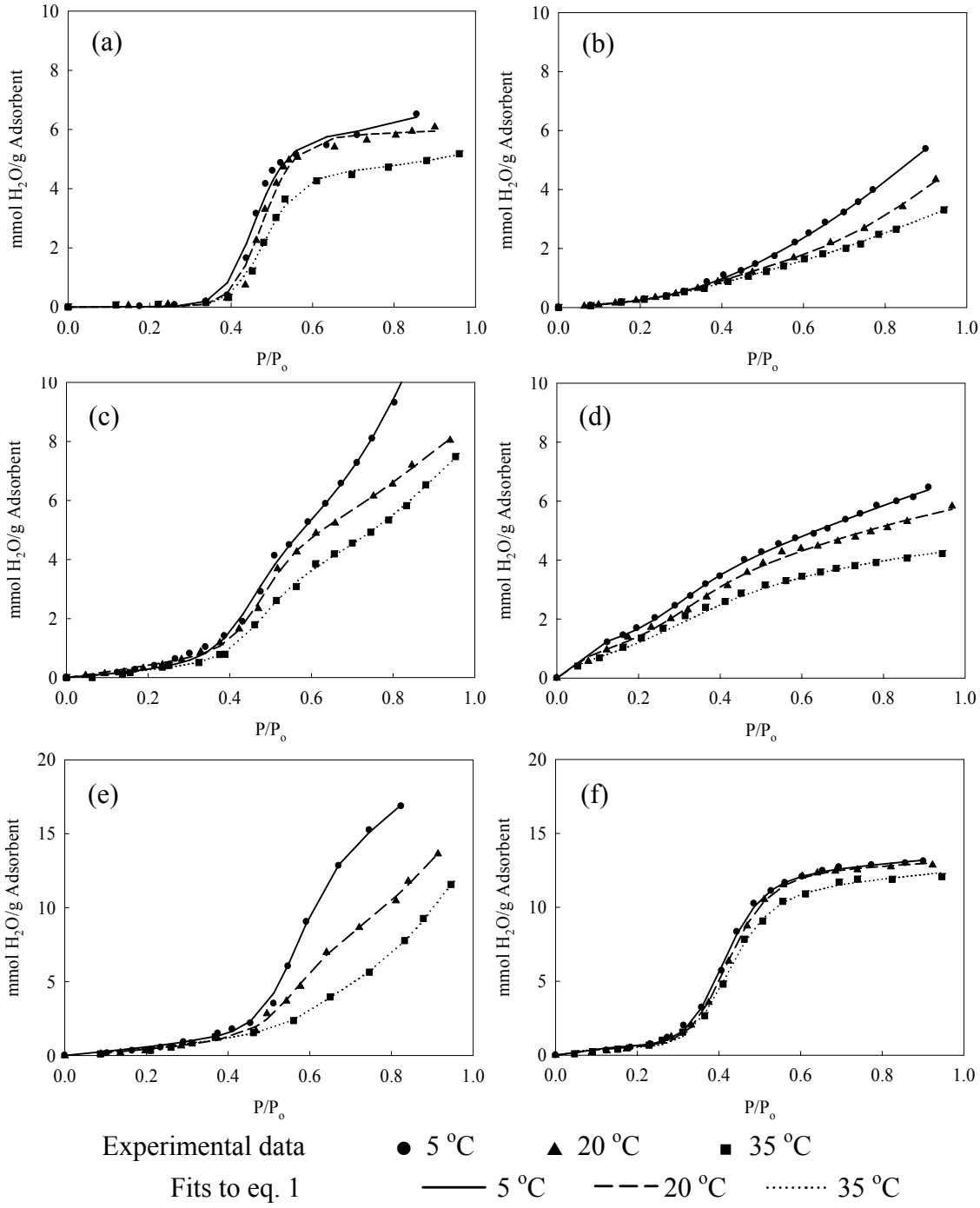

Figure 3.9 Water adsorption isotherms collected by gravimetric measurements and fitted to eq. 1 at T = 5, 20 and 35 ^{o}C. (a) SWNT1, (b) SWNT2, (c) SWNT3 and (d) SWNT4, and activated carbon samples (e) AC and (f) ACF10.

The maximum adsorption capacity of SWNTs ranged from 4 to 10 mmol/g while that of activated carbon varied between 10 to 16 mmol/g. The effect of total surface oxygen on a sample, as measured by XPS, was apparent from the shape of the isotherm curve. Sample SWNT1 had the least amount of oxygen (1.8%, Figure 2) resulting in a type V curve, while SWNT4 had the most surface oxygen (13.9%, Figure 2) which became known as a result of the appearance of a type IV curve. Sample SWNT1 and ACF10 were the only samples that clearly exhibited the characteristics of a type V isotherm common for water adsorption on carbon.

All isotherms were fitted to the CIMF model (eq. 2.9)[75] using the curve fitting toolbox available in Matlab. The non-linear least-square optimizer was used to determine the values of model parameters, the details of which are present in our previous work.[37]

$$C_\mu = S_O \frac{K_f \sum_{i=1}^{n} i * \left(\frac{P}{P_O}\right)^i}{1 + K_f \sum_{i=1}^{n} \left(\frac{P}{P_O}\right)^i} + C_{\mu s} \frac{K_\mu \left(\frac{P}{P_O}\right)^{m+1}}{K_\mu \left(\frac{P}{P_O}\right)^{m+1} + \left(\frac{P}{P_O}\right)} \qquad (2.9)$$

(1a) (1b)

where C_μ (mmol/g) is the amount of adsorbed water at a specific $P/P_{o,}$ n is the maximum number of water molecules adsorbed onto the functional groups, m is the average number of water molecules forming the clusters that migrate into the micropores, S_o is the concentration of primary adsorption sites, $C_{\mu s}$ is the maximum adsorption capacity (mmol/g), K_f is the equilibrium constant including water chemisorption on functional groups and hydrogen bonding of water on pre-adsorbed water molecules and K_μ is the equilibrium constant for water cluster filling into the micropores.

The CIMF model was developed for water-activated carbon isotherms. The rationale for it being most suitable of all models we tested to water-SWNTs isotherms is the central theme of our previous work.[37] The details of model development are reported elsewhere[75] and a brief description is provided here. The CIMF model is a modified version of the Do & Do equation[35] which assumes that the total adsorption follows a two-stage mechanism. In the first stage, water strongly bonds to the functional groups (BET type adsorption behavior) and forms clusters via hydrogen bonding. This is described by the first term of the eq. 2.9 (eq. 2.9a). When the cluster size equals six, a group of five molecules separates and fills the micropore. The second term of eq. 2.9 refers to the desorption of water from functional groups and its adsorption into the micropores as pentamers (eq. 2.9b). Based on experimental and theoretical evidence that clusters larger than pentamers migrate into the pores, Marban et al.[75] removed the restriction of size for these migrating clusters. This allows the pore filling cluster to be of varying size to be dependent on structural and thermodynamic parameters. In our previous work,[37] we evaluated the applicability of several common water isotherm models, including various versions of the Do & Do model, to water-SWNT experimental isotherms. We also tested the validity of the fitting parameters by following a different approach. We characterized the samples for properties similar to those quantified by the fitting parameters. By comparing the parameters to an independent sample characterization, we determined whether the parameters were true indicators of sample properties or merely a mathematical affectation with little physical meaning. As an example, the S_o fitting parameter that represents the concentration of primary sites was compared to the intensity ratio of D and G peaks (I_D/I_G) in the Raman spectra of samples. This was used because

the I_D/I_G ratio is a measure of total surface fracture, and therefore, must be related to the concentration of primary sites if the S_o value is correct. We found that several models fit well ($R^2 > 0.95$), however, the parameters obtained from the CIMF model[75] were the most compatible to independent measurements of sample properties: N_2 adsorption (77 K) for micropore volume, surface-chemistry from Raman scattering and relation of pore widths with cluster sizes.

For this study, eq. 2.9 was applied to the water adsorption isotherms collected at 5, 20 and 35 ^oC. Eq. 1 was found to fit extremely well with the experimental data regardless of the temperature and sample type ($R^2 > 0.995$, presented here as smooth lines in Figure 3.9). The accuracy of the fitting parameters was tested by relating them with sample characterization: S_o was compared to the % O from the XPS spectra of samples and $C_{\mu s}$ was compared to the N_2 adsorption (77 K) micropore volume. Representative fitting parameters at T = 5 ^oC with complementary sample properties are presented in Table 3.2. A detailed analysis of the fitting parameters is presented further on in this publication. It can be observed that the S_o sample-to-sample trends followed those of % O trends by XPS measurements. This is consistent with the trends in the I_D/I_G ratio of Raman spectra of the samples performed in our previous work.[37] The sample-to-sample trends in $C_{\mu s}$ were similar to those for the micropore volume, $C_{\mu s\text{-}N2}$. It can also be observed that $C_{\mu s} < C_{\mu s\text{-}N2}$ regardless of sample type, which strengthens the accuracy of $C_{\mu s}$ values as nitrogen is expected to fill the pores more effectively than water-clusters.[91] The only exception to this secondary constraint was found in the activated carbon sample, AC ($C_{\mu s}$ = 0.2 cm^3/g and $C_{\mu s\text{-}N2}$ = 0.18 cm^3/g), which is likely due to the higher degree of structural heterogeneity present in activated carbons.

Table 3.2 CIMF model parameters from fitting of isotherms collected at 5 °C

	Fitting parameter						Sample characterization		
	n	m	K_f	K_μ	S_o (mmol/g)	$C_{\mu s}$ (cm^3/g)	% O[a]	$C_{\mu s\text{-}N2}$[b] (cm^3/g)	Pore size[c] (nm)
SWNT1	15	11.4	0.1	6954	0.37	0.10	1.8	0.16	1.52
SWNT2	9	3.7	0.7	8	1.12	0.03	3.2	0.05	0.9
SWNT3	9	9.7	0.3	1818	1.11	0.06	4.0	0.10	1.1
SWNT4	6	4.3	23.8	112	1.39	0.04	13.9	0	1.1
AC	13	11.5	11.3	2541	1.52	0.20	7.2	0.18	3.5
ACF10	6	8.9	1.8	564	0.69	0.20	5.7	0.24	3.1

[a] Atomic O % determined from XPS survey scans for comparison with S_o, n and K_f values.
[b] Reproduced from Table 1 for comparison with $C_{\mu s}$
[c] Reproduced from Table 1 for comparison with m and K_μ.

3.3.2. Pseudo-experimental isotherms on functional groups and micropores: Effect of % O and T

The deconvolution of experimental isotherms of samples SWNT1, 2, 3 and 4 at T = 5, 20 and 35 °C is presented in Figure 4. For every sample, the first term of eq. 2.9 (eq. 2.9a) is plotted in the left-hand figures and the second term (eq. 2.9b) is plotted in the corresponding right-hand figures. The sum of two terms is plotted as smooth lines in Figure 3.10, where a high correlation coefficient ($R^2 > 0.99$) with experimental isotherms can be observed. We suggest that the individual terms can be interpreted as pseudo-experimental isotherms on functional groups (eq. 2.9a) and in micropores (eq. 2.9b) of SWNTs. It is emphasized that a purely experimental method to determine these two adsorptive components can not be traced in present literature. Therefore, as reported in our recent work,[37] a semi-empirical approach of fitting experimental isotherms to eq. 2.9 may be the most advanced method available to date.

The effect of total surface-oxygen on water adsorption onto a sample's functional groups was apparent from the plots of eq. 2.9a (Figure 3.10, left). It can be observed that

as the total surface oxygen progressively increased from 1.8% O in SWNT1 to 13.9% O in SWNT4, the amount of water adsorbed onto the functional groups at a given relative pressure increased as well. At T = 20 ^{o}C and $P/P_o \approx 0.6$, SWNT1, 2, 3 and 4 adsorbed 0.1, 1.2, 2.0 and 2.8 mmol/g of water on functional groups, respectively. The isotherms exhibited a type III shape that is typical for hydrophobic materials. Because of structural dissimilarities the adsorption in micropores (plots of eq. 2.9b, Figure 310, right) did not seem to have a direct correlation with surface oxygen. However, the least oxygenated sample SWNT1 exhibited the most adsorption in micropores. The pseudo-experimental isotherms suggest that at a given relative pressure water should simultaneously adsorb onto functional groups and into micropores. Increasing the temperature reduced both adsorptive contributions. However, at the low relative pressures adsorption was almost independent of temperatures between 5 and 35 ^{o}C. This trend may be due to the strong interaction of water molecules with functional groups. However, for sample SWNT4, regardless of temperature, the pseudo-experimental isotherms on functional groups suddenly increased at the initial relative pressure of $P/P_o \approx 0.05$. This was followed by a gradual increase for the rest of the adsorption sequence until near saturation was achieved. For this sample, noticeable adsorption in micropores could be observed at low $P/P_o < 0.2$. This is unexpected because morphologically this sample is similar to SWNT3. We believe that the leftward shift in micropore isotherm to 0.2 P/P_o is due to a much higher % O in this sample. This also suggests that a majority of surface-oxygen may be located at the pore entry.[68] As expected from the total adsorption isotherm, all samples exhibited a decreasing adsorption capacity and a pseudo-isotherm shift towards increasing relative pressures with an increasing temperature.

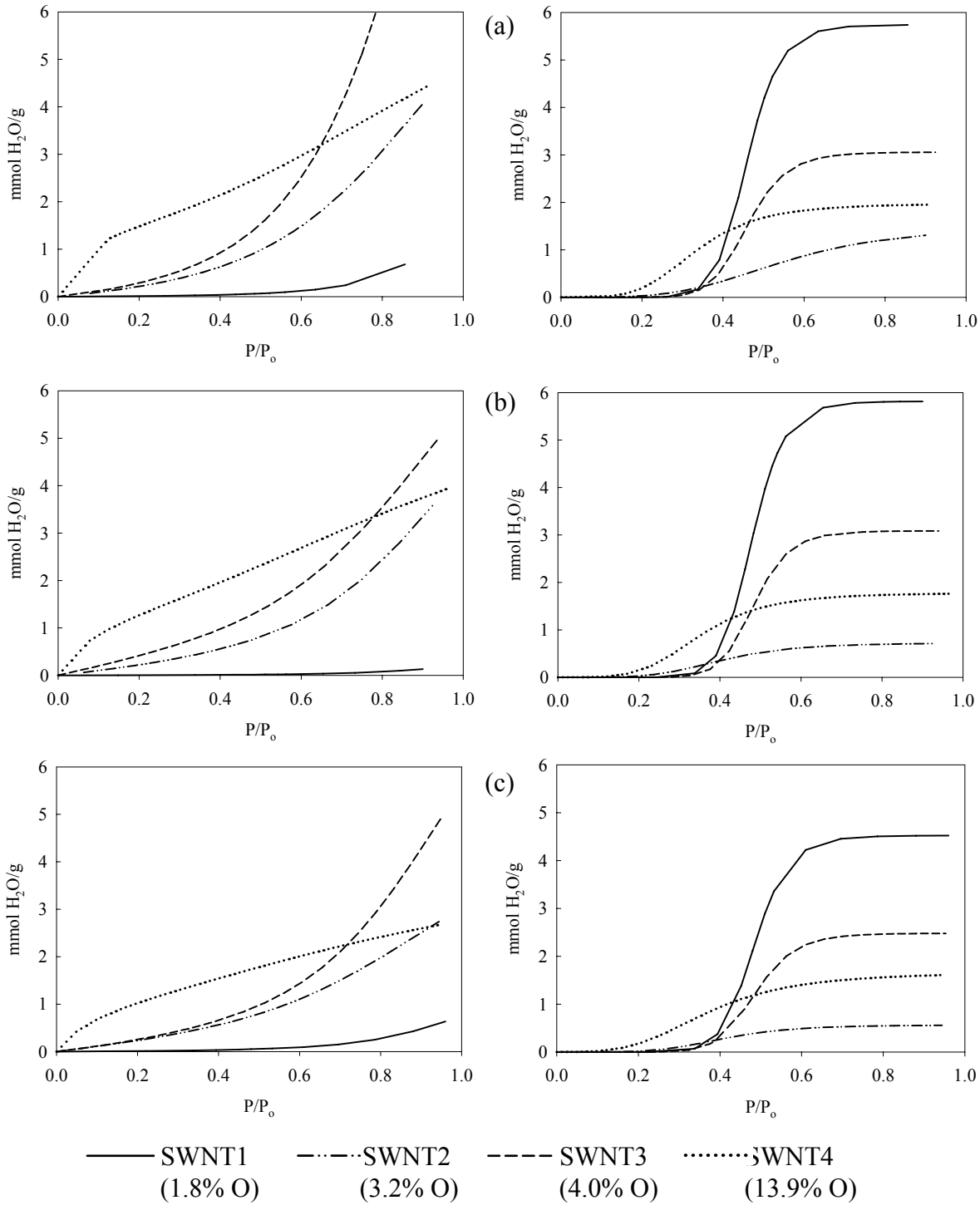

Figure 3.10 Effect of total oxygen and temperature on pseudo-experimental isotherms of water adsorption on functional groups (left) and in micropores (right) of SWNT samples at T = 5 ^{o}C (a), 20 ^{o}C (b) and 35 ^{o}C (c).

3.3.3. Heat of Adsorption

The isosteric heat of water adsorption is a differential molar quantity typically derived from the temperature dependency of an isotherm. In the case of water, it should describe the energy released from H_2O-primary site interaction and H_2O-H_2O interaction. Here, the isosteric heat of adsorption, Q_{st} (kJ/mol), was calculated by applying the Clausius-Clapeyron equation, eq. 3.1.[31] It was calculated from the experimental data pertaining to the total isotherms (Figure 3.11) and from the pseudo-experimental isotherms modeled from eq. 2.8 (Figure 3.10).

$$Q_{st} = L_{st} + q_{st}\big|_{isotherm} = L_{st} + RT^2 \frac{d\ln(P/P_o)}{dT} \qquad (3.1)$$

where, latent heat of water condensation (L_{st}) is 45 kJ/mol;[101] $q_{st}\big|_{isotherm}$ is the net isosteric heat of adsorption (kJ/mol) calculated from a particular isotherm; P/P_o are the values of relative pressures, at different temperature, T (K), which corresponded to the same amount of water adsorbed; R is the gas constant (8.314 J/mol·K). At a specific water adsorption capacity, P/P_o values are determined at different T. The slope in the plot of $\ln(P/P_o)$ versus $1/T$ equals the ratio $-q_{st}/R$.[102] This procedure was repeated for several equinumerical adsorption capacities to yield the dependency of $q_{st}\big|_{isotherm}$ on the amount adsorbed (mmol/g). The heat of adsorption calculated from total experimental isotherms (Q_{st}), and pseudo-experimental isotherms on functional groups ($q_{st}\big|_{func}$) and in micropores ($q_{st}\big|_{micro}$) is presented in Figure 3.11.

3.3.3.1. Total (Q_{st})

Figure 3.11a shows the isosteric heat of water adsorption, Q_{st}, calculated from experimental isotherms of samples SWNT1, 2, 3, 4, AC and ACF10. The values of Q_{st} ranged from 46 to 58 kJ/mol, specific to a sample and the mmol/g water adsorbed. The exceptionally high Q_{st} value of 58 kJ/mol was exhibited by sample SWNT4 in the low coverage region. This sample has a relatively high concentration of surface oxygen, a likely cause for its high heat of adsorption. Using microcalorimetric technique, Terzyk et al.[63] have also reported Q_{st} as high as 60 to 70 kJ/mol at very low adsorption capacities (equivalent to $P/P_o < 0.1$) for certain acid-treated carbons. Initially, the Q_{st} values drop with increasing mmol/g of water adsorbed because adsorption onto the functional groups is no longer the dominating mechanism.[65, 103] Q_{st} should approach the latent heat of condensation, L_{st} to denote water binding to pre-adsorbed water molecules. A minima is achieved where the first point of inflexion is observed in the isotherm beyond which $Q_{st} \geq L_{st}$ depending upon the proximity of P/P_o to micropore filling. Each sample exhibited increasing Q_{st} values with increasing amounts of water adsorbed, with the exception of SWNT4. At lower water adsorption capacities (prior to the first point of inflexion, $P/P_o < 0.2$), Q_{st} could not be calculated for other samples as the temperature dependency of their isotherms could not be determined from the experimental data. This suggests that the H_2O-primary site interaction may be stronger than the H_2O-H_2O interaction, and therefore is not easily affected by increasing T from 5 to 35 ^oC. At adsorption corresponding to $0.2 < P/P_o < 0.5$, where water molecules simultaneously adsorb onto functional groups and in micropores, $Q_{st} \approx$ 45 to 48 kJ/mol for samples SWNT1, 2, 3, AC

and ACF10. This value of Q_{st} is close to the heat of condensation of water (45 kJ/mol) and is consistent with the current carbon literature.[77-79] Sample SWNT4, however, exhibited high Q_{st} value of 58 kJ/mol at 0.15 P/P_o which decreased to 51 kJ/mol at 0.3 to 0.4 P/P_o and then steeply increased to 57 kJ/mol. All samples exhibited gradually increasing Q_{st} with mmol/g of water adsorbed in regions closer to the micropore filling. Such trends are consistent with those previously reported by experiments[63] and molecular simulations.[62]

3.3.3.2. Functional groups ($q_{st}\big|_{func}$) and micropores ($q_{st}\big|_{micro}$)

The heat of adsorption calculated from fitting eq. 3.1 to the pseudo-experimental isotherms on functional groups and micropores are presented in Figure 3.11b and 3.11c, respectively. It should be noted that L_{st} is not added to either of these quantities in order to avoid data misrepresentation. This is because we cannot determine if L_{st} is released solely upon adsorption onto functional groups and not in micropores or vice versa.

The $q_{st}\big|_{func}$ ranged from as high as 16 kJ/mol to as low as 0.5 kJ/mol, specific to sample chemistry and mmol/g of water adsorbed (Figure 3.11b). The highest of this value was exhibited by the most oxygenated sample, SWNT4. The $q_{st}\big|_{func}$ for samples SWNT1, 2, 3 and ACF10 were much lower, between 5 and 0.5 kJ/mol.

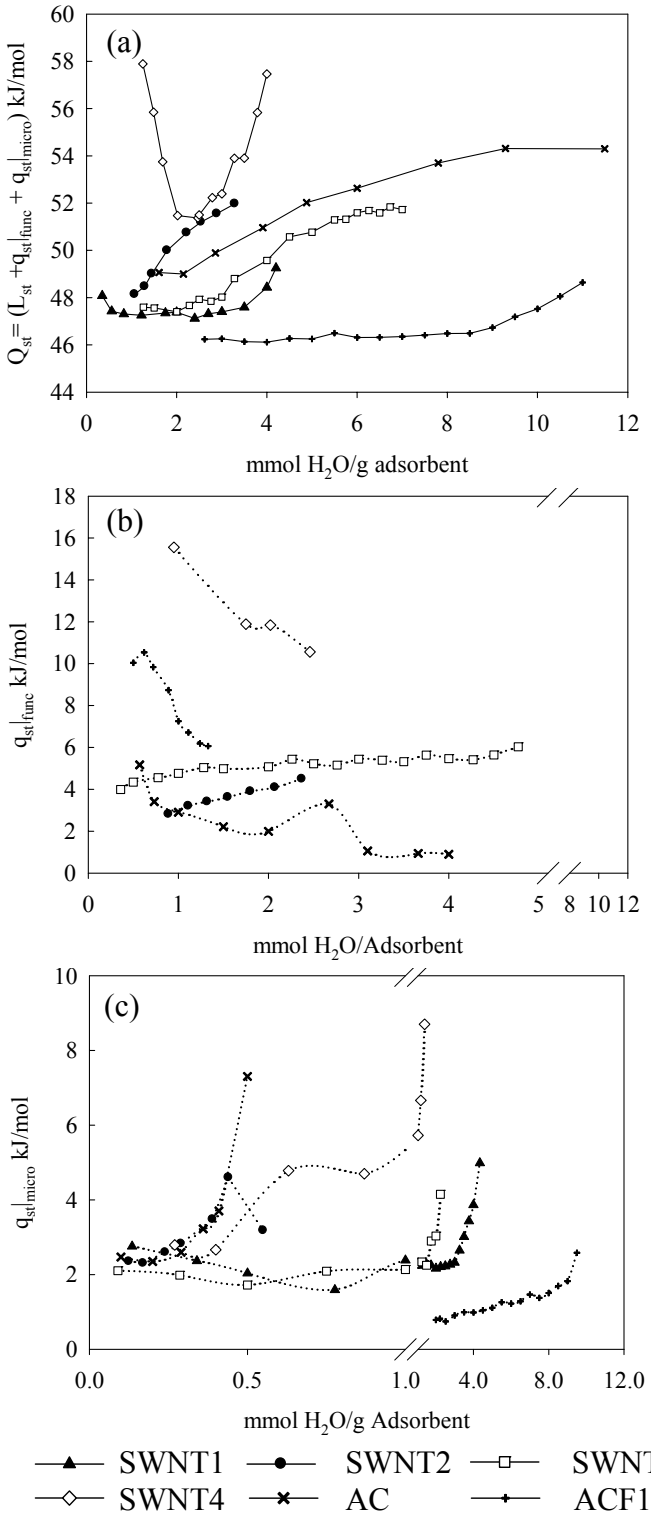

Figure 3.11 Heat of water adsorption calculated from (a) total water adsorption isotherms, and pseudo-isotherm adsorption isotherms (b) on functional groups and (c) micropores as calculated by eq. 1a. and 1b, respectively.

In general $q_{st}\big|_{func}$ decreased with increasing adsorption because after saturating the surface oxygen, water molecules continue to bind to the pre-adsorbed water. The $q_{st}\big|_{micro}$ was comparatively lower than $q_{st}\big|_{func}$ (Figure 3.11c). It varied between 1 and 3 kJ/mol for most of the isotherms, corresponding to the threshold values of P/P_o where micropore adsorption takes place prior to complete filling. These values are much lower than the heat of condensation.[65, 104] A sharp increase in $q_{st}\big|_{micro}$ was observed closer to saturation which was most likely due to micropore filling at P/P_o corresponding to the second point of inflexion in the isotherm. Our trends are consistent with those found by the microcalorimetric technique[63] and molecular simulations.[62] Both, Kimura et al.[63] and Striolo et al.[62] have reported increasing heat of adsorption with mmol/g of water during micropore filling in slit pores and SWNTs. They hypothesized that it is due to the stabilization of water clusters upon stacking and their dispersive interaction with the pore walls.

3.3.4. Analysis of fitting parameters

Eq. 2.9 was fitted to experimental isotherms measured at T = 5, 20 and 35 ^{o}C. All fitting parameters for SWNTs are presented in Figure 3.12, where their dependency upon temperature is apparent and the verity of their values can be evaluated by comparison with results from independent sample characterization. *First*, the numerical value of the fitting parameter S_o, which delineates the concentration of hydrophilic functional groups, was found related to the total % O of sample (Figure 3.12a). SWNT1 with the least 1.8% O had the lowest S_o values (0.4 to 0.05 mmol/g) while SWNT4 with the most 13.9% O

had the highest S_o values (1.4 to 1.2 mmol/g). Furthermore, in all samples increasing temperature caused S_o to drop which is unexpected as the temperatures in our study are not high enough to permanently remove surface oxygen. The lowering of S_o with temperature then suggests that water is adsorbed on fewer primary sites. Therefore, in essence, S_o denotes that concentration of hydrophilic functional groups that is being "detected" by water at any given thermodynamic state. Therefore, the observed lowering in S_o suggests the presence of primary sites with different activation energies. Some research suggests that at T ≈ 50 ^oC functional groups can interact with each other which lowers the concentration available for water to bind.[105]

Second, the numerical value of $C_{\mu s}$, which is a measure of the maximum micropore volume occupied by water, was found to relate to the sample's N_2 adsorption (77 K) micropore volume, $C_{\mu s\text{-}N2}$ (Figure 3.12b). SWNT1 with maximum $C_{\mu s\text{-}N2}$ = 0.15 cm^3/g also had the highest $C_{\mu s}$ of 0.1 to 0.8 cm^3/g. However, it was noted that although SWNT4 has zero N_2 microporosity, it had significant $C_{\mu s.}$ We believe that in this sample the extremely high surface oxygen was blocking the pore opening completely. Increasing temperature reduced the $C_{\mu s}$ values regardless of the sample type, which is expected of a physisorption process.

Third, the numerical value of the fitting parameter *n,* which describes the maximum number of water molecules per cluster bonded to primary sites, was also found to relate to the total surface oxygen; however, this parameter seems to be inversely related to atomic % O of a sample (Figure 3.12c). The least oxygenated sample, SWNT1 had the highest *n* values (15 to 17) whereas the most oxygenated SWNT4 sample had the

lowest *n* values (5 to 6). This trend indicates that a high degree of oxygenation results in formation of smaller aggregates of water molecules on primary adsorption sites. The average gap between neighboring functional groups is expected to be smaller in highly oxidized samples. This should lead to smaller size of water clusters (i.e., lower *n* in more oxidized samples) per functional group. It was also observed that *n* is a function of T. For all samples, increasing temperature caused their *n* value to increase. We believe that when temperature is raised adsorption is restricted to a lesser number of functional groups: only those that have an activation energy equal to or higher than those limited by T. This would make the SWNTs appear less hydrophilic thus allowing clusters to grow slightly larger in size.

Fourth, the numerical value of the fitting parameter *m,* which represents the average number of water molecules per cluster migrating into micropores, was discovered to relate directly to the pore width (Figure 3.12d). It is emphasized that the pore width presented here was extracted from the Raman spectra of the samples. The experimental details were presented in our previous work.[106] The pore width plotted here is the SWNT diameter that corresponded to that value of cm^{-1} which exhibited the tallest radial breathing mode peak (Figure 2.2). This method of determining SWNTs' pore sizes is far more accurate than adsorption based methods. Only the tallest peak was taken into consideration for the following comparative analysis as the effects of largest-sized nanotube on water-cluster size should be the most obvious. It was noticed that the sample with the widest nanotubes, SWNT1 (1.5 nm) had the highest *m* values (11 to 12). The smallest pore width sample, SWNT2 (0.9 nm) defied expectation of the lowest *m* ranking (*m* = 3.7 to 4.89) appearing above the most oxidized sample, SWNT4 (1.1 nm). The

lowest *m* values exhibited by SWNT4 indicate that in addition to geometric restriction, high concentration of functional groups can also influence the size of clusters entering the pores.

Fifth, the fitting parameter, K_f, is the equilibrium constant for water adsorption onto functional groups. It expresses the ratio of equilibrium constants for H_2O-primary site bonding versus H_2O-H_2O bonding around the functional groups.[75] We found that K_f was directly related to the total % O of the sample (Figure 3.12e). The least oxygenated sample, SWNT1 had the lowest K_f values (0.1 to 0.4) while SWNT4 with the most 13.9% O had the highest K_f values (11 to 24). Furthermore, with the exception of SWNT4, increasing temperature caused K_f to increase in all samples. This is due to the fact that H_2O-primary site interaction is much stronger ($q_{st}\big|_{func} \approx$ 50 to 70 kJ/mol) than H_2O-H_2O interaction ($q_{st}\big|_{func} \approx L_{st}$). Increasing temperature, within the limits of these experiments, will affect H_2O-H_2O bonding far more than H_2O-primary site bonding.

Last, the numerical value of the fitting parameter K_μ, which represents the equilibrium constant for water cluster insertion into micropores, was found directly related to the sample pore width and inversely related to the sample % O (Figure 3.12f). The least oxygenated sample which also had the widest nanotubes, sample SWNT1, had exceptionally high values of K_μ (4,200 to 7,000) while the most oxygenated sample SWNT4 had one of the lowest values (K_μ = 31 to 112). For all samples, increasing temperature lowered K_μ values. This is typical in a physisorption process.

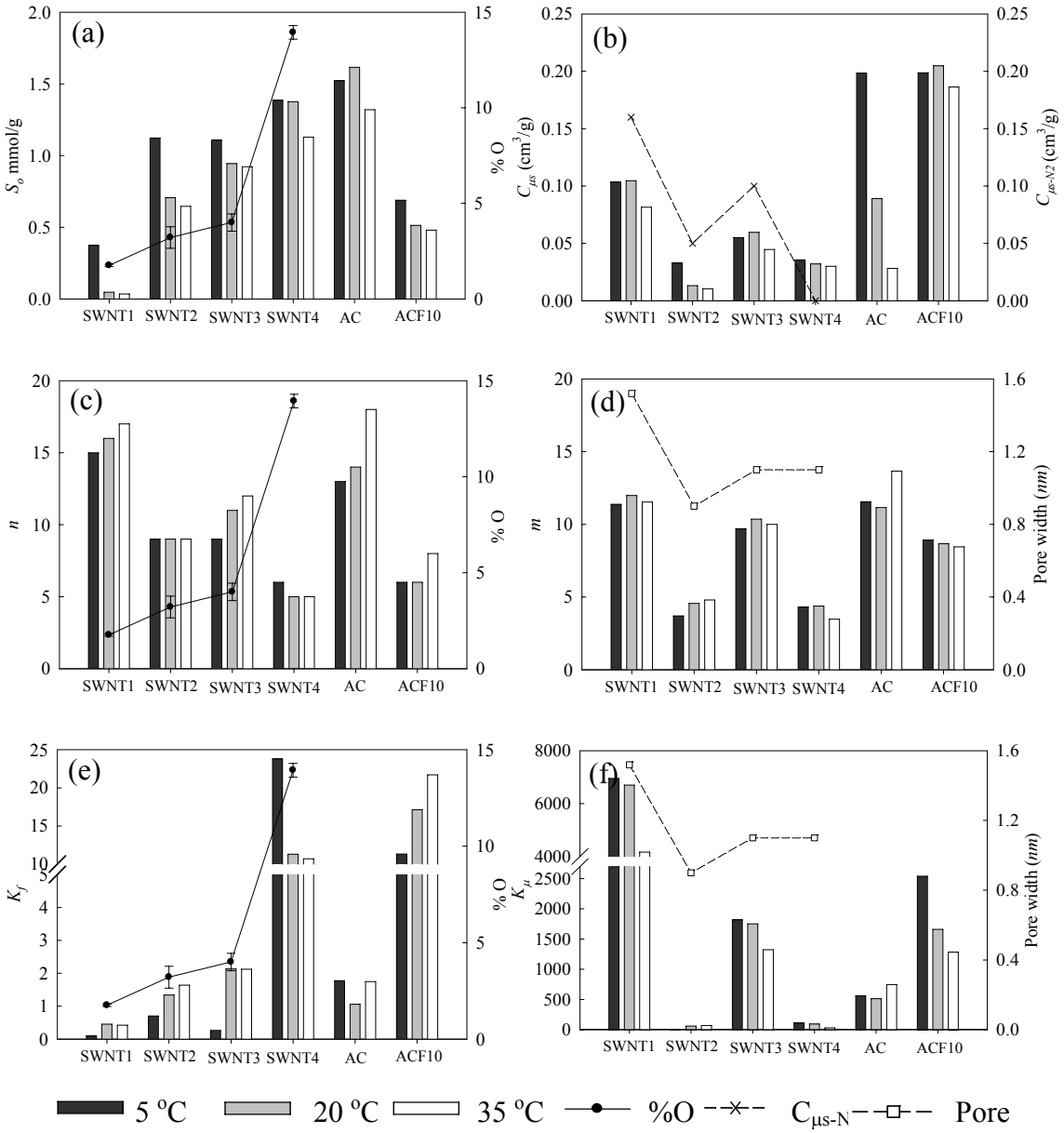

Figure 3.12 Analysis of the numerical value of fitting parameters obtained by applying eq. 1 to gravimetric water isotherms measured at T = 5, 20, 35 °C. (a) Concentration of primary sites, S_o. (b) Micropore volume by water, $C_{\mu s}$. (c) Maximum number of molecules comprising water clusters that grow onto the functional groups, n. (d) Average number of molecules per cluster in water clusters that fill micropores, m. (e) Equilibrium constant for water adsorption onto primary sites followed by growth of n size clusters, K_f, and (f) Equilibrium constant for m size water clusters filling into micropores.

3.3.5. Summary

We collected water adsorption isotherms ($0 < P/P_o < 0.95$) on several samples of single-walled carbon nanotubes (SWNTs) at three isotherms conditions, T = 5, 20 and 35 ^oC. The samples were characterized for surface oxygen, micropore volume and pore sizes. The isotherms were fitted to a semi-empirical model. This data fitting was employed as a methodology to calculate the heat of water adsorption in SWNT micropores and on functional groups, and to determine the size of water clusters, the concentration of functional groups and the limiting pore volumes. The validity of fitting parameters was determined by comparison of their values with sample characterization for total % O by x ray photoelectron spectroscopy, micropore volume by N_2 adsorption at 77 K and pore sizes by Raman spectroscopy. The total heat of adsorption (46 to 58 kJ/mol) calculated for several chemically and morphologically different SWNTs was found to be similar to those reported in literature derived from other methods such as calorimetry and molecular simulations. Individual heats of adsorption on functional groups (0.5 to 16 kJ/mol) and micropores (1 to 8.6 kJ/mol) were extracted from pseudo-experimental isotherms on functional groups and micropores. They were found to be inversely related to the size of water clusters. The equilibrium constant on functional groups increases with increasing temperature while equilibrium constant of micropore filling decreases. As expected, the concentration of surface functional groups and micropore volumes decreased with an increase of temperature.

4. Conclusions

The adsorption of water in microporous carbons such as activated carbons, carbon molecular sieves and carbon nanotubes is being widely investigated. In particular, the water adsorption in carbon nanotubes is an important process affecting a variety of scientific fields including electrochemistry, chromatography, catalysis, drug delivery and membrane separation. However, it remains ambiguous and not fully understood on adsorption property of water on carbon nanotubes, compared to activated carbons with which the interaction of water was described by several semiempirical tools. Therefore, the main objective of this study is to understand the interaction of water with single walled carbon nanotubes (SWNTs) implementing semiempirical models that were developed to interpret adsorption isotherms of water in common carbonaceous adsorbents. This study consists of three parts; 1) conducting gravimetric adsorption equilibrium and kinetics of water vapor in SWNTs and comparing them with those of activated carbons, 2) identifying the most suitable water adsorption models for SWNTs from existing adsorption models for activated carbons and 3) applying the most appropriate model to interpret adsorption property of water in nanocarbons.

Adsorption isotherms and kinetics of water vapor in several chemically and structurally distinct samples of SWNTs including two activated carbon samples were performed by gravimetric measurement at 20 ^{o}C. Adsorption was facilitated in an open-configuration. Adsorption capacities of SWNTs were found to be approximately one half of that of activated carbon and activated carbon fiber. The adsorption isotherms for SWNTs followed type V characteristics which are typically observed for a surface

chemistry mediated adsorption of water. The adsorption and desorption rate constants were calculated for all SWNT samples as a function of relative pressure using the linear-driving force model commonly used for activated carbons. The rate constants for both carbon types were in the general range of 1 x 10-3 to 3 x 10-3 s-1 with values decreasing with increasing vapor pressure; however, the distinction between adsorption on the primary sites versus capillary condensation was not apparent for SWNTs. This work can provide descriptive experimental data (detection limit = 0.1 □g) to aid molecular simulation studies of water adsorption in micro and nanoporous carbons.

To understand the interactions of water in novel nanocarbons, the semi-empirical equations developed to interpret adsorption isotherms at 20 oC of water in common carbonaceous adsorbents were implemented. Water adsorption isotherms gravimetrically determined on several SWNTs and activated carbon samples were fitted to the Dubinin-Serpinsky (DS) equation, Dubinin-Astakov equation, the Cooperative multi-molecular sorption theory, and the Do and Do equations. The applicability of models was evaluated by correlation coefficients, and physical significance of fitting parameters such as concentration of hydrophilic functional groups, micropore volume and the size of water clusters all of which were compared to complementary data from sample characterization by Raman spectroscopy and standard N2 adsorption at 77 K and were found to be relatable to the same. We conclude that the D. D. Do equation modified by Marban et al. is one of the most suitable equation for predicting from experimental isotherms alone the size of molecular clusters facilitating adsorption in SWNTs, deconvoluting experimental isotherms into individual contributions from hydrophilic groups and filling of micropores, and quantifying the concentration of hydrophilic functional groups and determining the

micropore volume. With the exception of the DS equation, the applicability of other water isotherm models to SWNTs is not computationally tractable.

Gravimetric water adsorption experiments (T = 5, 20 and 35 ^{o}C and $0 < P/P_o < 0.95$) were performed on SWNT and activated carbons. The isotherms were fitted to a semi-empirical model which allowed distinguishing with statistical confidence the adsorptive contributions of primary sites and micropores (referred to here as pseudo-experimental isotherms). The isosteric heats of water adsorption calculated from experimental isotherms ranged between 46 to 58 kJ/mol. The same calculations were performed on the separated adsorptive components: functional groups and micropore isotherms, and were found to be 0.5 to 16 kJ/mol and 1 to 8.6 kJ/mol, respectively. These values are similar to those available in the current literature reportedly estimated by calorimetric and molecular simulation techniques. From semi-empirical modeling, we were also able to qualitatively estimate temperature sensitive water specific sample properties such as the concentration of primary sites (found directly related to % O), and the size of water clusters aggregating on primary sites (found inversely related to % O) and those filling micropores (found directly related to the dominant pore size) and adsorption equilibrium constants.

The findings from this research should be useful in supporting molecular simulation studies of water adsorption in SWNTs which remains to be the most popular approach for understanding the microscopic behavior of water in nanocarbons.

5. Future Research

5.1. Chemical modification of carbon nanotubes by extremely low ozone vapor for further applications

Ozonation is one of the oxidation processes, which does not require any further subsequent elaboration for purification and functionalization of carbon nanotubes [107]. Ozone reaction with SWNTs produces functional moieties and morphological heterogeneity at the pore entry and sidewalls [108]. Several studies reported that 70~95% O_3 concentrations were applied to oxidize and etch carbon nanotubes, significantly destroying nanotubes' properties [13, 23, 107]. Other studies also applied 2~10 % O_3 concentrations for purification and functionalization on carbon nanotubes, producing extremely high defect density at the pore entry and sidewalls [109-111]. It is, therefore, essential to apply ozone concentrations to controllably functionalize SWNTs with minimal sample distortion.

It is proposed that the chemical and morphological modifications of SWNTs should be characterized by Raman spectroscopy, XPS, FTIR and nitrogen adsorption at 77K for surface area and pore volume. The characterized SWNT samples shoud be used to gravimetrically collect water adsorption isotherms and are applied to fit into the CIMF model for determining the product of functional groups at the pore entry and sidewalls and for interpreting water-carbon interactions in functionalized SWNTs.

5.2. Solubility of carbon nanotubes in ozonation process of drinking water treatment

Ozone has been widely used as pre-oxidant before conventional water treatment processes to remove algae, taste, odors, color and viruses as well as to enhance the coagulation for decreasing coagulant dosage, destabilizing the aggregation of particles and increasing the length of filter runs.[112] Effective ozone dose for preozonation has been known to suggest less than 3 mg/L to destabilize particle suspension and a residual ozone level for disinfection should remain 0.4 mg/L for a period of 4 minutes.

Carbon-based nanomaterials with different forms, such as fullerenes, SWNTs, MWNTs, carbon nanoparticles, nanofibers, and so forth are currently one of the most attractive nanomaterials and some of them have been already massively produced and for SWNTs and MWNTs synthetic methods for massive production have been considerably improved in last 5 years. It is imperative, therefore, to investigate the health and environmental implication of carbon nanomaterials. Carbon nanomaterials have been known to be hydrophobic and not dispersed into aquatic system. It is proposed that in case that massive dose of carbon nanomaterials in river and ground water inflows into drinking water process in which ozonation process is adapted, they are easily exposed to ozone oxidation. It has been suggested that higher than 2% ozone concentrations introduce carbon nanomaterials to be dispersed in water and increased turbidity. This research applies lower ozone concentrations, less than 3 mgO_3/L to oxidize carbon nanomaterials and analyze solubility by spectroscopic techniques and turbidity and coagulation capacity for characterization of oxidized CNTs.

Reference

(1) Iijima, S.; Ichihashi, T.; Ando, Y., PENTAGONS, HEPTAGONS AND NEGATIVE CURVATURE IN GRAPHITE MICROTUBULE GROWTH. *Nature* **1992,** *356*, 776.

(2) Qin, L. C.; Ichihashi, T.; Iijima, S., On the measurement of helicity of carbon nanotubes. *Ultramicroscopy* **1997,** *67*, 181.

(3) Saito, Y.; Uemura, S., Field emission from carbon nanotubes and its application to electron sources. *Carbon* **2000,** *38*, 169.

(4) Frackowiak, E.; Beguin, F., Electrochemical storage of energy in carbon nanotubes and nanostructured carbons. *Carbon* **2002,** *40*, 1775.

(5) Gevorgian, L. A.; Ispirian, K. A.; Ispirian, R. K., High energy particle channeling in nanotubes. *Nuclear Instruments and Methods in Physics Research Section B: Beam Interactions with Materials and Atoms* **1998,** *145*, 155.

(6) Striolo, A.; Gubbins, K. E.; Chialvo, A. A.; Cummings, P. T., Simulated water adsorption isotherms in carbon nanopores. *Mol. Phys.* **2004,** *102*, 243.

(7) Yang, Q. H.; Hou, P. X.; Bai, S.; Wang, M. Z.; Cheng, H. M., Adsorption and capillarity of nitrogen in aggregated multi-walled carbon nanotubes. *Chem. Phys. Lett.* **2001,** *345*, 18.

(8) Dillon, A. C.; Heben, M. J., Hydrogen storage using carbon adsorbents: past, present and future. *Appl. Phys. A-Mater. Sci. Process.* **2001,** *72*, 133.

(9) Baddour, C.; Briens, C., Carbon nanotube synthesis: A review. *Int. J. Chem. React. Eng.* **2005,** *3*, 22.

(10) Zeng, H.; Zhu, L.; Hao, G. M.; Sheng, R. S., Synthesis of various forms of carbon nanotubes by AC arc discharge. *Carbon* **1998,** *36*, 259.

(11) Puretzky, A. A.; Geohegan, D. B.; Fan, X.; Pennycook, S. J., Dynamics of single-wall carbon nanotube synthesis by laser vaporization. *Appl. Phys. A-Mater. Sci. Process.* **2000,** *70*, 153.

(12) Dupuis, A. C., The catalyst in the CCVD of carbon nanotubes - a review. *Prog. Mater. Sci.* **2005,** *50*, 929.

(13) Byl, O.; Liu, J.; Yates, J. T., Etching of carbon nanotubes by ozone - A surface area study. *Langmuir* **2005,** *21*, 4200.

(14) Chiang, I. W.; Brinson, B. E.; Huang, A. Y.; Willis, P. A.; Bronikowski, M. J.; Margrave, J. L.; Smalley, R. E.; Hauge, R. H., Purification and characterization of single-wall carbon nanotubes (SWNTs) obtained from the gas-phase decomposition of CO (HiPco process). *J. Phys. Chem. B* **2001,** *105*, 8297.

(15) Dujardin, E.; Ebbesen, T. W.; Krishnan, A.; Treacy, M. M. J., Purification of single-shell nanotubes. *Adv. Mater.* **1998,** *10*, 611.

(16) Bandow, S.; Rao, A. M.; Williams, K. A.; Thess, A.; Smalley, R. E.; Eklund, P. C., Purification of single-wall carbon nanotubes by microfiltration. *J. Phys. Chem. B* **1997,** *101*, 8839.

(17) Dai, H., Carbon nanotubes: opportunities and challenges. *Surface Science* **2002,** *500*, 218.

(18) Ando, T.; Matsumura, H.; Nakanishi, T. In *Theory of ballistic transport in carbon nanotubes*, 2002; Elsevier Science Bv: 2002; pp 44.

(19) Agnihotri, S.; Mota, J. P. B.; Rostam-Abadi, M.; Rood, M. J., Adsorption site analysis of impurity embedded single-walled carbon nanotube bundles. *Carbon* **2006,** *44*, 2376.

(20) Yarris, L., Legos for the nano-age. *Research review-Berkeley Lab* 2001.

(21) Misra, K.; Aggarwal, P.; Kapoor, S. K.; Bhalla, A. K.; Bansal, R. C., Adsorption isotherm studies of trinitrotoluene on granular activated carbon from aqueous solution. *Indian J. Chem. Technol.* **1998,** *5*, 87.

(22) Bansal, R. C.; Chhabra, P., EFFECT OF SURFACE OXIDATION ON THE ADSORPTION OF WATER-VAPOR BY PAN CARBON-FIBERS. *Indian J. Technol.* **1986,** *24*, 7.

(23) Mawhinney, D. B.; Naumenko, V.; Kuznetsova, A.; Yates, J. T.; Liu, J.; Smalley, R. E., Infrared spectral evidence for the etching of carbon nanotubes: Ozone oxidation at 298 K. *J. Am. Chem. Soc.* **2000,** *122*, 2383.

(24) Chingombe, P.; Saha, B.; Wakeman, R. J., Surface modification and characterisation of a coal-based activated carbon. *Carbon* **2005,** *43*, 3132.

(25) Biniak, S.; Szymanski, G.; Siedlewski, J.; Swiatkowski, A., The characterization of activated carbons with oxygen and nitrogen surface groups. *Carbon* **1997,** *35*, 1799.

(26) Villacanas, F.; Pereira, M. F. R.; Orfao, J. J. M.; Figueiredo, J. L., Adsorption of simple aromatic compounds on activated carbons. *J. Colloid Interface Sci.* **2006,** *293*, 128.

(27) Curulli, A.; Cesaro, S. N.; Coppe, A.; Silvestri, C.; Palleschi, G., Functionalization and dissolution of single-walled carbon nanotubes by chemical-physical and electrochemical treatments. *Microchimica Acta* **2006,** *152*, 225.

(28) Kuznetsova, A.; Popova, I.; Yates, J. T.; Bronikowski, M. J.; Huffman, C. B.; Liu, J.; Smalley, R. E.; Hwu, H. H.; Chen, J. G. G., Oxygen-containing functional groups on single-wall carbon nanotubes: NEXAFS and vibrational spectroscopic studies. *J. Am. Chem. Soc.* **2001,** *123*, 10699.

(29) Lafi, L.; Cossement, D.; Chahine, R., Raman spectroscopy and nitrogen vapour adsorption for the study of structural changes during purification of single-wall carbon nanotubes. *Carbon* **2005,** *43*, 1347.

(30) Ruthven, D. M., *Principles of adsorption and adsorption processs*. Wiley-Interscience Publication: New York, 1984.

(31) Alcaniz-Monge, J.; Linares-Solano, A.; Rand, B., Water adsorption on activated carbons: Study of water adsorption in micro- and mesopores. *J. Phys. Chem. B* **2001,** *105*, 7998.

(32) Cinke, M.; Li, J.; Chen, B.; Cassell, A.; Delzeit, L.; Han, J.; Meyyappan, M., Pore structure of raw and purified HiPco single-walled carbon nanotubes. *Chemical Physics Letters* **2002,** *365*, 69.

(33)Dresselhaus, M. S.; Eklund, P. C., Phonons in carbon nanotubes. *Adv. Phys.* **2000,** *49*, 705.

(34) Agnihotri, S.; Rostam-Abadi, M.; Rood, M. J., Temporal changes in nitrogen adsorption properties of single-walled carbon nanotubes. *Carbon* **2004,** *42*, 2699.

(35) Do, D. D.; Do, H. D., A model for water adsorption in activated carbon. *Carbon* **2000,** *38*, 767.

(36) Bansode, R. R.; Losso, J. N.; Marshall, W. E.; Rao, R. M.; Portier, R. J., Adsorption of volatile organic compounds by pecan shell- and almond shell-based granular activated carbons. *Bioresource Technology* **2003,** *90*, 175.

(37) Kim, P.; Agnihotri, S., Application of water-activated carbon isotherm models to water adsorption isotherms of single-walled carbon nanotubes. *J. Colloid Interface Sci.* **2008,** *325*, 64.

(38) Agnihotri, S.; Rood, M. J.; Rostam-Abadi, M., Adsorption equilibrium of organic vapors on single-walled carbon nanotubes. *Carbon* **2005,** *43*, 2379.

(39) Qi, N.; LeVan, M. D., Coadsorption of organic compounds and water vapor on BPL activated carbon. 5. Methyl ethyl ketone, methyl isobutyl ketone, toluene, and modeling. *Industrial & Engineering Chemistry Research* **2005,** *44*, 3733.

(40) Radovic, L. R.; Moreno-Castilla, C.; Rivera-Utrilla, J., Carbon materials as adsorbents in aqueous solutions. In *Chemistry and Physics of Carbon, Vol 27*, Marcel Dekker: New York, 2001; Vol. 27, pp 227.

(41) Jung, M. J.; Kim, J. W.; Im, J. S.; Park, S. J.; Lee, Y. S., Nitrogen and hydrogen adsorption of activated carbon fibers modified by fluorination. *J. Ind. Eng. Chem.* **2009,** *15*, 410.

(42) Crespo, D.; Yang, R. T., Adsorption of organic vapors on single-walled carbon nanotubes. *Industrial & Engineering Chemistry Research* **2006,** *45*, 5524.

(43) Chen, W.; Duan, L.; Zhu, D. Q., Adsorption of polar and nonpolar organic chemicals to carbon nanotubes. *Environmental Science & Technology* **2007,** *41*, 8295.

(44) Jorda-Beneyto, M.; Suarez-Garcia, F.; Lozano-Castello, D.; Cazorla-Amoros, D.; Linares-Solano, A., Hydrogen storage on chemically activated carbons and carbon nanomaterials at high pressures. *Carbon* **2007,** *45*, 293.

(45) Lua, A. C.; Guo, J., Adsorption of sulfur dioxide on activated carbon from oil-palm waste. *J. Environ. Eng.-ASCE* **2001,** *127*, 895.

(46) Pietrzak, R.; Bandosz, T. J., Activated carbons modified with sewage sludge derived phase and their application in the process of NO2 removal. *Carbon* **2007,** *45*, 2537.

(47)Long, R. Q.; Yang, R. T., Carbon nanotubes as a superior sorbent for nitrogen oxides. *Industrial & Engineering Chemistry Research* **2001,** *40*, 4288.

(48) Liu, J. C.; Monson, P. A., Monte Carlo simulation study of water adsorption in activated carbon. *Industrial & Engineering Chemistry Research* **2006,** *45*, 5649.

(49) Shi, W.; Johnson, J. K., Gas adsorption on heterogeneous single-walled carbon nanotube bundles. *Physical Review Letters* **2003,** *91*.

(50) Landi, B. J.; Ganter, M. J.; Cress, C. D.; DiLeo, R. A.; Raffaelle, R. P., Carbon nanotubes for lithium ion batteries. *Energy Environ. Sci.* **2009,** *2*, 638.

(51) Bondavalli, P.; Legagneux, P.; Pribat, D., Carbon nanotubes based transistors as gas sensors: State of the art and critical review. *Sens. Actuator B-Chem.* **2009,** *140*, 304.

(52) Zhang, X. X.; Zhu, C. C., Field-emission lighting tube with CNT film cathode. *Microelectron. J.* **2006,** *37*, 1358.

(53) Antolini, E., Carbon supports for low-temperature fuel cell catalysts. *Appl. Catal. B-Environ.* **2009,** *88*, 1.

(54) Lu, C. Y.; Tseng, H. H.; Wey, M. Y.; Chuang, K. H.; Kuo, J. H., Evaluating the potential of CNT-supported Co catalyst used for gas pollution removal in the incineration flue gas. *J. Environ. Manage.* **2009,** *90*, 1884.

(55) Shih, Y. H.; Li, M. S., Adsorption of selected volatile organic vapors on multiwall carbon nanotubes. *J. Hazard. Mater.* **2008,** *154*, 21.

(56) Ji, L. L.; Chen, W.; Duan, L.; Zhu, D. Q., Mechanisms for strong adsorption of tetracycline to carbon nanotubes: A comparative study using activated carbon and graphite as adsorbents. *Environ. Sci. Technol.* **2009,** *43*, 2322.

(57) Xu, M.; Sun, Z.; Chen, Q.; Tay, B. K. In *Effect of chemical oxidation on the gas sensing properties of multi-walled carbon nanotubes*, 2009; Inderscience Enterprises Ltd: 2009; pp 735.

(58) Rudisill, E. N.; Hacskaylo, J. J.; Levan, M. D., Coadsorption of Hydrocarbons and Water on Bpl Activated Carbon. *Industrial & Engineering Chemistry Research* **1992,** *31*, 1122.

(59) Ohba, T.; Kanoh, H.; Kaneko, K., Affinity transformation from hydrophilicity to hydrophobicity of water molecules on the basis of adsorption of water in graphitic nanopores. *J. Am. Chem. Soc.* **2004,** *126*, 1560.

(60) Ohba, T.; Kaneko, K., Surface oxygen-dependent water cluster growth in carbon nanospaces with GCMC simulation-aided in situ SAXS. *Journal of Physical Chemistry C* **2007,** *111*, 6207.

(61) Bekyarova, E.; Hanzawa, Y.; Kaneko, K.; Silvestre-Albero, J.; Sepulveda-Escribano, A.; Rodriguez-Reinoso, F.; Kasuya, D.; Yudasaka, M.; Iijima, S., Cluster-mediated filling of water vapor in intratube and interstitial nanospaces of single-wall carbon nanohorns. *Chem. Phys. Lett.* **2002,** *366*, 463.

(62) Striolo, A.; Gubbins, K. E.; Gruszkiewicz, M. S.; Cole, D. R.; Simonson, J. M.; Chialvo, A. A., Effect of temperature on the adsorption of water in porous carbons. *Langmuir* **2005,** *21*, 9457.

(63) Kimura, T.; Kanoh, H.; Kanda, T.; Ohkubo, T.; Hattori, Y.; Higaonna, Y.; Denoyel, R.; Kaneko, K., Cluster-associated filling of water in hydrophobic carbon micropores. *J. Phys. Chem. B* **2004,** *108*, 14043.

(64) Terzyk, A. P.; Gauden, P. A.; Rychlicki, G., Energetics of water adsorption and immersion on carbons. *Colloid Surf. A-Physicochem. Eng. Asp.* **1999,** *148*, 271.

(65) Rutherford, S. W., Probing the mechanism of water adsorption in carbon micropores with multitemperature isotherms and water preadsorption experiments. *Langmuir* **2006,** *22*, 9967.

(66) Furmaniak, S.; Gauden, P. A.; Terzyk, A. P.; Rychlicki, G.; Wesolowski, R. P.; Kowalczyk, P., Heterogeneous Do-Do model of water adsorption on carbons. *J. Colloid Interface Sci.* **2005,** *290*, 1.

(67) Dubinin, M. M.; Serpinsky, V. V., Isotherm equation for water vapor adsorption by microporous carbonaceous adsorbents. *Carbon* **1981,** *19*, 402.

(68) Mao, S.; Kleinhammes, A.; Wu, Y., NMR study of water adsorption in single-walled carbon nanotubes. *Chem. Phys. Lett* **2006,** *421*, 513.

(69) Vermisoglou, E. C.; Georgakilas, V.; Kouvelos, E.; Pilatos, G.; Viras, K.; Romanos, G.; Kanellopoulos, N. K., Sorption properties of modified single-walled carbon nanotubes. *Microporous and Mesoporous Materials* **2007,** *99*, 98.

(70) Slasli, A. M.; Jorge, M.; Stoeckli, F.; Seaton, N. A., Modelling of water adsorption by activated carbons: effects of microporous structure and oxygen content. *Carbon* **2004,** *42*, 1947.

(71) Talu, O.; Meunier, F., Adsorption of associating molecules in micropores and application to water on carbon. *AIChE J.* **1996,** *42*, 809.

(72) Rutherford, S. W., Modeling water adsorption in carbon micropores: Study of water in carbon molecular sieves. *Langmuir* **2006,** *22*, 702.

(73) Lagorsse, S.; Campo, M. C.; Magalhaes, F. D.; Mendes, A., Water adsorption on carbon molecular sieve membranes: Experimental data and isotherm model. *Carbon* **2005,** *43*, 2769.

(74) Zimny, T.; Finqueneisel, G.; Cossarutto, L.; Weber, J. V., Water vapor adsorption on activated carbon preadsorbed with naphtalene. *J. Colloid Interface Sci.* **2005,** *285*, 56.

(75) Marban, G.; Fuertes, A. B., Co-adsorption of n-butane/water vapour mixtures on activated carbon fibre-based monoliths. *Carbon* **2004,** *42*, 71.

(76) Striolo, A.; Chialvo, A. A.; Cummings, P. T.; Gubbins, K. E., Simulated water adsorption in chemically heterogeneous carbon nanotubes. *J. Chem. Phys.* **2006,** *124*.

(77) Velikov, A. A.; Grigor'ev, S. V.; Chuikin, A. V., Heats of sorption of nuclear-spin isomers of water on activated carbon. *Russ. J. Phys. Chem.* **2006,** *80*, 2047.

(78) Hassan, N. M.; Ghosh, T. K.; Hines, A. L.; Loyalka, S. K., Adsorption of water vapor on BPL activated carbon. *Carbon* **1991,** *29*, 681.

(79) Terzyk, A. P.; Rychlicki, G.; Cxiertnia, M. S.; Gauden, P. A.; Kowalczyk, P., Effect of the carbon surface layer chemistry on benzene adsorption from the vapor phase and from dilute aqueous solutions. *Langmuir* **2005,** *21*, 12257.

(80) Agnihotri, S., Zheng, Y., Mota, J. P. B., Ivanov, I , Kim, P., Practical Modeling of Heterogeneous Bundles of Single-Walled Carbon Nanotubes for Adsorption Application: Estimating the Fraction of Open-Ended Nanotubes in Samples. *J. Phys. Chem. C* **2007,** *111*, 13747.

(81) Yang, C. M.; Kaneko, K.; Yudasaka, M.; Iijima, S., Surface chemistry and pore structure of purified HiPco single-walled carbon nanotube aggregates. *Physica B-Condensed Matter* **2002,** *323*, 140.

(82) Dubinin, M. M., Adsorption in micropores. *J. Colloid Interface Sci.* **1967,** *23*, 487.

(83) Malakhov, A. O.; Volkov, V. V., Cooperative multimolecular sorption equation: Application to an alcohol-poly(1-trimethylsilyl-1-propyne) system. *Polymer Science Series A* **2000,** *42*, 1120.

(84) Barrer, R. M., *Intracrystalline diffusion*. ACS: 1971.

(85) Jorg Kärger, D. M. R., *Diffusion in zeolites and other microporous solids* A Wiley-Interscience publication: New York 1992.

(86) Sircar, S.; Hufton, J. R., Why does the Linear Driving Force model for adsorption kinetics work ? *Adsorption-Journal of the International Adsorption Society* **2000,** *6*, 137.

(87) Glueckauf, E., Theory of Chromatography .10. Formulae for Diffusion into Spheres and Their Application to Chromatography. *Transactions of the Faraday Society* **1955,** *51*, 1540.

(88) Fletcher, A. J.; Benham, M. J.; Thomas, K. M., Multicomponent vapor sorption on active carbon by combined microgravimetry and dynamic sampling mass spectrometry. *Journal of Physical Chemistry B* **2002,** *106*, 7474.

(89) Foley, N. J.; Thomas, K. M.; Forshaw, P. L.; Stanton, D.; Norman, P. R., Kinetics of water vapor adsorption on activated carbon. *Langmuir* **1997,** *13*, 2083.

(90) Reid, C. R.; Thomas, K. M., Adsorption of gases on a carbon molecular sieve used for air separation: Linear adsorptives as probes for kinetic selectivity. *Langmuir* **1999,** *15*, 3206.

(91) Alcaniz-Monge, J.; Linares-Solano, A.; Rand, B., Mechanism of adsorption of water in carbon micropores as revealed by a study of activated carbon fibers. *J. Phys. Chem. B* **2002,** *106*, 3209.

(92) Kuznetsova, A.; Mawhinney, D. B.; Naumenko, V.; Yates, J. T.; Liu, J.; Smalley, R. E., Enhancement of adsorption inside of single-walled nanotubes: opening the entry ports. *Chem. Phys. Lett* **2000,** *321*, 292.

(93) Cal, M. P.; Rood, M. J.; Larson, S. M., Gas phase adsorption of volatile organic compounds and water vapor on activated carbon cloth. *Energy Fuels* **1997,** *11*, 311.

(94) Barton, S. S.; Evans, M. J. B.; Holland, J.; Koresh, J. E., Water and cyclohexane vapour adsorption on oxidized porous carbon. *Carbon* **1984,** *22*, 265.

(95) Harding, A. W.; Foley, N. J.; Norman, P. R.; Francis, D. C.; Thomas, K. M., Diffusion barriers in the kinetics of water vapor adsorption/desorption on activated carbons. *Langmuir* **1998,** *14*, 3858.

(96) Fletcher, A. J.; Uygur, Y.; Thomas, K. M., Role of surface functional groups in the adsorption kinetics of water vapor on microporous activated carbons. *Journal of Physical Chemistry C* **2007,** *111*, 8349.

(97) Okoye, I. P.; Benham, M.; Thomas, K. M., Adsorption of gases and vapors on carbon molecular sieves. *Langmuir* **1997,** *13*, 4054.

(98) Fletcher, A. J.; Yuzak, Y.; Thomas, K. M., Adsorption and desorption kinetics for hydrophilic and hydrophobic vapors on activated carbon. *Carbon* **2006,** *44*, 989.

(99) Ohba, T.; Kanoh, H.; Kaneko, K., Water cluster growth in hydrophobic solid nanospaces. *Chemistry-a European Journal* **2005,** *11*, 4890.

(100) Neitsch, M.; Heschel, W.; Suckow, M., Water vapor adsorption by activated carbon: a modification to the isotherm model of Do and Do. *Carbon* **2001,** *39*, 1437.

(101) Ruthven, D. M., *Principles of Adsortpion and Adsorption Processes*. Wiley: New York, 1984.

(102) Jayendra Kumar, A.; Singh, R. R. B.; Patil, G. R.; Patel, A. A., Effect of temperature on moisture desorption isotherms of kheer. *LWT - Food Science and Technology* **2005,** *38*, 303.

(103) Brennan, J. K.; Bandosz, T. J.; Thomson, K. T.; Gubbins, K. E., Water in porous carbons. *Colloid Surf. A-Physicochem. Eng. Asp.* **2001,** *187*, 539.

(104) Ohba, T.; Kaneko, K., Cluster-associated filling of water molecules in slit-shaped graphitic nanopores. *Molucular Physics* **2007,** *105*, 139.

(105) Garcia-Perez, J. V.; Carcel, J. A.; Clemente, G.; Mulet, A., Water sorption isotherms for lemon peel at different temperatures and isosteric heats. *LWT-Food Sci. Technol.* **2008,** *41*, 18.

(106) Agnihotri, S.; Zheng, Y. J.; Mota, J. P. B.; Ivanov, I.; Kim, P. C., Practical Modeling of heterogeneous bundles of single-walled carbon nanotubes for adsorption applications: Estimating the fraction of open-ended nanotubes in samples. *Journal of Physical Chemistry C* **2007,** *111*, 13747.

(107) Cai, L. T.; Bahr, J. L.; Yao, Y. X.; Tour, J. M., Ozonation of single-walled carbon nanotubes and their assemblies on rigid self-assembled monolayers. *Chem. Mat.* **2002,** *14*, 4235.

(108) Simmons, J. M.; Nichols, B. M.; Baker, S. E.; Marcus, M. S.; Castellini, O. M.; Lee, C. S.; Hamers, R. J.; Eriksson, M. A., Effect of ozone oxidation on single-walled carbon nanotubes. *Journal of Physical Chemistry B* **2006,** *110*, 7113.

(109) Banerjee, S.; Wong, S. S., Rational Sidewall Functionalization and Purification of Single-Walled Carbon Nanotubes by Solution-Phase Ozonolysis. *The Journal of Physical Chemistry B* **2002,** *106*, 12144.

(110) Cataldo, F., A study on the action of ozone on multiwall carbon nanotubes. *Fuller. Nanotub. Carbon Nanostruct.* **2008,** *16*, 1.

(111) Li, M.; Boggs, M.; Beebe, T. P.; Huang, C. P., Oxidation of single-walled carbon nanotubes in dilute aqueous solutions by ozone as affected by ultrasound. *Carbon* **2008,** *46*, 466.

(112) Li, T.; Yan, X. M.; Wang, D. S.; Wang, F. L., Impact of preozonation on the performance of coagulated flocs. *Chemosphere* **2009,** *75*, 187.

APPENDIX

1. Raman Intensity (I_D/I_G) from Raman spectra

EA95 SWNT1

	G	D	D/G
1	7.392	0.365	0.049378
2	8.286	0.391	0.047188
3	8.225	0.35	0.042553
4	8.614	0.415	0.048177
5	9.907	0.426	0.043
6	6.777	0.314	0.046333
7	7.614	0.31	0.040714
8	7.379	0.335	0.045399
9	7.125	0.379	0.053193
10	7.171	0.323	0.045043
Avg.			0.046098
Standard deviation			0.003643

CVD90 SWNT2

	G	D	D/G
1	11.534	3.514	0.304664
2	13.792	4.984	0.361369
3	10.153	3.372	0.332119
4	9.976	3.467	0.347534
5	8.337	3.113	0.373396
6	8.572	2.893	0.337494
7	6.942	2.695	0.388217
8	8.795	3.517	0.399886
9	9.133	3.392	0.3714
10	8.602	3.104	0.360846
Avg.			0.357693
Standard deviation			0.02818

CS70 SWNT3

	G	D	D/G
1	1.735	0.335	0.193084
2	1.394	0.288	0.2066
3	1.692	0.349	0.206265
4	3.213	0.623	0.1939
5	4.081	0.786	0.1926
6	0.528	0.137	0.25947
7	1.539	0.298	0.193632
8	1.589	0.333	0.209566
9	1.247	0.29	0.232558
10	1.095	0.264	0.241096
Avg.			0.212877
Standard deviation			0.023528

CS80 SWNT4

	G	D	D/G
1	0.386	0.267	0.69171
2	0.33	0.288	0.872727
3	0.457	0.281	0.61488
4	0.334	0.27	0.808383
5	0.475	0.296	0.623158
6	0.376	0.271	0.720745
7	0.421	0.26	0.617577
8	0.361	0.28	0.775623
9	0.419	0.298	0.711217
10	0.406	0.315	0.775862
Avg.			0.721188
Standard deviation			0.087645

AC

	G	D	D/G
1	0.514	0.519	1.009728
2	0.417	0.497	1.191847
3	0.413	0.468	1.133172
4	0.423	0.438	1.035461
5	0.456	0.51	1.118421
6	0.382	0.456	1.193717
7	0.355	0.44	1.239437
8	0.335	0.397	1.185075
9	0.362	0.437	1.207182
10	0.384	0.417	1.085938
Avg.			1.139998
Standard deviation			0.076985

ACFC

	G	D	D/G
1	0.426	0.31	0.7277
2	0.323	0.236	0.73065
3	0.43	0.293	0.681395
4	0.353	0.269	0.76204
5	0.353	0.294	0.832861
6	0.429	0.344	0.801865
7	0.476	0.284	0.596639
8	0.404	0.338	0.836634
9	0.424	0.284	0.669811
10	0.42	0.284	0.67619
Avg.			0.731578
Standard deviation			0.078023

2. Water adsorption isotherms and kinetics at 20 ^{o}C

2.1 SWNT1 (EA95)

P/Po	Adsorbed net weigth (mmol/g) SWNT1-1	SWNT1-2	P/Po	SWNT1-1 Kinetics (s-1)	P/Po	SWNT1-2 Kinetics (s-1)
0	0	0	0		0	0
0.04699	0.02995	0.04023	0.04699		0.04699	0
0.09398	0.0599	0.06583	0.09398		0.09398	0
0.14097	0.08985		0.14097		0.14097	0
0.18796	0.1198	0.0768	0.18796		0.18796	0
0.23495	0.14975		0.23495		0.23495	0
0.28194	0.14975	0.13167	0.28194		0.28194	0
0.32893	0.14975		0.32893		0.32893	0
0.37592	0.32944	0.21213	0.37592		0.37592	0
0.42291	0.44924	0.32916	0.42291		0.42291	0.0004
0.4699	1.07817	1.74823	0.4699	0.0009	0.4699	0.0008
0.51689	2.60557	3.63909	0.51689	0.001	0.51689	0.001
0.56388	3.80353	4.08895	0.56388	0.0009	0.56388	0.0013
0.61087	4.25277		0.61087	0.0023	0.61087	0.0023
0.65786	4.49236	4.59001	0.65786	0.0014	0.65786	0.0014
0.70485	4.64211		0.75184	0.0018	0.75184	0.0009
0.75184	4.8817		0.79883	0.0016	0.79883	0.0013
0.79883	4.97155	5.1313	0.9398	0.001	0.84582	0.0007
0.84582	5.0614				0.9398	0.0009
0.89281	5.24109					
0.9398	5.39084	5.52264				

	SWNT1-1	
P/Po	Desorbed net weight (mmol/g)	Kinetics
0.80444	5.372687	
0.66248	5.050838	
0.61516	4.92301	0.0012
0.56784	4.73291	0.0003
0.52052	4.297418	0.001
0.4732	3.448906	0.001
0.42588	1.543413	0.0012
0.37856	0.709531	0.0017
0.33124	0.587129	0.0025
0.28392	0.453515	0.002
0.18928	0.354766	
0.09464	0.274303	

2.2 SWNT2 (CVD90)

P/Po	SWNT2-1 net weight (mmol/g)	SWNT2-2 net weight (mmol/g)
0	0	0
0.04699	0.111832	
0.09398	0.217778	
0.14097	0.310481	0.300181
0.18796	0.473815	
0.23495	0.719551	
0.28194	0.969702	0.99766
0.32893	1.325799	
0.37592	1.764299	
0.42291	2.170426	
0.4699	2.582439	2.379376
0.51689	3.056255	
0.56388	3.42118	
0.61087	3.877338	
0.65786	4.274636	4.07893
0.70485	4.758752	
0.75184	5.236981	
0.79883	5.732868	5.363528
0.84582	5.971247	
0.89281	6.573081	
0.9398	7.335305	6.864433
0.80444		6.503921
0.7098		6.058064
0.56784		4.995659
0.42588		3.687517
0.28392		1.765771
0.14196		0.975588

P/Po	Kinetics(s-1)
0.04699	0.001
0.09398	0.0013
0.14097	0.0014
0.18796	0.0015
0.23495	0.0011
0.28194	0.0008
0.32893	0.0007
0.37592	0.001
0.42291	0.001
0.4699	0.0009
0.51689	0.0008
0.56388	0.0008
0.61087	0.0008
0.65786	0.0012
0.70485	0.0007
0.75184	0.0007
0.79883	0.0007

2.3 SWNT3 (CS70)

P/Po	net weight (mmol/g) SWNT3-1	SWNT3-2	SWNT3-3
0	0	0	
0.04699	0.074994		
0.09398	0.134989	0.090017	0.150575
0.14097	0.194984		
0.18796	0.317975		0.291984
0.23495	0.434965	0.31506	
0.28194	0.614951		0.594443
0.32893	0.86993	0.63012	
0.37592	1.184905		1.154843
0.42291	1.649868		
0.4699	2.339813	2.010382	2.385629
0.51689	3.689705	3.195607	3.566659
0.56388	4.259659		4.421662
0.61087	4.889609		
0.65786	5.234581		5.503182
0.70485	5.669546		
0.75184	6.149508		6.506141
0.79883	6.554476		
0.84582	7.199424		7.612538
0.9398	8.039357	7.756474	8.980805
0.85176			8.1342
0.75712			7.8912
0.66248			7.3289
0.56784			6.1275
0.4732			4.739833
0.37856			2.4236
0.28392			1.298871
0.18928			0.823579
0.09464			0.484458
0			0.137481

P/Po	Kinetics (s-1) SWNT3-1
0.04699	0.0017
0.09398	0.0013
0.14097	0.0022
0.18796	0.0008
0.23495	0.0013
0.28194	0.0012
0.32893	0.0014
0.37592	0.0012
0.42291	0.001
0.4699	0.0009
0.51689	0.0009
0.56388	0.0009
0.61087	0.0009
0.65786	0.0016
0.70485	0.0014
0.75184	0.0013
0.84582	0.0006
0.9398	0.0006

P/Po	Kinetics (s-1) SWNT3-2
0	
0.04699	
0.09398	0.0013
0.18796	0.0016
0.28194	0.0012
0.37592	0.0011
0.4699	0.0007
0.51689	0.0004
0.56388	0.0007
0.65786	0.0009
0.75184	0.0006
0.84582	0.0006
0.9398	0.0006

2.4 SWNT4 (CS80)

	net weight (mmol/g)		
P/Po	SWNT4-1	SWNT4-2	SWNT4-3
0	0	0	0
0.04699	0.854835	0.558641	0.567884
0.09398	1.300608	0.971859	
0.14097	1.667716	1.338966	1.365796
0.18796	2.001608		
0.23495	2.309279	1.94017	1.960636
0.28194	2.664149		
0.32893	3.039997	2.567977	2.562665
0.37592	3.433326		
0.42291	3.898329	3.447615	3.339012
0.4699	4.370324	3.944186	
0.51689	4.674498		4.323823
0.56388	5.01888	4.671306	
0.65786	5.609748	5.253002	
0.75184		6.036874	
0.79883	6.461087		
0.9398	7.097406	6.74626	6.462372
0.80444		6.586648	
0.7098			6.3891
0.66248		6.320628	
0.4732		5.682181	5.454199
0.18928			3.137737
0.14196		2.933311	
0		0.929296	0.965043

	Kinetics (s-1)		
P/Po	SWNT4-1	P/Po	SWNT4-1
0.04699	0.0013	0.04699	0.0014
0.14097	0.0013	0.09398	0.0012
0.23495	0.001	0.14097	0.0006
0.32893	0.001	0.18796	0.0016
0.42291	0.0005	0.23495	0.0008
0.51689	0.0009	0.28194	0.0005
0.705	0.0011	0.32893	0.0008
0.846	0.0011	0.37592	0.0006
0.9398	0.0006	0.42291	0.0009
		0.4699	0.0006
		0.51689	0.0008
		0.56388	0.0007
		0.61087	0.0007
		0.65786	0.001
		0.75184	0.0004
		0.84582	0.0005
		0.9398	0.0005

2.5 Activated Carbons (AC)

Adsorption				
P/Po	AC-1 (mmol/g)	Kinetics	AC-2 (mmol/g)	kINTICS-2
0	0	0	0	
0.04699	0.204541	0.0024	0.316069	0.0026
0.09398	0.322959	0.0016	0.540167	0.002
0.14097	0.537437	0.0012	0.757788	0.0017
0.18796	0.796632	0.0013	1.053131	0.0016
0.23495	1.101373	0.0013	1.455989	0.0016
0.28194	1.583327	0.0012	2.012995	0.0014
0.32893	2.282243	0.001	2.67104	0.0013
0.37592	3.036642	0.001	3.443077	0.0014
0.42291	4.061829	0.001	4.449574	0.0011
0.4699	4.805463	0.0009	5.300628	0.0012
0.51689	5.790902	0.0008	6.048053	0.0012
0.56388	6.649641	0.0009	6.78641	0.0011
0.61087	7.583737	0.0006	7.848608	0.0008
0.65786	8.462351	0.0007	9.333095	0.0007
0.70485	9.678002	0.0004	10.56758	0.0007
0.75184			11.97823	0.0004
0.79883			12.60648	0.0009
0.84582			13.96674	0.0005
0.89281			15.12855	0.0008
0.9398			16.76978	0.0004

Desorption		
P/Po	AC-1 (mmol/g)	Kinetics
0.85176	16.33713	0.002
0.75712	15.64411	0.0012
0.66248	14.70497	0.0009
0.56784	11.54428	0.0008
0.4732	8.377117	0.0013
0.37856	5.015648	0.0006
0.28392	2.79669	0.001
0.18928	1.589411	0.0014
0.14196	1.187848	0.0019
0.09464	0.932662	0.0017
0.04732	0.663226	0.0021
0	0.257777	0.0015

2.6 Activated Carbon Fiber (ACF0

Adsorption (ACF)			Desorption		
P/Po	mmol/g	Kinetics	P/Po	mmol/g	Kinetics
0	0		0.85176	13.24437	0.0009
0.04732	0.119276	0.0024	0.75712	13.10537	0.0015
0.09464	0.200046	0.0019	0.66248	12.89406	0.0016
0.14196	0.31087	0.0018	0.56784	12.56253	0.0014
0.18928	0.457383	0.0018	0.4732	10.71139	0.0004
0.2366	0.692179	0.0013	0.42588	7.371656	0.0006
0.28392	1.077244	0.0013	0.37856	3.719169	0.0012
0.33124	1.792902	0.0012	0.33124	2.238076	0.0014
0.37856	3.236428	0.001	0.18928	0.801124	0.0021
0.42588	5.683942	0.0007	0.14196	0.64428	0.0022
0.4732	9.005836	0.0004	0.09464	0.501524	0.0023
0.52052	11.32374	0.0008	0.04732	0.410423	0.0026
0.56784	12.1737	0.0012	0.02366	0.365343	0.0011
0.61516	12.57004	0.0014	0	0.25358	0.0012
0.66248	12.80296	0.0015			
0.7098	12.93256				
0.75712	13.08565				
0.80444	13.19741				
0.85176	13.29885				
0.89908	13.3984				
0.9464	13.47447				

3. Fitting parameters of existing isotherm equations on carbon materials

Parameter			SWNT1	SWNT2	SWNT3	SWNT4	AC	ACF10
DS	S_o	mmol/g	0.07	1.24	0.51	5	2.75	0.44
	c	-	1.90	1.24	2.05	1.91	1.55	2.75
	k	g/mmol	0.09	0.07	0.07	0.09	0.026	0.05

Parameter			SWNT1	SWNT2	SWNT3	SWNT4	AC	ACF10
DA	E_V	kJ/mol	17.65	0.2568	16.98	26.41	0.07	27.41
	E_1	kJ/mol	12.57	14.77	0.35	2922	15.24	20.61
	$C_{\mu S}$	cm^3/g	0.07	0.02	0.13	0.06	0.25	0.16
	S_o	mmol/g	2.03	5.484	2.39	1.65	14.67	8.74
	N_5	-	9.75	2.78	1.92	1.31	0.19	2.37
	N_1	-	1.094	1.01	0.20	0.09	1.229	7.33

	Parameter		SWNT1	SWNT2	SWNT3	SWNT4	AC	ACF10
DDDo	n	-	5	8	7	5	8	4
	$C_{\mu S}$	cm^3/g	0.1	0.01	0.1	0.02	0.11	0.26
	K_f	-	$1.26E^{-13}$	1.152	2.28	13.27	2.96	$2.93E^{-14}$
	$K\mu$	-	22.1	107.1	18.69	114.7	9.734	60.39
	S_o	mmol/g	0.07	1.109	0.55	2.086	2.7	0.4

	Parameter		SWNT1	SWNT2	SWNT3	SWNT4	AC	ACF10
CMMS	b_L	-	9865	0.49	1.05	10	1.49	1.58
	$C_{\mu S}$	cm^3/g	0.09	0.04	0.04	0.1	0.09	0.23
	S_o	mmol/g	0.05	1.59	0.97	1.63	1.60	1.67
	K_o	-	0.0094	0.20	0.012	0.35	0.09	0.02
	K_1	-	1.99	1.56	2.02	1.45	1.49	2.26
	K_{as}	-	-	0.59	0.74	-	0.64	-

	Do and Do				Marban's			
	SWNT1	SWNT2	SWNT3	SWNT4	SWNT1	SWNT2	SWNT3	SWNT4
n	9	9	9	8	15	8-9	9-11	5
m	5	5	5	5	9.4	4.0-4.3	7.9	3.0
So	0	1.25	0.92	2.8	0.07	1.2-1.4	0.8-1.1	1.71
Kf	0	1.9	0.5	5.3	1.8	1.4-1.7	1.5-2.2	14.2
Qu	5.855	1.8	5.2	0	4.8	1.8-2.2	3.5-4.0	2.3
Ku	22	77	28.14	0.8	589	28-44	215-503	12
R^2	0.971	0.9992	0.9942	0.996	0.9936	0.9993	0.9986	0.994

	Lagorsse				Zinmy			
	SWNT1	SWNT2	SWNT3	SWNT4	SWNT1	SWNT2	SWNT3	SWNT4
n	7	7	7	7	-	-	-	-
m	7	7	7	7	6.9	1.9	3.7	2.4
So	0.23	0.87	0.53	3902	0.86	6.27	0.093	0.26
Kf	1.5	1.9	1.9	0.003	360	0	8887	0.8
Qu	4.548	2	5.2	0	5.9	22.06	8.9	3.7
Ku	19.38	0.03	0.42	0	23	0.52	5.958	2.4
R^2	0.9809	0.9992	0.9872	0.931	0.9833	0.999	0.9929	0.9988

4. Do and Do equation modified by Marbon et al. at 5 and 35 ^{o}C

5 ^{o}C

	n	m	Kf	Kus	So	Cus
SWNT1	15	11.4	0.09681	6954	0.3726	0.10
SWNT2	9	3.7	0.7024	7.683	1.122	0.03
SWNT3	9	9.7	0.263	1818	1.109	0.06
SWNT4	6	4.3	23.8	111.8	1.385	0.04
AC	13	11.5	11.32	2541	1.522	0.20
ACF10	6	8.9	1.775	563.6	0.6883	0.20

35 ^{o}C

	n	m	Kf	Kus	So	Cus
SWNT1	17	11.5	0.4215	4165	0.03437	0.08
SWNT2	9	4.8	1.638	70.96	0.6461	0.01
SWNT3	12	10.0	2.121	1323	0.922	0.04
SWNT4	5	3.5	10.69	30.97	1.129	0.03
AC	18	13.7	21.7	1285	1.319	0.03
ACF10	8	8.5	1.746	747.4	0.4803	0.19

5. Calculation of Heat of adsorption

5.1. SWNT1
5.1.1 Isotherm of Total adsorption

	5°C	20°C	35°C	1/T2-1/T1			Slop	R^2	qst(KJ/mol)	Qst(KJ/mol)
mmol/g	p/po	p/po	p/po	0.000184	0.00035	0.000166	qst/R			
0.35	0.3458	0.37	0.3938	-0.06764	-0.12998	-0.06234	370.4	0.9997	3.0795056	48.079506
0.56	0.37	0.39	0.41	-0.05264	-0.10265	-0.05001	291.85	0.9981	2.4264409	47.426441
0.83	0.39	0.41	0.43	-0.05001	-0.09764	-0.04763	277.54	0.9979	2.30746756	47.307468
1.22	0.4	0.42	0.44	-0.04879	-0.09531	-0.04652	270.89	0.9978	2.25217946	47.252179
1.75	0.42	0.439	0.465	-0.04424	-0.10178	-0.05754	282.45	0.9064	2.3482893	47.348289
2	0.4332	0.4562	0.4792	-0.05173	-0.10092	-0.04919	286.89	0.998	2.38520346	47.385203
2.4	0.4458	0.4666	0.4877	-0.0456	-0.08983	-0.04423	254.98	0.9962	2.11990372	47.119904
2.7	0.4542	0.475	0.502	-0.04478	-0.10006	-0.05529	278.79	0.9297	2.31786006	47.31786
3	0.4624	0.4854	0.5124	-0.04854	-0.10268	-0.05413	288.33	0.9671	2.39717562	47.397176
3.5	0.4792	0.505	0.5354	-0.05244	-0.1109	-0.05846	311.43	0.9672	2.58922902	47.589229
4	0.4854	0.52	0.5624	-0.06886	-0.14724	-0.07838	412.82	0.9605	3.43218548	48.432185
4.2	0.49	0.535	0.5874	-0.08786	-0.1813	-0.09344	510.99	0.9801	4.24837086	49.248371

5.1.2. Isotherm of Micropore filling

	5°C	20°C	35°C				Slop	R^2	qst(KJ/mol)	Qst(KJ/mol)
mmol/g	p/po	p/po	p/po	0.000184	0.00035	0.000166	qst/R			
0.135	0.314	0.335	0.3522	-0.06474	-0.11481	-0.05007	331.5	0.9028	2.756091	47.756091
0.34	0.3522	0.37	0.3896	-0.0493	-0.10092	-0.05162	284.79	0.9837	2.36774406	47.367744
0.5	0.3688	0.385	0.4022	-0.04299	-0.08669	-0.04371	245.2	0.9895	2.0385928	47.038593
0.777	0.398	0.4168	0.4314	-0.04615	-0.08058	-0.03443	191.56	0.9642	1.59262984	46.59263
1	0.4332	0.4562	0.4792	-0.05173	-0.10092	-0.04919	286.89	0.998	2.38520346	47.385203
1.287	0.4084	0.4314	0.448	-0.05479	-0.09255	-0.03776	269.49	0.9523	2.24053986	47.24054
1.5	0.4168	0.4396	0.4584	-0.05326	-0.09514	-0.04188	274.36	0.9866	2.28102904	47.281029
1.74	0.425	0.448	0.4668	-0.0527	-0.09381	-0.04111	270.71	0.9851	2.25068294	47.250683
2	0.4334	0.4542	0.475	-0.04688	-0.09165	-0.04478	260.46	0.9976	2.16546444	47.165464
2.25	0.4418	0.4626	0.4854	-0.04601	-0.09412	-0.04811	265.61	0.9839	2.20828154	47.208282
2.5	0.45	0.4688	0.4958	-0.04093	-0.09693	-0.056	267.93	0.8815	2.22757002	47.22757
2.75	0.4564	0.48	0.5042	-0.05042	-0.0996	-0.04919	273.49	0.8347	2.27379586	47.273796
3	0.4646	0.4834	0.5146	-0.03967	-0.10221	-0.06255	279.5	0.8043	2.323763	47.323763
3.26	0.4708	0.4918	0.5292	-0.04364	-0.11693	-0.07329	318.24	0.7682	2.64584736	47.645847
3.5	0.4772	0.5	0.5458	-0.04667	-0.13432	-0.08764	362.55	0.7047	3.0142407	48.014241

5.2 SWNT2

5.2.1 Isotherm of Total adsorption

	5°C	20°C	35°C	1/T2-1/T1			Slop	R^2	qst(KJ/mol)	Qst(KJ/mol)
mmol/g	p/po	p/po	p/po	0.000184	0.00035	0.000166	qst/R			
1.07	0.4058	0.4334	0.4638	-0.0658	-0.13359	-0.06779	377.45	0.987	3.1381193	48.138119
1.29	0.4484	0.4834	0.5194	-0.07516	-0.14699	-0.07183	417.7	0.9976	3.4727578	48.472758
1.45	0.4764	0.5222	0.5634	-0.09179	-0.16773	-0.07594	481.89	0.9946	4.00643346	49.006433
1.79	0.5236	0.593	0.643	-0.12447	-0.20542	-0.08095	600.64	0.9323	4.99372096	49.993721
2.22	0.581	0.6708	0.736	-0.14372	-0.23648	-0.09276	691.84	0.9295	5.75195776	50.751958
2.54	0.618	0.7222	0.7972	-0.15581	-0.25462	-0.0988	745.84	0.9222	6.20091376	51.200914
2.89	0.6582	0.7706	0.8636	-0.15766	-0.2716	-0.11394	788.15	0.9667	6.5526791	51.552679
3.29	0.7012	0.8136	0.9428	-0.14868	-0.29606	-0.14739	838.97	0.9935	6.97519658	51.975197

5.2.2 Isotherm of Functional groups

	5°C	20°C	35°C	1/T2-1/T1			Slop	R^2	qst(KJ/mol)	Qst(KJ/mol)
mmol/g	p/po	p/po	p/po	0.000184	0.00035	0.000166	qst/R			
0.89	0.475	0.51	0.5332	-0.0711	-0.11558	-0.04449	338.89	0.987	2.81753146	47.817531
1.11	0.5312	0.57	0.6082	-0.0705	-0.13537	-0.06487	385.79	0.9997	3.20745806	48.207458
1.32	0.5728	0.62	0.6604	-0.07918	-0.14231	-0.06313	409.98	0.9946	3.40857372	48.408574
1.55	0.6082	0.66	0.7082	-0.08174	-0.15222	-0.07049	435.97	0.9985	3.62465458	48.624655
1.8	0.654	0.7186	0.7686	-0.0942	-0.16146	-0.06727	468.96	0.9633	3.89893344	48.898933
2.07	0.6894	0.756	0.8186	-0.09222	-0.17177	-0.07955	491.95	0.9985	4.0900723	49.090072
2.37	0.7248	0.7936	0.879	-0.09068	-0.19289	-0.10221	541.23	0.9638	4.49978622	49.499786

5.2.3 Isotherm of Micropore filling

	5°C	20°C	35°C	1/T2-1/T1			Slop	R^2	qst(KJ/mol)	Qst(KJ/mol)
mmol/g	p/po	p/po	p/po	0.000184	0.00035	0.000166	qst/R			
0.125	0.2834	0.3	0.3124	-0.05692	-0.09743	-0.0405	283.04	0.9622	2.35319456	47.353195
0.17	0.3124	0.33	0.3438	-0.05481	-0.09578	-0.04097	277.24	0.9997	2.30497336	47.304973
0.24	0.3478	0.37	0.3874	-0.06188	-0.10783	-0.04595	312.29	0.974	2.59637906	47.596379
0.29	0.3728	0.4	0.4188	-0.07042	-0.11635	-0.04593	340.14	0.9333	2.82792396	47.827924
0.39	0.4146	0.45	0.4792	-0.08193	-0.1448	-0.06287	418.36	0.9633	3.47824504	48.478245
0.44	0.4352	0.48	0.529	-0.09798	-0.19518	-0.0972	553.07	0.9169	4.59822398	49.598224
0.55	0.4748	0.5144	0.541	-0.08011	-0.13053	-0.05042	382.54	0.9199	3.18043756	48.180438

5.3 SWNT3

5.3.1 Isotherm of Total adsorption

	5C	20C	35C	$1/T_2-1/T_1$ (ln(P2/P1))			Slop			
mmol/g	p/po	p/po	p/po	0.000184	0.00035	0.000166	qst/R	R^2	qst(KJ/mol)	Qst(KJ/mol)
0.0745	0.0469	0.08	0.1188	-0.53401	-0.92942	-0.39541	2692.3	0.9732	22.3837822	
0.11	0.074	0.1	0.1375	-0.30111	-0.61956	-0.31845	1744	0.9814	14.499616	
0.13	0.0927	0.12	0.1448	-0.25812	-0.44599	-0.18786	1293	0.9687	10.750002	
0.17	0.12	0.138	0.1573	-0.13976	-0.27066	-0.1309	770	0.999	6.40178	
0.31	0.1875	0.21	0.2282	-0.11333	-0.19644	-0.08311	569	0.9707	4.730666	49.730666
1.26	0.375	0.396	0.4188	-0.05449	-0.11047	-0.05598	312.18	0.9875	2.59546452	47.595465
1.5	0.3938	0.4146	0.4396	-0.05147	-0.11002	-0.05855	308.49	0.9607	2.56478586	47.564786
2	0.43	0.45	0.4772	-0.04546	-0.10415	-0.05869	289.19	0.9099	2.40432566	47.404326
2.28	0.4396	0.4668	0.4918	-0.06004	-0.11221	-0.05217	321.18	0.999	2.67029052	47.670291
2.5	0.448	0.4792	0.5064	-0.06732	-0.12253	-0.05521	352.27	0.9475	2.92877278	47.928773
2.76	0.4646	0.4918	0.525	-0.0569	-0.12222	-0.06533	342.45	0.9576	2.8471293	47.847129
3	0.475	0.5022	0.5418	-0.05568	-0.13158	-0.0759	363.83	0.8834	3.02488262	48.024883
3.28	0.4792	0.5164	0.5646	-0.07476	-0.164	-0.08924	458.13	0.9434	3.80889282	48.808893
3.54	0.498	0.5104	0.573	-0.02459	-0.14029	-0.11569	357.65	0.355	2.9735021	47.973502
4	0.5042	0.5396	0.6188	-0.06786	-0.20481	-0.13695	549.94	0.665	4.57220116	49.572201
4.5	0.5314	0.5792	0.6812	-0.08613	-0.24834	-0.16221	670.18	0.7031	5.57187652	50.571877
5	0.5772	0.6272	0.748	-0.08308	-0.25921	-0.17614	693.59	0.6388	5.76650726	50.766507
5.5	0.6104	0.6812	0.8042	-0.10974	-0.27573	-0.16599	756.38	0.8277	6.28854332	51.288543
5.75	0.6272	0.7104	0.823	-0.12456	-0.27169	-0.14713	759.58	0.9474	6.31514812	51.315148
6	0.6376	0.7376	0.8418	-0.14569	-0.27783	-0.13214	792.67	1	6.59025838	51.590258
6.26	0.6542	0.7646	0.8646	-0.15594	-0.27885	-0.12291	804.04	0.9871	6.68478856	51.684789
6.5	0.6688	0.7876	0.8772	-0.16351	-0.27125	-0.10774	792.4	0.937	6.5880136	51.588014
6.73	0.6834	0.8084	0.9062	-0.16798	-0.28218	-0.1142	822.48	0.9479	6.83809872	51.838099
7	0.698	0.825	0.9208	-0.16716	-0.27702	-0.10986	809.42	0.9361	6.72951788	51.729518

5.3.2 Isotherm of Functional groups

mmol/g	5C	20C	35C	$1/T_2-1/T_1$ (ln(P2/P1))			Slop	R^2	qst(KJ/mol)	Qst(KJ/mol)
	p/po	p/po	p/po	0.000184	0.00035	0.000166	qst/R			
0.36	0.2626	0.287	0.3106	-0.08885	-0.16787	-0.07902	479.67	0.9875	3.98797638	48.987976
0.5	0.2938	0.325	0.3522	-0.10093	-0.1813	-0.08037	522.36	0.9889	4.34290104	49.342901
0.774	0.3688	0.405	0.448	-0.09363	-0.19454	-0.10091	547.74	0.9787	4.55391036	49.55391
1	0.4168	0.46	0.5106	-0.09862	-0.20298	-0.10436	572.32	0.9812	4.75826848	49.758268
1.28	0.4646	0.523	0.573	-0.1184	-0.20971	-0.0913	605.65	0.9827	5.0353741	50.035374
1.5	0.498	0.556	0.6146	-0.11017	-0.21037	-0.1002	600	1	4.9884	49.9884
2	0.5542	0.617	0.6876	-0.10734	-0.21568	-0.10834	610.35	0.9907	5.0744499	50.07445
2.26	0.5792	0.6564	0.7272	-0.12512	-0.22755	-0.10243	654.27	0.9932	5.43960078	50.439601
2.76	0.625	0.705	0.775	-0.12045	-0.21511	-0.09467	620.38	0.9865	5.15783932	50.157839
3	0.6356	0.72	0.798	-0.12468	-0.22754	-0.10286	653.85	0.9942	5.4361089	50.436109
3.26	0.6542	0.7376	0.8208	-0.11999	-0.22687	-0.10688	648.16	0.999	5.38880224	50.388802
3.5	0.671	0.76	0.8376	-0.12455	-0.22177	-0.09722	639.9	0.9852	5.3201286	50.320129
3.75	0.6814	0.775	0.8628	-0.12871	-0.23603	-0.10732	677.72	0.9956	5.63456408	50.634564
4	0.698	0.7814	0.8814	-0.11287	-0.23329	-0.12042	657.37	0.9793	5.46537418	50.465374
4.27	0.7146	0.8	0.9	-0.11289	-0.23067	-0.11778	651.1	0.9844	5.4132454	50.413245
4.5	0.723	0.82	0.9168	-0.1259	-0.23748	-0.11159	678.74	0.9998	5.64304436	50.643044

5.3.3 Isotherm of Micropore filling

mmol/g	5C	20C	35C	1/T2-1/T1 (ln(P2/P1))			Slop	R^2	qst(KJ/mol)	Qst(KJ/mol)
	p/po	p/po	p/po	0.000184	0.00035	0.000166	qst/R			
0.09	0.3188	0.335	0.348	-0.04957	-0.08764	-0.03807	253.18	0.9819	2.10493852	47.104939
0.286	0.3626	0.38	0.3938	-0.04687	-0.08254	-0.03567	238.62	0.9799	1.98388668	46.983887
0.5	0.3896	0.405	0.4188	-0.03877	-0.07227	-0.03351	206.96	0.9986	1.72066544	46.720665
0.75	0.4272	0.4542	0.446	-0.06129	-0.04307	0.018219	251.88	0.9995	2.09413032	47.09413
1	0.4292	0.4522	0.4688	-0.0522	-0.08825	-0.03605	256.95	0.953	2.1362823	47.136282
1.25	0.446	0.4708	0.4918	-0.05411	-0.09775	-0.04364	281.38	0.991	2.33939332	47.339393
1.5	0.4604	0.4834	0.5064	-0.04875	-0.09523	-0.04648	270.67	0.9978	2.25035038	47.25035
1.75	0.475	0.51	0.5354	-0.0711	-0.1197	-0.0486	348.76	0.9497	2.89959064	47.899591
2	0.4938	0.53	0.5604	-0.07075	-0.12652	-0.05577	364.8	0.9871	3.0329472	48.032947
2.24	0.5146	0.56	0.6146	-0.08455	-0.17758	-0.09303	499.2	0.971	4.1503488	49.150349

5.4 SWNT4

5.4.1 Isotherm of Total adsorption

	5C	20C	35C	$1/T_2-1/T_1$ (ln(P2/P1))			Slop	R^2	qst(KJ/mol)	Qst(KJ/mol)
mmol/g	p/po	p/po	p/po	0.000184	0.00035	0.000166	qst/R			
0.175	0.075	0.098	0.1356	-0.26748	-0.59222	-0.32474	1652.2	0.9367	13.7363908	58.736391
1.25	0.1252	0.173	0.22	-0.32338	-0.56372	-0.24034	1550.5	0.9248	12.890857	57.890857
1.488	0.1584	0.2064	0.248	-0.26469	-0.44831	-0.18361	1304.8	0.9544	10.8481072	55.848107
1.69	0.1938	0.2376	0.2792	-0.20376	-0.3651	-0.16134	1052.4	0.9879	8.7496536	53.749654
2.02	0.2398	0.2772	0.3148	-0.14493	-0.27213	-0.1272	778.36	0.9994	6.47128504	51.471285
2.47	0.2898	0.3334	0.3792	-0.14015	-0.26887	-0.12872	766.38	0.9998	6.37168332	51.371683
2.5	0.2916	0.3374	0.3832	-0.14589	-0.27317	-0.12729	781.68	0.9992	6.49888752	51.498888
2.79	0.3252	0.3772	0.443	-0.14834	-0.30913	-0.16079	869.99	0.9752	7.23309686	52.233097
3	0.354	0.4124	0.4854	-0.1527	-0.31568	-0.16298	889.48	0.9792	7.39513672	52.395137
3.28	0.377	0.4374	0.5582	-0.1486	-0.39247	-0.24387	1070	0.7815	8.89598	53.89598
3.5	0.4104	0.4582	0.6166	-0.11017	-0.40709	-0.29691	1071	0.5255	8.904294	53.904294
3.79	0.4416	0.5	0.727	-0.1242	-0.49852	-0.37432	1303	0.4815	10.833142	55.833142
4	0.4604	0.5394	0.8124	-0.15836	-0.5679	-0.40954	1499	0.5432	12.462686	57.462686

5.4.2 Isotherm of Functional groups

	5C	20C	35C	$1/T_2-1/T_1$ (ln(P2/P1))			Slop	R^2	qst(KJ/mol)	Qst(KJ/mol)
mmol/g	p/po	p/po	p/po	0.000184	0.00035	0.000166	qst/R			
0.95	0.091	0.129	0.175	-0.34895	-0.65393	-0.30497	1871	0.9031	15.555494	60.555494
1.75	0.2814	0.3398	0.4772	-0.18858	-0.52816	-0.33958	1430	0.7284	11.88902	56.88902
2.02	0.3606	0.46	0.598	-0.24346	-0.50582	-0.26236	1424	0.9767	11.839136	56.839136
2.46	0.4834	0.54	0.789	-0.11072	-0.48992	-0.3792	1270	0.4378	10.55878	55.55878

5.3.3 Isotherm of Micropore filling

	5C	20C	35C	$1/T_2-1/T_1$ (ln(P2/P1))			Slop	R^2	qst(KJ/mol)	Qst(KJ/mol)
mmol/g	p/po	p/po	p/po	0.000184	0.00035	0.000166	qst/R			
0.27	0.2166	0.23	0.2438	-0.06003	-0.1183	-0.05827	335.76	0.9961	2.79150864	47.791509
0.4	0.2426	0.259	0.2708	-0.06541	-0.10997	-0.04455	320.48	0.9485	2.66447072	47.664471
0.63	0.2782	0.31	0.34	-0.10823	-0.20061	-0.09237	574.99	0.9977	4.78046686	49.780467
0.87	0.3156	0.351	0.3844	-0.10631	-0.19721	-0.0909	565.17	0.9979	4.69882338	49.698823
1.05	0.3448	0.3874	0.4406	-0.11649	-0.24517	-0.12868	689	0.9699	5.728346	50.728346
1.2	0.3688	0.4198	0.4916	-0.12952	-0.28741	-0.15789	801.57	0.935	6.66425298	51.664253
1.4	0.4084	0.49	0.5916	-0.18216	-0.37058	-0.18843	1046.7	0.9862	8.7022638	53.702264

6.1. Example of Isoster of SWNT3 (Micropore adsorption)

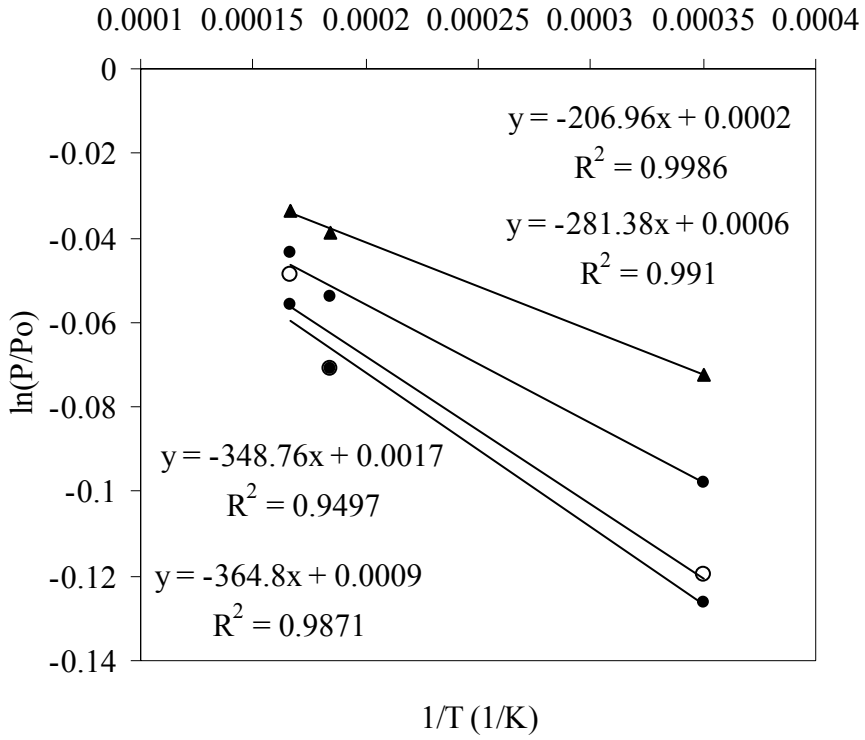

V I T A

Pyoungchung Kim was born in Yeosu, South Korea on April 1, 1971. He obtained his bachelor's degree in environmental engineering from the KonKuk University in 1996. He obtained his M.S. degree in environmental engineering in 1998 in the same school. Upon graduation, he worked as research assistant at the drinking water division in the National Institute of Environmental Research (NIER) for 2 years and worked as a researcher in the Korea Institute of Environmental Science and Technology (KIEST) for 2years. On his serving, he won a letter of official commendation from the Minister of Environment in Korea in 2001. He returned to school for Ph.D. degree at the department of civil and environmental engineering in the university of Tennessee, Knoxville, Tennessee in 2005 and earned Ph.D. in 2009. During his graduate study, he received scholarship from Korean-American Scientists and Engineers Association (KSEA) and was invited to present his research achievement. He published three peer reviewed journal articles as a first author and three journal articles as co-authors, and gave several oral presentations at national conferences.